



A11103 711480

REFERENCE

NIST  
PUBLICATIONS**NISTIR 4590**

# **Applications of the Generalized Global Equivalence Ratio Model (GGERM) for Predicting the Generation Rate and Distribution of Products of Combustion in Two-Layer Fire Environments - - Methane and Hexanes**

**Leonard Y. Cooper**

**U.S. DEPARTMENT OF COMMERCE  
National Institute of Standards  
and Technology  
Building and Fire Research Laboratory  
Gaithersburg, MD 20899**

**U.S. DEPARTMENT OF COMMERCE  
Robert A. Mosbacher, Secretary  
NATIONAL INSTITUTE OF STANDARDS  
AND TECHNOLOGY  
John W. Lyons, Director**

QC

100

.U56

#4590

1991

**NIST**



**Applications of the Generalized  
Global Equivalence Ratio Model  
(GGERM) for Predicting the  
Generation Rate and Distribution  
of Products of Combustion in  
Two-Layer Fire Environments - -  
Methane and Hexanes**

**Leonard Y. Cooper**

**U.S. DEPARTMENT OF COMMERCE  
National Institute of Standards  
and Technology  
Building and Fire Research Laboratory  
Gaithersburg, MD 20899**

**June 1991**



**U.S. DEPARTMENT OF COMMERCE  
Robert A. Mosbacher, Secretary  
NATIONAL INSTITUTE OF STANDARDS  
AND TECHNOLOGY  
John W. Lyons, Director**



TABLE OF CONTENTS

	<u>Page</u>
TABLE OF CONTENTS . . . . .	iii
LIST OF FIGURES . . . . .	iv
ABSTRACT . . . . .	1
INTRODUCTION - THE EXTENDED UPPER LAYER IN A ROOM CONTAINING A FIRE . . .	2
Background . . . . .	2
An Overview of the GGERM . . . . .	2
INITIAL VALUE PROBLEM FOR THE MASS FRACTION OF FUEL, OXYGEN, AND OTHER PRODUCTS OF COMBUSTION . . . . .	4
FIRE SCENARIOS WHERE ALL OXYGEN INFLOW IS FROM AN AMBIENT ATMOSPHERE . . .	5
CONSTRUCTING ANALYTIC REPRESENTATIONS FOR THE PRODUCT GENERATION FUNCTIONS AND THE STEADY STATE MASS FRACTIONS FROM EXPERIMENTAL DATA . . . . .	8
General Considerations . . . . .	8
The Product Generation Functions and the Steady State Mass Fractions for the Combustion of Methane Using Data of [2] . . .	11
The Product Generation Functions and the Steady State Mass Fractions for the Combustion of Hexane Using Data of [6] . . .	16
Plots of the Product Generation Functions and the Steady State Mass Fractions for the Combustion of Methane and Hexanes . . .	19
SIMULATING EXPERIMENTS OF REFERENCES [2] AND [3] . . . . .	19
The Combustion of Methane in Figure-3b Test Configurations . . . . .	19
The Combustion of Hexanes in Figure-3l Test Configurations - One of Two Hexane Experiments Reported in [3] . . . . .	21
The Combustion of Hexanes in Figure-3l Test Configurations - A Hypothetical Reference-[3]-Type Hexane Experiment . . . . .	24
SUMMARY AND CONCLUSIONS . . . . .	25
REFERENCES . . . . .	26
NOMENCLATURE . . . . .	27

LIST OF FIGURES





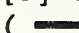
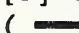


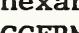
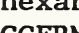
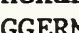
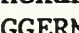
	<u>Page</u>
Figure 1. The extended upper layer in a room of fire origin which includes the assumed negligible-volume fire plume. . . . .	29
Figure 2. The GGERM representation of combustion and flow dynamics in the extended upper-layer of Figure 1 . . . . .	30
Figure 3. The experimental configuration used in [6], [7], and [8] (a) and in [2], [4], [5], and [9] (b). . . . .	31
Figure 4. Combustion of methane ( $\text{CH}_4$ ). Data from [2]. Analytic representations of $c_{\text{CH}_4, \text{REACTOUT}}^{(\text{SS})}$ : for complete stoichiometric combustion, Eqs. (51)-(53) or Eqs. (55) and (56) ( - - - ); and for the curve-fit of Eq. (58) ( ——— ). . . . .	32
Figure 5. Combustion of methane ( $\text{CH}_4$ ). Data from [2]. Analytic representations of $c_{\text{O}_2, \text{REACTOUT}}^{(\text{SS})}$ : for complete stoichiometric combustion, Eq. (59) ( - - - ); and for the curve-fit of Eq. (61) ( ——— ). . . . .	33
Figure 6. Combustion of methane ( $\text{CH}_4$ ). Data from [2]. Analytic representations of $c_{\text{CO}_2, \text{REACTOUT}}^{(\text{SS})}$ : for complete stoichiometric combustion, Eq. (62) ( - - - ); and for the curve-fit of Eq. (64) and (65) ( ——— ) . . . . .	34
Figure 7. Combustion of methane ( $\text{CH}_4$ ). Data from [2]. Analytic representations of $c_{\text{H}_2\text{O}, \text{REACTOUT}}^{(\text{SS})}$ : for complete stoichiometric combustion, Eq. (63) ( - - - ); and for the curve-fit of Eq. (66) and (67) ( ——— ) . . . . .	35
Figure 8. Combustion of methane ( $\text{CH}_4$ ). Data from [2]. Analytic representations of $c_{\text{CO}, \text{REACTOUT}}^{(\text{SS})}$ for the curve fit of Eqs. (68) and (69). . . . .	36
Figure 9. Combustion of methane ( $\text{CH}_4$ ). Data from [2]. Analytic representations of $c_{\text{H}_2, \text{REACTOUT}}^{(\text{SS})}$ for the curve fit of Eq. (70) . . . . .	37
Figure 10. Combustion of hexanes ( $\text{C}_6\text{H}_{14}$ ). Data from [6]. Analytic representations of $f_{\text{C}_6\text{H}_{14}}$ : for complete stoichiometric combustion, Eqs. (51)-(53) and (71) ( ——— ); and for the curve-fit of Eqs. (71)-(73) ( ——— ) . . . . .	38
Figure 11. Combustion of hexanes ( $\text{C}_6\text{H}_{14}$ ). Data from [6]. Analytic representations of $f_{\text{O}_2}$ : for complete stoichiometric combustion, Eqs. (51)-(53) and (71) ( ——— ); and for the curve-fit of Eqs. (71)-(73) ( ——— ). . . . .	39



Figure 12.	Combustion of hexanes ( $C_6H_{14}$ ). Data from [6]. Analytic representations of $f_{CO_2}$ : for complete stoichiometric combustion, Eqs. (51)-(53) and (71) ( — ); and for the curve-fit of Eqs. (71)-(73) ( ——— ). . . . .	40
Figure 13.	Combustion of hexanes ( $C_6H_{14}$ ). Data from [6]. Analytic representations of $f_{H_2O}$ : for complete stoichiometric combustion, Eqs. (51)-(53) and (71) ( — ); and for the curve-fit of Eqs. (71)-(73) ( ——— ). . . . .	41
Figure 14.	Combustion of hexanes ( $C_6H_{14}$ ). Data from [6]. Analytic representation of $f_{CO}$ according to the curve fit of Eq. (74) . . . . .	42
Figure 15.	Combustion of hexanes ( $C_6H_{14}$ ). Data from [6]. Analytic representation of $f_{H_2}$ according to the curve fit of Eq. (75) . . . . .	43
Figure 16.	Combustion of methane ( $CH_4$ ). TOP - Analytic representations of $c_{CH_4, REACTOUT}^{(SS)}$ : for complete stoichiometric combustion, Eqs. (51)-(53) or Eqs. (55) and (56) ( — ); and for the curve-fit of Eq. (58) ( ——— ). BOTTOM - Corresponding analytic representations of $f_{CH_4}$ according to Eq. (23) . . . . .	44
Figure 17.	Combustion of methane ( $CH_4$ ): TOP - Analytic representations of $c_{O_2, REACTOUT}^{(SS)}$ : for complete stoichiometric combustion, Eq. (59) ( — ); and for the curve fit of Eq. (61) ( ——— ). BOTTOM - Corresponding analytic representations of $f_{O_2}$ according to Eq. (24) . . . . .	45
Figure 18.	Combustion of methane ( $CH_4$ ): TOP - Analytic representations of $c_{CO_2, REACTOUT}^{(SS)}$ for complete stoichiometric combustion, Eq. (62) ( — ), and for the curve fit of Eq. (64) and (65) ( ——— ). BOTTOM - Corresponding analytic representations of $f_{CO_2}$ according to Eq. (25). . . . .	46
Figure 19.	Combustion of methane ( $CH_4$ ): TOP - Analytic representations of $c_{H_2O, REACTOUT}^{(SS)}$ for complete stoichiometric combustion, Eq. (63) ( — ), and for the curve fit of Eqs. (66) and (67) ( ——— ). BOTTOM - Corresponding analytic representations of $f_{H_2O}$ according to Eq. (25). . . . .	47
Figure 20.	Combustion of methane ( $CH_4$ ): TOP - Analytic representation of $c_{CO, REACTOUT}^{(SS)}$ according to Eqs. (68) and (69). BOTTOM - Corresponding analytic representations of $f_{CO}$ according to Eq. (25) . . . . .	48
Figure 21.	Combustion of methane ( $CH_4$ ): TOP - Analytic representation of $c_{H_2, REACTOUT}^{(SS)}$ according to Eq. (70). BOTTOM - Corresponding analytic representation of $f_{H_2}$ according to Eq. (25) . . . . .	49

Figure 22.	Combustion of hexanes ( $C_6H_{14}$ ): TOP - Analytic representations of $f_{C_6H_{14}}$ for complete stoichiometric combustion, Eqs. (51)-(53) and (71) ( ——— ), and of the curve-fit of Eqs. (71)-(73) ( ——— ). BOTTOM - Corresponding analytic representations of $c_{C_6H_{14},REACTOUT}^{(SS)}$ according to Eq. (20)	50
Figure 23.	Combustion of hexanes ( $C_6H_{14}$ ): TOP - Analytic representations of $f_{O_2}$ for complete stoichiometric combustion, Eqs. (51)-(53) and (71) ( ——— ), and of the curve-fit of Eqs. (71)-(73) ( ——— ). BOTTOM - Corresponding analytic representations of $c_{O_2,REACTOUT}^{(SS)}$ according to Eq. (21)	51
Figure 24.	Combustion of hexanes ( $C_6H_{14}$ ): TOP - Analytic representations of $f_{CO_2}$ for complete stoichiometric combustion, Eqs. (51)-(53) and (71) ( ——— ), and of the curve-fit of Eqs. (71)-(73) ( ——— ). BOTTOM - Corresponding analytic representations of $c_{CO_2,REACTOUT}^{(SS)}$ according to Eq. (22)	52
Figure 25.	Combustion of hexanes ( $C_6H_{14}$ ): TOP - Analytic representations of $f_{H_2O}$ for complete stoichiometric combustion, Eqs. (51)-(53) and (71) ( ——— ), and of the curve-fit of Eqs. (71)-(73) ( ——— ). BOTTOM - Corresponding analytic representations of $c_{H_2O,REACTOUT}^{(SS)}$ according to Eq. (22)	53
Figure 26.	Combustion of hexanes ( $C_6H_{14}$ ): TOP - Analytic representations of $f_{CO}$ for the curve-fit of Eq. (74). BOTTOM - Corresponding analytic representation of $c_{CO,REACTOUT}^{(SS)}$ according to Eq. (22)	54
Figure 27.	Combustion of hexanes ( $C_6H_{14}$ ): TOP - Analytic representations of $f_{H_2}$ for the curve-fit of Eq. (75). BOTTOM - Corresponding analytic representation of $c_{H_2,REACTOUT}^{(SS)}$ according to Eq. (22)	55
Figure 28.	Results of GGERM simulation of test 1 of Appendix B of [2] using the real combustion model ( ——— ) and the complete stoichiometric combustion model ( ——— ). TOP: Plots of $c_{CH_4,U}$ . BOTTOM: Plots of $c_{O_2,U}$	56
Figure 29.	Results of GGERM simulation of test 1 of Appendix B of [2] using the real combustion model ( ——— ) and the complete stoichiometric combustion model ( ——— ). TOP: Plots of $c_{CO_2,U}$ . BOTTOM: Plots of $c_{H_2O,U}$	57
Figure 30.	Results of GGERM simulation of test 1 of Appendix B of [2] using the real combustion model ( ——— ) and the complete stoichiometric combustion model ( ——— ). TOP: Plots of $c_{CO,U}$ . BOTTOM: Plots of $c_{H_2,U}$	58



Figure 31.	Test configuration for the experiments of [3]. . . . .	59
Figure 32.	Large-burn hexane experiment of [3]. Temperature data from the thermocouple located approximately at the mid-elevation of the upper layer data. Curve fit of the data used in the analysis . . . . .	60
Figure 33.	Large-burn hexane experiment of [3]. TOP - Hexane pyrolysis rate data and curve fit of the data used in the analysis; BOTTOM - air flow rate data and curve fit of the data used in the analysis to approximate $\dot{P}_{FUEL, FLOWIN}$ . . . . .	61
Figure 34.	Plot of $\phi^{(SS)}$ for the large-burn hexane experiment of [3]. . . . .	62
Figure 35.	Results of simulating the large-burn hexane experiment of [3] using the real combustion model: The GGERM simulation (  ) and the quasi-steady approximation (  ). TOP: Plots of $c_{HEX,U}$ [vol]. BOTTOM: Plots of $c_{O_2,U}$ [vol]. . . . .	63
Figure 36.	Results of simulating the large-burn hexane experiment of [3] using the real combustion model: The GGERM simulation (  ) and the quasi-steady approximation (  ). TOP: Plots of $c_{CO_2,U}$ [vol]. BOTTOM: Plots of $c_{H_2O,U}$ [vol] . . . . .	64
Figure 37.	Results of simulating the large-burn hexane experiment of [3] using the real combustion model: The GGERM simulation (  ) and the quasi-steady approximation (  ). TOP: Plots of $c_{CO,U}$ [vol]. BOTTOM: Plots of $c_{H_2,U}$ [vol] . . . . .	65
Figure 38.	Hypothetical reference-[3]-type hexane experiment. TOP - Assumed hexane pyrolysis rate used in the analysis; BOTTOM - Assumed air flow rate used in the analysis . . . . .	66
Figure 39.	Results of simulating the hypothetical reference-[3]-type hexane experiment using the real combustion model: The GGERM simulation (  ) and the quasi-steady approximation (  ). TOP: Plots of $c_{HEX,U}$ [vol]. BOTTOM: Plots of $c_{O_2,U}$ [vol]. . . . .	67
Figure 40.	Results of simulating the hypothetical reference-[3]-type hexane experiment using the real combustion model: The GGERM simulation (  ) and the quasi-steady approximation (  ). TOP: Plots of $c_{CO_2,U}$ [vol]. BOTTOM: Plots of $c_{H_2O,U}$ [vol] . . . . .	68
Figure 41.	Results of simulating the hypothetical reference-[3]-type hexane experiment using the real combustion model: The GGERM simulation (  ) and the quasi-steady approximation (  ). TOP: Plots of $c_{CO,U}$ [vol]. BOTTOM: Plots of $c_{H_2,U}$ [vol]. . . . .	69



**APPLICATIONS OF THE GENERALIZED GLOBAL EQUIVALENCE RATIO MODEL (GGERM) FOR  
PREDICTING THE GENERATION RATE AND DISTRIBUTION OF PRODUCTS OF COMBUSTION  
IN TWO-LAYER FIRE ENVIRONMENTS - METHANE AND HEXANES**

**Leonard Y. Cooper  
National Institute of Standards and Technology  
Gaithersburg, MD 02899**

**ABSTRACT**

The Generalized Global Equivalence Ratio Model (GGERM) was developed to predict the generation rates of oxygen, fuel, and other products of combustion in rooms containing fires. The GGERM extends to general transient conditions the global equivalence ratio model established during times of steady-state in experimental studies involving two-layer compartment fires. The present work uses the GGERM to predict the time-dependent upper-layer mass fractions of products of combustion (fuel, oxygen, CO, and others) in these two-layer fire experiments. All predicted results are found to be plausible and, where transient data are available, predicted and measured results compare favorably. However, available data are limited and additional validation of the GGERM under more varied fire conditions is required before it can be used with confidence in two-layer zone-type compartment fire models.

**Keywords:** building fires; combustion; compartment fires; computer models; equivalence ratio; fire models; global equivalence ratio; mathematical models; zone models.

# INTRODUCTION - THE EXTENDED UPPER LAYER IN A ROOM CONTAINING A FIRE

## Background

This paper presents results of applying and validating a general model, usable in two-layer zone-type compartment fire analyses, for predicting the generation rate and accumulation of combustion products throughout a multi-room facility. The model is called the Generalized Global Equivalence Ratio Model (GGERM) [1]<sup>1</sup>. In this work, the GGERM is used to simulate the mass fractions of products of combustion that developed during the transient portions of the two-layer fire experiments reported in references [2] and [3]. Model predictions are presented and they are compared to experimental results when available.

Consider a multi-room compartment fire and assume an upper-layer/lower-layer zone-type of description of the environment in each of the rooms. As indicated in Figure 1, for the purpose of describing combustion processes in any room, the GGERM defines the fire and plume, which may originate in the lower layer, as part of the upper-layer zone. Also, the volumes of the fire and plume are assumed to be negligible compared to the total volume of the room. Thus, the GGERM treats all combustion processes in any room with a fire as occurring in the upper layer. The actual combustion process is modeled as if it occurs in a well-stirred reactor with a relatively rapid throughflow and a correspondingly negligible residence time.

## An Overview of the GGERM

Presented here is a brief summary of the essential features of the GGERM, the details of which are presented at length in [1].

Let  $P_{k,U}$ <sup>2</sup> represent the total mass of a combustion product  $k$  in the upper layer of any room containing a fire during an arbitrary multi-room fire scenario. The goal of the GGERM is to estimate the combustion contribution to the instantaneous value of  $dP_{k,U}/dt$ , the rate of change of product  $k$  in the upper layer.

Conservation of species leads to the following general representation for  $dP_{k,U}/dt$

$$dP_{k,U}/dt = \dot{P}_{k,U} \quad (1)$$

where the right-hand-side term,  $\dot{P}_{k,U}$ , represents the net rate of product of combustion  $k$  flowing to the upper layer. This term is the sum of material transfers of product  $k$  to the extended upper layer from all plumes, jets,

---

<sup>1</sup>Numbers in brackets refer to the list of REFERENCES at the end of this report.

<sup>2</sup>A list of NOMENCLATURE is included at the end of this report.



near-boundary flows, combustion zones, and other isolated or distributed sources.

The material flowing into and out of the extended upper layer generally includes various amounts of the combustion products  $k$  associated with a fuel of interest and other inert flow components. The total rates of mass inflow and outflow,  $\dot{m}_{\text{FLOWIN}}$  and  $\dot{m}_{\text{FLOWOUT}}$ , and the corresponding individual rates of inflow and outflow of products  $k$ ,  $\dot{P}_{k,\text{FLOWIN}}$  and  $\dot{P}_{k,\text{FLOWOUT}}$ , respectively, are established from a variety of compartment fire modeling considerations. These rates are assumed to be known.

The combustion contributions to  $\dot{P}_{k,U}$  are modeled by the GGERM. As depicted in Figure 2, the GGERM has two components: the accumulator, which simulates spatially-averaged properties of the generally unsteady upper layer environment; and the quasi-steady reactor, which simulates the actual combustion processes taking place there.

As indicated in Figure 2, all of the flow into the layer is modeled as immediately "entering" the reactor where it may participate in the reaction process. As depicted in the figure, the model also includes a "feedback loop" which brings flow from the bulk upper layer atmosphere into the reactor and the reaction process. A critical feature of the overall model is the means of evaluating the feedback mass flow rate,  $\dot{m}_{\text{FEEDBK}}$ . This is presented in Eqs. (42), (43), (46), (47), and (49) of [1].

The global equivalence ratio,  $\phi$ , is introduced as a normalized ratio of the rates of fuel to oxygen entering the reactor.  $\phi$  is defined and determined by

$$\phi = (\dot{P}_{\text{FUEL,REACTIN}} / \dot{P}_{\text{O}_2,\text{REACTIN}}) / r \quad (2)$$

where  $\dot{P}_{\text{FUEL,REACTIN}}$  and  $\dot{P}_{\text{O}_2,\text{REACTIN}}$  are the mass flow rate of FUEL and O<sub>2</sub>, respectively, flowing into the reactor;  $\dot{P}_{k,\text{REACTIN}}$  is generally defined as the mass flow rate into the reactor of these and any other products  $k$ ; and  $r$  is the known fuel-to-oxygen ratio for idealized stoichiometric combustion of a fuel of interest. Note that the  $\phi$  definition of Eq. (2) is consistent with the  $\phi$  definitions of references in the list at the end of this work.

According to the GGERM,  $\dot{\omega}_k$ , the rate of generation of an arbitrary product  $k$  due to combustion, is given by

$$\dot{\omega}_k / \dot{P}_{\text{FUEL,REACTIN}} = f_k(\phi) \quad (3)$$

where the  $f_k$  functions for the fuel would be determined from steady state experiments of the type carried out in references [2]-[9].

Having obtained values for  $\dot{\omega}_k$ , the right-hand side of Eq. (1) can be evaluated from

$$\dot{P}_{k,U} = \dot{P}_{k,\text{FLOWIN}} - \dot{P}_{k,\text{FLOWOUT}} + \dot{\omega}_k \quad (4)$$



and integration of Eq. (1) can proceed. This leads to solutions for the  $P_{k,U}$ .

#### INITIAL VALUE PROBLEM FOR THE MASS FRACTION OF FUEL, OXYGEN, AND OTHER PRODUCTS OF COMBUSTION

In [1], the GGERM implementation of Eq. (1) is also formulated in terms of  $c_{k,U}$ , the upper-layer mass fractions of products  $k$ , instead of  $P_{k,U}$ . These are defined by

$$c_{k,U} \equiv P_{k,U}/m_U \quad (5)$$

where  $m_U$  is the instantaneous total mass of material in the upper layer.

The governing equations for  $c_{FUEL,U}$ ,  $c_{O_2,U}$ , and the other  $c_{k,U}$  of interest are [1]:

$$m_U dc_{FUEL,U}/dt = c_{FUEL,U} \dot{m}_{FEEDBK} f_{FUEL}(\phi) - c_{FUEL,U} \dot{m}_{FLOWIN} + \dot{P}_{FUEL, FLOWIN} [1 + f_{FUEL}(\phi)] \quad (6)$$

$$m_U dc_{O_2,U}/dt = c_{O_2,U} \dot{m}_{FEEDBK} \phi f_{O_2}(\phi) r - c_{O_2,U} \dot{m}_{FLOWIN} + \dot{P}_{O_2, FLOWIN} [1 + \phi f_{O_2}(\phi) r] \quad (7)$$

$$m_U dc_{k,U}/dt + c_{k,U} \dot{m}_{FLOWIN} = (c_{FUEL,U} \dot{m}_{FEEDBK} + \dot{P}_{FUEL, FLOWIN}) f_k(\phi) \quad (8)$$

$$= (c_{O_2,U} \dot{m}_{FEEDBK} + \dot{P}_{O_2, FLOWIN}) \phi f_k(\phi) r \quad (9)$$

$$= \lambda_k(t) \quad (10)$$

where initial conditions for  $c_{FUEL,U}$ ,  $c_{O_2,U}$ , and the  $c_{k,U}$  must be specified. Following Figure 2 and the above GGERM description, the value of  $\phi$  in Eqs. (6)-(9) is calculated from Eq. (2) to be

$$\phi = [(\dot{P}_{FUEL, FLOWIN} + c_{FUEL,U} \dot{m}_{FEEDBK}) / (\dot{P}_{O_2, FLOWIN} + c_{O_2,U} \dot{m}_{FEEDBK})] / r \quad (11)$$

Also, the value of  $\dot{m}_{FEEDBK}$ , is calculated from

$$\dot{m}_{FEEDBK} = \dot{m}_{FEEDBK}(\text{layer inflow conditions}, c_{FUEL,U}, c_{O_2,U}) \quad (12)$$

which represents the generalized  $\dot{m}_{FEEDBK}$  equation set presented in [1]. Finally, the  $f_k$  functions and  $r$  are assumed to be known and specified properties of a fuel of interest.

In specific fire scenarios, a closure to the above problems for the  $c_{k,U}$ 's requires specification of the time-dependent values of  $m_U$ ,  $\dot{m}_{FLOWIN}$ ,  $\dot{P}_{FUEL,FLOWIN}$ , and  $\dot{P}_{O_2,FLOWIN}$ . Experimental data or analytic models would be expected to provide these latter input specifications.

As can be seen from Eqs. (6) and (7), for a particular fire scenario the initial value problems for  $c_{FUEL,U}$  and  $c_{O_2,U}$  are coupled, but independent of the initial value problems for the other  $c_{k,U}$ . In solving a given problem, first solutions for  $c_{FUEL,U}$  and  $c_{O_2,U}$  would be obtained. Then the  $\lambda_k(t)$  of Eq. (10) would be determined from the representations of the right-hand sides of Eqs. (8) or (9). Finally, the  $c_{k,U}$  for other combustion products of interest would be obtained from solutions of Eqs. (10).

#### FIRE SCENARIOS WHERE ALL OXYGEN INFLOW IS FROM AN AMBIENT ATMOSPHERE

Experiments of [2]-[10] involved test configurations depicted in Figures 3(a) and 3(b). In these tests all components of  $\dot{P}_{O_2,FLOWIN}$  were from a standard atmosphere, i.e., with an oxygen mass fraction of 0.232. Unless noted otherwise, analyses and results throughout the remainder of this work are generally applicable only for fire scenarios where  $\dot{P}_{O_2,FLOWIN}$  is similarly from a standard atmosphere. In such scenarios it can be shown from [1] that Eqs. (6)-(11) can be written as

$$\begin{aligned} (m_U/\dot{m}_{FLOWIN})dc_{FUEL,U}/dt &= c_{FUEL,U} [f_{FUEL}(\phi)(\dot{m}_{FEEDBK}/\dot{m}_{FLOWIN}) - 1] \\ &+ 0.232r\phi^{(SS)} [1 + f_{FUEL}(\phi)]/[1 + 0.232r\phi^{(SS)}] \end{aligned} \quad (13)$$

$$\begin{aligned} (m_U/\dot{m}_{FLOWIN})dc_{O_2,U}/dt &= c_{O_2,U} [r\phi f_{O_2}(\phi)(\dot{m}_{FEEDBK}/\dot{m}_{FLOWIN}) - 1] \\ &+ 0.232[1 + r\phi f_{O_2}(\phi)]/[1 + 0.232r\phi^{(SS)}] \end{aligned} \quad (14)$$

$$\begin{aligned} (m_U/\dot{m}_{FLOWIN})dc_{k,U}/dt + c_{k,U} &= \{c_{FUEL,U}(\dot{m}_{FEEDBK}/\dot{m}_{FLOWIN}) \\ &+ 0.232\phi^{(SS)}r/[1 + 0.232r\phi^{(SS)}]\}f_k(\phi) \end{aligned} \quad (15)$$

$$\begin{aligned} &= \{c_{O_2,U}(\dot{m}_{FEEDBK}/\dot{m}_{FLOWIN}) \\ &+ 0.232/[1 + 0.232r\phi^{(SS)}]\}r\phi f_k(\phi) \end{aligned} \quad (16)$$

$$= \Lambda_k(t) \quad (17)$$

$$\phi = \phi^{(SS)} \{1 + (\dot{m}_{FEEDBK}/\dot{m}_{FLOWIN})c_{FUEL,U}[1 + 1/(0.232r\phi^{(SS)})]\} / \{1 + (\dot{m}_{FEEDBK}/\dot{m}_{FLOWIN})c_{O_2,U}\phi^{(SS)}r[1 + 1/(0.232r\phi^{(SS)})]\} \quad (18)$$

As in [1],  $\phi^{(SS)}$  in Eqs. (13)-(18) is defined as the value of  $\phi$  under virtual steady-state conditions, i.e., the value of  $\phi$  when  $\dot{m}_{FEEDBK} = 0$  and when  $\dot{P}_{FUEL, FLOWIN}$  and  $\dot{P}_{O_2, FLOWIN}$  are maintained at their current values, i.e.,

$$\phi^{(SS)} = (\dot{P}_{FUEL, FLOWIN} / \dot{P}_{O_2, FLOWIN}) / r \quad (19)$$

As is also defined in [1],  $c_{k, REACTOUT}^{(SS)}(\phi^{(SS)})$  is the product-k mass fraction flowing out of a GGERM reactor under steady state conditions when the Global Equivalence Ratio of the inflow to the reactor is  $\phi^{(SS)}$ .

As presented in [1], for any product k there is a one-to-one correspondence between  $c_{k, REACTOUT}^{(SS)}(\phi^{(SS)})$  and  $f_k(\phi^{(SS)})$

$$c_{FUEL, REACTOUT}^{(SS)} = 0.232\phi^{(SS)}r[1 + f_{FUEL}(\phi^{(SS)})] / (1 + 0.232\phi^{(SS)}r) \quad (20)$$

$$c_{O_2, REACTOUT}^{(SS)} = 0.232[1 + r\phi^{(SS)}f_{O_2}(\phi^{(SS)})] / (1 + 0.232r\phi^{(SS)}) \quad (21)$$

$$c_{k, REACTOUT}^{(SS)} = 0.232r\phi^{(SS)}f_k(\phi^{(SS)}) / (1 + 0.232r\phi^{(SS)}) \quad \text{for k other than fuel or oxygen} \quad (22)$$

Solving for the  $f_k$  in the above leads to

$$f_{FUEL} = [1 + 1/(0.232r\phi^{(SS)})]c_{FUEL, REACTOUT}^{(SS)}(\phi^{(SS)}) - 1 \quad (23)$$

$$f_{O_2} = c_{O_2, REACTOUT}^{(SS)}(\phi^{(SS)}) + [c_{O_2, REACTOUT}^{(SS)}(\phi^{(SS)}) - 0.232] / (0.232r\phi^{(SS)}) \quad (24)$$

$$f_k = [1 + 1/(0.232r\phi^{(SS)})]c_{k, REACTOUT}^{(SS)}(\phi^{(SS)}) \quad \text{for k other than fuel or oxygen} \quad (25)$$

When data for the  $c_{k, REACTOUT}^{(SS)}(\phi^{(SS)})$  functions for a particular fuel are presented in reports of Figure-3-type experiments in a standard atmosphere, it is possible to determine analytic representations of these and to then

construct the  $f_k$  functions, required for use in the GGEM, by using Eqs. (23)-(25). Similarly, known  $f_k$  functions can be used to construct the  $c_{k,REACTOUT}^{(SS)}$  by using Eqs. (20)-(22).

Eqs. (13)-(15) are completed with specification of  $\dot{m}_{FEEDBK}/\dot{m}_{FLOWIN}$ . For fire scenarios considered here, this is found from [1] to be

$$\dot{m}_{FEEDBK}/\dot{m}_{FLOWIN} = \max(\dot{m}_{FEEDBK,1}/\dot{m}_{FLOWIN}, \dot{m}_{FEEDBK,3}/\dot{m}_{FLOWIN}) \quad (26)$$

where

$$\dot{m}_{FEEDBK,1}/\dot{m}_{FLOWIN} = \begin{cases} 0 & \text{if } \phi^{(SS)}/\phi_{FUEL} \leq 1 \text{ or } c_{O_2,U} - c_{O_2,REACTOUT}^{(SS)} \leq 0; \\ [(1 - \phi_{FUEL}/\phi^{(SS)})/(\phi_{FUEL}/\phi^{(SS)} + 0.232r\phi_{FUEL})] \cdot \\ [(c_{O_2,U} - c_{O_2,REACTOUT}^{(SS)})/(0.232 - c_{O_2,REACTOUT}^{(SS)})] \\ & \text{if } \phi^{(SS)}/\phi_{FUEL} > 1 \text{ and } c_{O_2,U} - c_{O_2,REACTOUT}^{(SS)} > 0 \end{cases} \quad (27)$$

$$\dot{m}_{FEEDBK,3}/\dot{m}_{FLOWIN} = \begin{cases} 0 & \text{if } \phi_{O_2}/\phi^{(SS)} \leq 1 \text{ or } c_{FUEL,U} - c_{FUEL,REACTOUT}^{(SS)} \leq 0; \\ [(\phi_{O_2}/\phi^{(SS)} - 1)(0.232r\phi^{(SS)})/(1 + 0.232r\phi^{(SS)})] \cdot \\ [(c_{FUEL,U} - c_{FUEL,REACTOUT}^{(SS)})/(1 - c_{FUEL,REACTOUT}^{(SS)})] \\ & \text{if } \phi_{O_2}/\phi^{(SS)} > 1 \text{ and } c_{FUEL,U} - c_{FUEL,REACTOUT}^{(SS)} > 0 \end{cases} \quad (28)$$

and where,  $c_{FUEL,REACTOUT}^{(SS)}$  and  $c_{O_2,REACTOUT}^{(SS)}$  are obtained from Eqs. (20) and (21), respectively.

In the above,  $\phi_{FUEL}$  is defined as in [1] as the maximum value of  $\phi$  which leads to complete combustion of the fuel, i.e., the maximum value of  $\phi$  where  $\dot{\omega}_{FUEL} = -\dot{P}_{FUEL,REACTIN}$ . Using Eq. (3)

$$\phi_{FUEL} = \text{maximum root of } f_{FUEL}(\phi_{FUEL}) + 1 = 0 \quad (29)$$

It is assumed that  $\phi_{FUEL} > 0$  and is bounded.

Similarly,  $\phi_{O_2}$  is defined as in [1] as the minimum value of  $\phi$  which leads to complete consumption of oxygen, i.e., the minimum value of  $\phi$  which leads to  $\dot{P}_{O_2,REACTIN} = 0$ . Using Eq. (3)



$$\phi_{O_2} = \text{minimum root of } \phi_{O_2} f_{O_2}(\phi_{O_2})r + 1 = 0 \quad (30)$$

It is assumed that  $\phi_{O_2} > 0$  and is bounded.

## CONSTRUCTING ANALYTIC REPRESENTATIONS FOR THE PRODUCT GENERATION FUNCTIONS AND THE STEADY STATE MASS FRACTIONS FROM EXPERIMENTAL DATA

### General Considerations

In general, application of the GGEM for a given fuel requires calculations based on analytic representations of its  $f_k$ 's and  $c_{k, \text{REACTOUT}}^{(SS)}$ 's. These would be obtained from steady state experiments of the kind described in references [2], and [4]-[9].

If, as in [2], [4], [5], and [9], reduced data points are provided for the  $c_{k, \text{REACTOUT}}^{(SS)}$ 's, then these data points must be used to construct analytic, curve-fitted representations of these functions. These latter representations would be used, in turn, to calculate a consistent set of the  $f_k$ 's. The calculation would use Eqs. (23)-(25).

If, as in [7] and [8], reduced data points are provided for the  $f_k$ , then these data points can be used to construct analytic curve-fitted representations of these functions. These latter representations would be used, in turn, to calculate a consistent set of the  $c_{k, \text{REACTOUT}}^{(SS)}$ 's. In this case, the calculation would use Eqs. (20)-(22).

The curve-fitting task must be carried out so that the resulting  $f_k(\phi)$  and  $c_{k, \text{REACTOUT}}^{(SS)}(\phi^{(SS)})$  functions are physically and analytically well-behaved for arbitrary non-negative values of  $\phi$  and  $\phi^{(SS)}$ . The following mutually-consistent physical and analytic constraints are required:

1. The  $f_k(\phi)$ 's and  $c_{k, \text{REACTOUT}}^{(SS)}(\phi^{(SS)})$ 's are continuous functions for arbitrary non-negative values of  $\phi$  and  $\phi^{(SS)}$ .
2. According to the Eq.-(29) definition of  $\phi_{\text{FUEL}}$ , for  $0 \leq \phi \leq \phi_{\text{FUEL}}$  and for  $\phi \rightarrow 0$  in particular, all fuel entering the reactor is completely consumed, i.e.,

$$\dot{\omega}_{\text{FUEL}} = - \dot{P}_{\text{FUEL}, \text{REACTIN}} \quad \text{for } 0 \leq \phi \leq \phi_{\text{FUEL}} \quad (31)$$

Consistent with whatever reactor chemistry is applicable as  $\phi \rightarrow 0$ , the generation/consumption rate of oxygen and all products  $k$  will be directly proportional to the generation/consumption rate of fuel. The constants of proportionality are designated in terms of the characteristic product- $k$  constants,  $\Gamma_{k, 0}$ ,



$$\lim_{\phi \rightarrow 0} \dot{\omega}_k = - \Gamma_{k,0} \dot{\omega}_{\text{FUEL}} \quad (32)$$

$$\Gamma_{\text{FUEL},0} \equiv 1 \quad (33)$$

where

$$\Gamma_{\text{O}_2,0} = - 1/r \text{ for complete stoichiometric combustion at } \phi = 0 \quad (34)$$

Using Eq. (3) and (32), with  $k \rightarrow \text{O}_2$  (i.e.,  $k$  representing  $\text{O}_2$ ), and Eq. (31), and then using Eq. (21) leads to

$$\lim_{\phi \rightarrow 0} f_{\text{O}_2}(\phi) = \Gamma_{\text{O}_2,0} \quad (35)$$

$$\lim_{\phi^{(\text{SS})} \rightarrow 0} c_{\text{OXY},\text{REACTOUT}}^{(\text{SS})}(\phi^{(\text{SS})}) = 0.232[1 + r\phi^{(\text{SS})}\Gamma_{\text{O}_2,0}(1 - 0.232/\Gamma_{\text{O}_2,0}) + O(\phi^{(\text{SS})^2})] \quad (36)$$

Using Eq. (3) with  $k \rightarrow \text{FUEL}$  and Eq. (31), and then using Eq. (20) leads to

$$f_{\text{FUEL}}(\phi) = - 1 \text{ for } 0 \leq \phi \leq \phi_{\text{FUEL}} \quad (37)$$

$$c_{\text{FUEL},\text{REACTOUT}}^{(\text{SS})}(\phi^{(\text{SS})}) = 0 \text{ for } 0 \leq \phi^{(\text{SS})} \leq \phi_{\text{FUEL}} \quad (38)$$

Using Eqs. (3) and (32) with  $k$  other than FUEL or  $\text{O}_2$ , and Eq. (31), and then using Eq. (22) leads to

For  $k$  other than FUEL or  $\text{O}_2$ :

$$\lim_{\phi \rightarrow 0} f_k(\phi) = \Gamma_{k,0} \quad (39)$$

$$\lim_{\phi^{(\text{SS})} \rightarrow 0} c_{k,\text{REACTOUT}}^{(\text{SS})}(\phi^{(\text{SS})}) = 0.232r\phi^{(\text{SS})}\Gamma_{k,0} \quad (40)$$

3. According to the Eq. (30) definition of  $\phi_{O_2}$ , for  $\phi \geq \phi_{O_2} > 0$ , and for  $\phi \rightarrow \infty$  in particular, all oxygen entering the reactor is completely consumed, i.e.,

$$\dot{\omega}_{O_2} = - \dot{P}_{O_2, REACTIN} \text{ when } \phi \geq \phi_{O_2} > 0 \quad (41)$$

Consistent with whatever reactor chemistry is applicable as  $\phi \rightarrow \infty$ , the generation/consumption rate of oxygen and all products k will be directly proportional to the generation/consumption rate of fuel. The constants of proportionality are designated in terms of the characteristic product-k constants,  $\Gamma_{k, \infty}$ .

$$\lim_{\phi \rightarrow \infty} \dot{\omega}_k = - \Gamma_{k, \infty} \dot{\omega}_{FUEL} \quad (42)$$

$$\Gamma_{FUEL, \infty} \equiv 1 \quad (43)$$

where

$$\Gamma_{O_2, \infty} = - 1/r \text{ for complete stoichiometric combustion at } \phi \rightarrow \infty \quad (44)$$

Using Eq. (3), with  $k \rightarrow O_2$ , and Eqs. (2) and (41), and then using Eq. (21) leads to

$$f_{O_2}(\phi) = - 1/(r\phi) \text{ when } \phi \geq \phi_{O_2} > 0 \quad (45)$$

$$c_{OXY, REACTOUT}^{(SS)}(\phi^{(SS)}) = 0 \text{ when } \phi^{(SS)} \geq \phi_{O_2} > 0 \quad (46)$$

Using Eqs. (3) and (42), with  $k \rightarrow FUEL$ , and Eqs. (2) and (41), and then using Eq. (20) leads to

$$\lim_{\phi \rightarrow \infty} f_{FUEL}(\phi) = 1/(r\phi\Gamma_{O_2, \infty}) \text{ when } \phi \geq \phi_{FUEL} > 0 \quad (47)$$

$$\lim_{\phi^{(SS)} \rightarrow \infty} c_{FUEL, REACTOUT}^{(SS)}(\phi^{(SS)}) = 1 + (1 - \Gamma_{O_2, \infty}/0.232)[1/(r\phi^{(SS)}\Gamma_{O_2, \infty})] + O(1/\phi^{(SS)2}) \quad (48)$$

Using Eqs. (3) and (42) with k other than FUEL or  $O_2$ , Eq. (2) and Eq. (41), and then using Eq. (22) leads to

For k other than FUEL or O<sub>2</sub> :

$$\lim_{\phi \rightarrow \infty} f_k(\phi) = - \Gamma_{k, \infty} / (r\phi\Gamma_{O_2, \infty}) \quad (49)$$

$$\lim_{\phi^{(SS)} \rightarrow \infty} c_{FUEL, REACTOUT}^{(SS)}(\phi^{(SS)}) = - \Gamma_{k, \infty} / (r\phi^{(SS)}\Gamma_{O_2, \infty}) \quad (50)$$

As discussed in [1], when reaction processes only involve complete stoichiometric combustion,  $\phi_{FUEL}$ ,  $\phi_{O_2}$ , and the  $f_k$  are given by

$$\phi_{FUEL}^{(STOICH)} = \phi_{O_2}^{(STOICH)} = 1 \quad (51)$$

$$f_k^{(STOICH)}(\phi) = \begin{cases} \Gamma_k & \text{if } 0 \leq \phi \leq 1 \\ \Gamma_k/\phi & \text{if } \phi > 1 \end{cases} \quad (52)$$

where

$$\Gamma_{FUEL} = -1, \Gamma_{O_2} = -1/r \quad (53)$$

and where the other  $\Gamma_k$  can be determined from the stoichiometric reaction of the particular fuel of interest. These results are consistent with the results of items 1-3 above.

### The Product Generation Functions and the Steady State Mass Fractions for the Combustion of Methane Using Data of [2]

Reference [2] provides reduced  $c_{k, REACTOUT}^{(SS)}$  data for steady state combustion of natural gas in the test configuration of Figure 3b. These data were acquired over a wide range of layer temperatures, but these never exceeded 800K.  $\phi^{(SS)}$  values were in the range  $0 < \phi^{(SS)} < 3$ . In these tests, in addition to the rate of oxygen supply to the extended upper layer through entrainment into the burner's fire plume, the gas in the upper layer collector was injected with a specified flow of air and its associated oxygen. Some of the reference-[2] test results and results of other natural gas tests using earlier versions of the same test configuration were presented in [4], [5], and [9].

It will be assumed here that the natural gas fuel used in the experiments of [2] can be modeled as pure methane, CH<sub>4</sub>.

$c_{k, REACTOUT}^{(SS)}$  data for  $k \rightarrow CH_4, O_2, CO_2, H_2O, CO,$  and  $H_2$  are presented in [2] and are reproduced here in Figures 4-10. Analytic approximations for the  $f_k$  and  $c_{k, REACTOUT}^{(SS)}$  functions which characterize the combustion of CH<sub>4</sub> will be constructed by using these data, the analytic constraints of the above items 1-3, and Eqs. (23)-(25). With these functions, the GGERM will be used to simulate the transient upper-layer environment in the methane combustion experiments of [2].

It is important to point out that the data of the reference-[5] experiments of Toner, included in Figures 4-9, were acquired at higher layer temperatures, greater than 900K, than were all the other data in the figures. Regarding the generation of  $\text{CH}_4$ , and especially  $\text{O}_2$ ,  $\text{CO}_2$ , and  $\text{H}_2\text{O}$ , Figures 4-7 show that at these temperatures the reactions closely simulate complete stoichiometric combustion. The Toner data suggest that GGERM simulations at higher temperatures would be improved if the  $f_k$ 's of Eq. (3) were generally assumed to be dependent on layer temperature as well as  $\phi$ . For now this temperature dependence is ignored and **IN ALL CASES THE DATA POINTS OF THE REFERENCE-[5] EXPERIMENTS OF TONER, INCLUDED IN FIGURES 5-10, WILL BE DISREGARDED IN THE ANALYSIS TO FOLLOW.** Further discussion of this will be presented toward the end of this work.

#### Methane ( $\text{CH}_4$ ):

The reduced data for  $c_{\text{CH}_4, \text{REACTOUT}}^{(\text{SS})}$  is presented in Figure 4 (a re-labelled version of Figure 4.5 of [2]). Included in the figure is a plot of  $c_{\text{CH}_4, \text{REACTOUT}}^{(\text{SS})}$  for complete stoichiometric combustion. The latter plot is obtained from Eq. (20) using Eqs. (51)-(53) and  $r = 1/4$ .

From visual observation of the data, the value of  $\phi_{\text{FUEL}} = \phi_{\text{CH}_4}$  is approximated as

$$\phi_{\text{FUEL}} = \phi_{\text{CH}_4} = 0.70 \quad (54)$$

It is now observed from Figure 4 and from the results of the items 1-3 that for  $\text{CH}_4$ , and possibly for other fuels, certain basic functional characteristics of the  $c_{\text{FUEL}, \text{REACTOUT}}^{(\text{SS})}$  are approximately similar for real combustion and for complete stoichiometric combustion, viz.,  $c_{\text{FUEL}, \text{REACTOUT}}^{(\text{SS})}$  is: identically zero for  $0 \leq \phi/\phi_{\text{FUEL}} \leq 1$ ; monotonically increasing with  $\phi/\phi_{\text{FUEL}}$  for  $\phi/\phi_{\text{FUEL}} > 1$ ; increasing with a positive slope (designated here as  $\sigma$ ) from zero at  $\phi/\phi_{\text{FUEL}} = 1$ ; and asymptotic to 1 as  $\phi/\phi_{\text{FUEL}} \rightarrow \infty$ .

All of the above characteristics are shared by the following two-parameter representation which satisfies the required asymptotic behavior of Eq. (48)

$$c_{\text{FUEL}, \text{REACTOUT}}^{(\text{SS})} = [1 - (\phi_{\text{FUEL}}/\phi)] / \{1 + [1/(\sigma\phi_{\text{FUEL}}) - 1](\phi_{\text{FUEL}}/\phi)\} \quad \text{if } \phi/\phi_{\text{FUEL}} > 1 \quad (55)$$

where

$$\sigma = \lim_{\phi/\phi_{\text{FUEL}} \downarrow 1} dc_{\text{FUEL}, \text{REACTOUT}}^{(\text{SS})} / d\phi \quad (56)$$

Eq. (55) is exact in the case of complete stoichiometric combustion where, according to Eqs. (20) and (47)-(49),  $\phi_{\text{FUEL}} = 1$  and  $\sigma = 1/[1 + 1/(0.232r)]$ . Indeed, it is precisely the  $c_{\text{FUEL}, \text{REACTOUT}}^{(\text{SS})}$  of Eq. (55), with the latter values of  $\phi_{\text{FUEL}}$  and  $\sigma$ , that is plotted in Figure 4.

The Eq. (55) representation is used here to fit the  $c_{\text{CH}_4, \text{REACTOUT}}^{(\text{SS})}$  data.

From the Figure 4 data,  $\sigma$  is approximated as

$$\sigma = 0.037 \quad (57)$$

The desired curve-fit is therefore taken to be

$$c_{\text{CH}_4, \text{REACTOUT}}^{(\text{SS})} = \begin{cases} 0 & \text{if } \phi \leq 0.70 = \phi_{\text{FUEL}} = \phi_{\text{CH}_4} \\ [1 - (0.70/\phi)] / \{1 + [1/(0.037 \cdot 0.70) - 1](0.70/\phi)\} & \\ & \text{if } \phi > 0.70 = \phi_{\text{FUEL}} = \phi_{\text{CH}_4} \end{cases} \quad (58)$$

This is plotted in Figure 4.

$\text{O}_2$ :

The reduced data for  $c_{\text{O}_2, \text{REACTOUT}}^{(\text{SS})}$  is presented in Figure 5 (a re-labelled version of Figure 4.3 of [2]). Included is a plot of  $c_{\text{O}_2, \text{REACTOUT}}^{(\text{SS})}$  for complete stoichiometric combustion. This is obtained from Eq. (21) using Eqs. (51)-(53) and  $r = 1/4$

$$c_{\text{O}_2, \text{REACTOUT}, \text{STOICH}}^{(\text{SS})} = \begin{cases} 0.232(1 - \phi) / (1 + 0.232\phi/4) & \text{if } 0 \leq \phi \leq 1 \\ 0 & \text{if } 1 < \phi \end{cases} \quad (59)$$

As can be seen in the figure, when  $0 \leq \phi \leq 0.60$  an approximation of complete stoichiometric combustion provides a good estimate for the real combustion data. This approximation will be used for the desired curve-fit in this range of  $\phi$ .

From extrapolation of data in Figure 5,  $\phi_{\text{O}_2}$  is approximated as

$$\phi_{\text{O}_2} = 3.50 \quad (60)$$

In the range  $0.60 < \phi < 3.50$  the function  $\lambda(3.50 - \phi)/\phi^{1/2}$ , with  $\lambda$  chosen to force continuity with Eq. (59) at  $\phi = 0.6$ , is found to fit well the Figure 5 data.

Consistent with the above, the desired  $c_{\text{O}_2, \text{REACTOUT}}^{(\text{SS})}$  curve-fit is taken to be



$$c_{O_2, REACTOUT}^{(SS)} = \begin{cases} c_{O_2, REACTOUT, STOICH}^{(SS)} & \text{if } 0 \leq \phi \leq 0.60 \\ \{(0.232)(0.40)/[1 + (0.232)(0.60)/4]\} \cdot \\ \quad [(3.50 - \phi)/2.90]/(\phi/0.60)^{1/2} & \text{if } 0.60 \leq \phi \leq 3.5 \\ c_{O_2, REACTOUT, STOICH}^{(SS)} = 0 & \text{if } 3.50 < \phi \end{cases} \quad (61)$$

This is plotted in Figure 5.

CO<sub>2</sub> and H<sub>2</sub>O:

The reduced data for  $c_{CO_2, REACTOUT}^{(SS)}$  and  $c_{H_2O, REACTOUT}^{(SS)}$  are presented in Figures 6 and 7 (re-labelled versions of Figures 4.7 and 4.8 of [2]), respectively. Included are plots of these  $c_{k, REACTOUT}^{(SS)}$  for complete stoichiometric combustion. These are designated as  $c_{k, REACTOUT, STOICH}^{(SS)}$  and they are computed from

$$c_{CO_2, REACTOUT, STOICH}^{(SS)} = \begin{cases} (0.232/4)(11/4)\phi/(1 + 0.232\phi/4) & \text{if } 0 \leq \phi \leq 1 \\ (0.232/4)(11/4)/(1 + 0.232\phi/4) & \text{if } 1 < \phi \end{cases} \quad (62)$$

$$c_{H_2O, REACTOUT, STOICH}^{(SS)} = (9/11)c_{CO_2, REACTOUT, STOICH}^{(SS)} \quad (63)$$

Eqs. (62) and (63) were obtained from Eq. (22) using Eqs. (52),  $r = 1/4$ , and  $\Gamma_{CO_2} = 11/4$  and  $\Gamma_{H_2O} = 9/4$  [1].

As can be seen in Figure 6, when  $0 \leq \phi \leq 0.60$ , a complete stoichiometric combustion approximation provides a good estimate for the real combustion data of  $c_{CO_2, REACTOUT}^{(SS)}$ . For simplicity, this approximation will be used here for the somewhat extended range  $0 \leq \phi \leq 0.70$ . Then, for the range  $0.70 \leq \phi \leq 3.00$ ,  $c_{CO_2, REACTOUT}^{(SS)}$  will be approximated as being constant. Finally, consistent with the required asymptotic behavior of Eq. (49),  $c_{CO_2, REACTOUT}^{(SS)}$  will be approximated as being proportional to  $1/\phi$  for  $\phi > 3.00$ .

Consistent with the above, and with the required continuity of the approximating function, the desired  $c_{O_2, REACTOUT}^{(SS)}$  curve-fit is taken to be

$$c_{\text{CO}_2, \text{REACTOUT}}^{(\text{SS})} = \begin{cases} c_{\text{CO}_2, \text{REACTOUT}, \text{STOICH}}^{(\text{SS})} & \text{if } 0 \leq \phi \leq 0.70 \\ \lambda_{\text{CO}_2, 1} & \text{if } 0.70 < \phi \leq 3.00 \\ (3.00/\phi)\lambda_{\text{CO}_2, 1} & \text{if } \phi > 3.00 \end{cases} \quad (64)$$

where

$$\lambda_{\text{CO}_2, 1} = (0.232/4)(11/4)(0.70)/[1 + (0.232)(0.70)/4] = 0.107\dots \quad (65)$$

This is plotted in Figure 6.

As can be seen in Figure 7, when  $0 \leq \phi \leq 0.70$  and  $2.25 < \phi$  it is reasonable to use the complete stoichiometric combustion approximation to estimate the real combustion data of  $c_{\text{H}_2\text{O}, \text{REACTOUT}}^{(\text{SS})}$ . In the range  $0.70 < \phi \leq 2.25$  the fitted function is completed by the straight-line segment, plotted in the figure, that joins the curves applicable in the two outer- $\phi$  ranges.

Consistent with the above, the desired  $c_{\text{H}_2\text{O}, \text{REACTOUT}}^{(\text{SS})}$  curve-fit is taken to be

$$c_{\text{H}_2\text{O}, \text{REACTOUT}}^{(\text{SS})} = \begin{cases} c_{\text{H}_2\text{O}, \text{REACTOUT}, \text{STOICH}}^{(\text{SS})} & \text{if } 0 \leq \phi \leq 0.70 \\ \lambda_{\text{H}_2\text{O}, 1}\phi - \lambda_{\text{H}_2\text{O}, 2} & \text{if } 0.70 < \phi \leq 2.25 \\ c_{\text{H}_2\text{O}, \text{REACTOUT}, \text{STOICH}}^{(\text{SS})} & \text{if } 2.25 < \phi \end{cases} \quad (66)$$

where

$$\begin{aligned} \lambda_{\text{H}_2\text{O}, 1} &= (c_{\text{H}_2\text{O}, 2}^{(\text{SS})} - c_{\text{H}_2\text{O}, 1}^{(\text{SS})})/(2.25 - 0.70) \\ \lambda_{\text{H}_2\text{O}, 2} &= (0.70c_{\text{H}_2\text{O}, 2}^{(\text{SS})} - 2.25c_{\text{H}_2\text{O}, 1}^{(\text{SS})})/(2.25 - 0.70) \\ c_{\text{H}_2\text{O}, 1}^{(\text{SS})} &= (0.232/4)(9/4)(0.70)/[1 + 0.232(0.70)/4] \\ c_{\text{H}_2\text{O}, 2}^{(\text{SS})} &= (0.232/4)(9/4)/[1 + 0.232(2.25)/4] \end{aligned} \quad (67)$$

CO, and H<sub>2</sub>:

The reduced data for  $c_{\text{CO}, \text{REACTOUT}}^{(\text{SS})}$  and  $c_{\text{H}_2, \text{REACTOUT}}^{(\text{SS})}$  are presented in Figures 8 and 9 (re-labelled versions of Figures 4.7 and 4.2 of [2]), respectively.

As seen in Figure 8, the data show that  $c_{\text{CO}, \text{REACTOUT}}^{(\text{SS})}$  is effectively zero for  $\phi$  less than approximately 0.55. For  $\phi > 0.55$  and as shown in the figure, the data curve-fit will be accomplished with straight-line segments in the ranges  $0.55 < \phi \leq 1.15$  and  $1.15 < \phi \leq 3.00$ . Also, consistent with the required asymptotic behavior of Eq. (49),  $c_{\text{CO}, \text{REACTOUT}}^{(\text{SS})}$  will be approximated as being proportional to  $1/\phi$  for  $\phi > 3.00$ .

Consistent with the above, the  $c_{\text{CO,REACTOUT}}^{(\text{SS})}$  curve-fit is taken to be

$$c_{\text{CO,REACTOUT}}^{(\text{SS})} = \begin{cases} 0 & \text{if } 0 \leq \phi < 0.55 \\ \lambda_{\text{CO},1}\phi - \lambda_{\text{CO},2} & \text{if } 0.55 < \phi \leq 1.15 \\ \lambda_{\text{CO},3}\phi - \lambda_{\text{CO},4} & \text{if } 1.15 < \phi \leq 3.00 \\ 0.0205(3.00)/\phi & \text{if } 3.00 < \phi \end{cases} \quad (68)$$

where

$$\begin{aligned} \lambda_{\text{CO},1} &= 0.0127/(1.15 - 0.55) \\ \lambda_{\text{CO},2} &= 0.55(0.0127)/(1.15 - 0.55) \\ \lambda_{\text{CO},3} &= (0.0205 - 0.0127)/(3.00 - 1.15) \\ \lambda_{\text{CO},4} &= [1.15(0.0205) - 3.00(0.0127)]/(3.00 - 1.15) \end{aligned} \quad (69)$$

The curve-fit of the  $c_{\text{H}_2\text{,REACTOUT}}^{(\text{SS})}$  data of Figure 9 is done with three curve segments, in a manner analogous to that of  $c_{\text{CO,REACTOUT}}^{(\text{SS})}$ . The resulting function, plotted in the figure, is taken to be

$$c_{\text{H}_2\text{,REACTOUT}}^{(\text{SS})} = \begin{cases} 0 & \text{if } 0 \leq \phi < 0.90 \\ [0.00145/(2.00 - 0.90)]\phi - 0.90(0.00145)/(2.00 - 0.90) & \text{if } 0.90 < \phi \leq 2.00 \\ 0.00145 & \text{if } 2.00 < \phi \leq 3.00 \\ 0.00145(3.00)/\phi & \text{if } 3.00 < \phi \end{cases} \quad (70)$$

### The Product Generation Functions and the Steady State Mass Fractions for the Combustion of Hexane Using Data of [6]

Reference [6] provides reduced  $f_k(\phi)$  data for steady state combustion of hexane,  $\text{C}_6\text{H}_{14}$ , in the test configuration of Figure 3a.

The plotted  $f_k$  data for  $k \rightarrow \text{C}_6\text{H}_{14}$ ,  $\text{O}_2$ ,  $\text{H}_2\text{O}$ ,  $\text{CO}_2$ ,  $\text{CO}$ , and  $\text{H}_2$  presented in [6] and are reproduced here in Figures 10-15. Analytic approximations for the  $f_k(\phi)$  and  $c_k^{(\text{SS})}(\phi^{(\text{SS})})$  functions which characterize the combustion of the fuel will be obtained by first applying the analytic constraints of the above items 1-3 to these data and then using Eqs. (20)-(22). With these

functions, the GGERM will then be used to simulate the transient upper-layer environment in the hexane combustion experiments of [3].

$\Gamma_k$  for  $k \rightarrow C_6H_{14}$ ,  $O_2$ ,  $H_2O$ , and  $CO_2$ :

The reduced data for  $f_k$ ,  $k \rightarrow FUEL$  (i.e.,  $C_6H_{14}$ ),  $O_2$ ,  $H_2O$ , and  $CO_2$ , are presented in Figures 10-13 (re-labelled versions of Figures 4-35, 4-34, 4-36, and 4-32 of [6]), respectively. These are all the components that would be involved in the complete stoichiometric reaction of the fuel. Included in each of the figures is a plot of the corresponding  $f_k$  function for the complete stoichiometric combustion reaction. The latter plots were obtained using Eqs. (51)-(53). Note that

For  $C_6H_{14}$ :

$$\begin{aligned} r = 43/152, \Gamma_{C_6H_{14}} = -1, \Gamma_{O_2} = -152/43, \\ \Gamma_{H_2O} = 63/43, \Gamma_{CO_2} = 132/43 \end{aligned} \quad (71)$$

It is now observed from Figures 10-13 that for  $C_6H_{14}$ , and possibly for other fuels, there are positive values of  $\phi$ , denoted by  $\phi_{k,STOICH1} > 0$ , such that in the range  $0 \leq \phi \leq \phi_{k,STOICH1}$ , data for the present  $f_k$  can be well-fitted by  $f_k^{(STOICH)}$  of Eq. (52). Such representations would satisfy the required criteria of Eqs. (35), (37), and (39). (Note that  $\phi_{FUEL,STOICH1} \equiv \phi_{FUEL}$ .) It is also possible to choose positive values of  $\phi$ , denoted by  $\phi_{k,STOICH2}$ , possibly out of the range of the  $f_k$  data or out of the range of  $\phi$ 's expected in real two-layer fire scenarios, such that in the range  $\phi \geq \phi_{k,STOICH2}$  the  $f_k^{(STOICH)}$  of Eq. (52) again provides representations for the  $f_k$  which are good fits to the data, if they exist in the range, or are at least consistent with the required criteria of Eqs. (45), (47), and (49). (Note that  $\phi_{OXY,STOICH1} \equiv \phi_{O_2}$ .)

$C_6H_{14}$ ,  $O_2$ ,  $H_2O$ , and  $CO_2$ :

Using the above ideas, choices for the  $\phi_{k,STOICH1}$  and  $\phi_{k,STOICH2}$  are made and the following analytic representations are used to construct (the four)  $f_k$  functions which are well-fitted to the data and continuous for all  $\phi$ , and which satisfy the required criteria of Eqs. (35), (37), (39), (45), (47), and (49):

$$f_k(\phi) = \begin{cases} \Gamma_k & \text{if } \phi \leq \phi_{k,STOICH1}; \\ (\Gamma_k/\phi)[1 - (1 - \phi_k)(\phi_{k,STOICH2} - \phi)/(\phi_{k,STOICH2} - \phi_{k,STOICH1})] & \text{if } \phi_{k,STOICH1} < \phi < \phi_{k,STOICH2}; \\ \Gamma_k/\phi & \text{if } \phi \geq \phi_{k,STOICH2} \end{cases} \quad (72)$$



The following values of  $\phi_{k, \text{STOICH1}}$  and  $\phi_{k, \text{STOICH2}}$  are chosen for the four curve fits:

$$\begin{aligned}
 \phi_{\text{C}_6\text{H}_{14}, \text{STOICH1}} &= \phi_{\text{FUEL}} = 0.85 \\
 \phi_{\text{O}_2, \text{STOICH1}} &= 0.80 \\
 \phi_{\text{H}_2\text{O}, \text{STOICH1}} &= 0.85 \\
 \phi_{\text{CO}_2, \text{STOICH1}} &= 0.70 \\
 \phi_{k, \text{STOICH2}} &= \phi_{\text{O}_2} = 10.0 \text{ for } k \rightarrow \text{C}_6\text{H}_{14}, \text{O}_2, \text{H}_2\text{O}, \text{ and } \text{CO}_2
 \end{aligned} \tag{73}$$

Note that Eq. (72) is exact for complete stoichiometric combustion in which case all  $\phi_{k, \text{STOICH1}} = \phi_{k, \text{STOICH2}} = 1$ , and the middle range of  $\phi$  shrinks to a point.

The  $f_k$  representations of Eqs. (72) and (73) are plotted in Figures 10-13.

CO, and H<sub>2</sub>:

The reduced data for  $f_{\text{CO}}$  and  $f_{\text{H}_2}$  are presented in Figures 14 and 15 (re-labelled Figures 4-33 and 4-37 of [6]), respectively.

As seen in Figure 14, the data show that  $f_{\text{CO}}$  is effectively zero for  $\phi$  less than approximately 0.55. For  $\phi > 0.55$  and as shown in the figure, the data curve-fit will be accomplished with straight-line segments in the ranges  $0.55 < \phi \leq 1.00$  and  $1.00 < \phi \leq 3.50$ . Also, consistent with the required asymptotic behavior of Eq. (49),  $f_{\text{CO}}$  will be approximated as being proportional to  $1/\phi$  for  $\phi > 3.50$ .

Consistent with the above, the  $f_{\text{CO}}$  curve-fit is taken to be

$$(43/84)f_{\text{CO}} = \begin{cases} 0 & \text{if } 0 \leq \phi < 0.55 \\ 0.200\phi - 0.110 & \text{if } 0.55 < \phi \leq 1.00 \\ 0.090 & \text{if } 1.00 < \phi \leq 3.50 \\ 0.090(3.50)/\phi & \text{if } 3.50 < \phi \end{cases} \tag{74}$$

The curve-fit of the  $f_{\text{H}_2}$  data of Figure 15 is done with three curve segments, in a manner analogous to that of  $f_{\text{CO}}$ . The resulting function, plotted in the figure, is taken to be



$$(43/7)f_{H_2} = \begin{cases} 0 & \text{if } 0 \leq \phi < 0.70 \\ 0.050(\phi/0.70 - 1) & \text{if } 0.70 < \phi \leq 1.40 \\ 0.050 & \text{if } 1.40 < \phi \leq 3.50 \\ 0.050(3.50)/\phi & \text{if } 3.50 < \phi \end{cases} \quad (75)$$

### Plots of the Product Generation Functions and the Steady State Mass Fractions for the Combustion of Methane and Hexanes

The  $f_k$  functions for  $CH_4$  were computed from Eqs. (23)-(25) using the  $c_{k,REACTOUT}^{(SS)}$  representations of Eqs. (54)-(70). The  $f_k, c_{k,REACTOUT}^{(SS)}$  pair for each of the six products are presented in Figures 16-21.

The  $c_{k,REACTOUT}^{(SS)}$  functions for  $C_6H_{14}$  were computed from Eqs. (20)-(22) using the  $f_k$  representations of Eqs. (71)-(75). The  $f_k, c_{k,REACTOUT}^{(SS)}$  pair for each of the six products are presented in Figures 22-27.

All the above  $f_k, c_{k,REACTOUT}^{(SS)}$  representations will be useful in GGERM-implemented two-layer zone-type compartment fire model simulations of fire scenarios involving the combustion of  $CH_4$  or  $C_6H_{14}$ . Results of such simulations will be presented in the next section.

### SIMULATING EXPERIMENTS OF REFERENCES [2] AND [3]

#### The Combustion of Methane in Figure-3b Test Configurations

Consider the 64  $CH_4$  tests reported in Appendix B of [2]. The test configuration for these is depicted in Figure 3b. Except for initial test time intervals (on the order of 1 to 2 minutes), which were relatively short compared to the times to reach steady state conditions (on the order of 20 to 30 minutes), the layer interface elevation in all of these tests was constant, slightly below the bottom of the upper layer collector. In the simulations to follow it is assumed that the elevation of the layer interface, i.e., the volume of the upper layer, is constant throughout a test run. From [2] the volume is estimated to be the volume of the collector,  $3.89 \text{ m}^3$ .

Each test was carried out with a fixed-elevation gas burner surface and with constant upper-layer supply rates of fuel and injected upper-layer air. Because of the constant-interface-elevation assumption, which implies a constant rate of air entrainment from the lower layer (i.e., the laboratory environment) to the fire plume, each test is simulated with constant values of  $\dot{m}_{FLOWIN}, \dot{P}_{FUEL, FLOWIN}$ , and  $\dot{P}_{O_2, FLOWIN}$  where

$$\dot{m}_{FLOWIN} = \dot{P}_{FUEL, FLOWIN} + \dot{P}_{AIR, FLOWIN} = \dot{P}_{FUEL, FLOWIN} + \dot{P}_{O_2, FLOWIN}/0.232 \quad (76)$$

In Eq. (76),  $\dot{P}_{AIR, FLOWIN}$  is defined as the mass rate of flow of air into the upper layer.

With the above assumptions, solutions to the GGERM Eqs. (13)-(30) have been carried out to simulate experiments of reference [2]. For each experiment simulated, calculations were carried out with the two different models of  $CH_4$  combustion, viz., real combustion and complete stoichiometric combustion. In the simulations it was assumed that the initial mass fractions of products of combustion in the upper layer were the same as those of an ambient atmosphere, which were approximated by  $c_{O_2, U}(t = 0) = 0.232$ , and all other  $c_{k, U}(t = 0) = 0$ .

Results from Appendix B of [2] are presented here for the simulation of test run 1. For this test the initial and characteristic final temperature of the layer were reported to be  $T_{U, INIT} = 296$  K and  $T_{U, FINAL} = 529.7$  K, respectively. In the simulation, the upper layer temperature was assumed to be at the constant reasonable value  $T_U = T_{U, INIT} + (2/3)(T_{U, FINAL} - T_{U, INIT}) = 451.8$  K. The mass of the upper layer was computed according to a perfect gas law model of the upper layer with the gas constant taken to be that of a standard atmosphere. The other conditions of the test were taken from [2] to be:

$$\begin{aligned} \dot{P}_{FUEL, FLOWIN} &= 0.00135 \text{ kg/s} \\ \dot{P}_{AIR, FLOWIN} &= 0.01030 \text{ kg/s} \end{aligned} \tag{77}$$

In this test run, all inflowing air was from plume entrainment. Using Eq. (77) in Eq. (19), the constant simulated value of  $\phi^{(SS)}$  for this experiment is found to be 2.33. The  $\phi^{(SS)}$  reported in [2] was 2.17. The difference in these two values is attributed to the fact that in the simulation the fuel was modeled as pure methane with  $r = 1/4$ , whereas the value in [2] is based on  $r = 1/3.82$ . The latter value was the result of an actual analysis of the natural gas used in the experiment.

The simulation was carried out twice, first using the real  $CH_4$  combustion model and then using the complete stoichiometric combustion model. Results of the simulations are presented in Figures 28-30 where the predicted mass fractions  $c_{k, U}(t)$  are plotted for  $k \rightarrow CH_4, O_2, CO_2, H_2O, CO,$  and  $H_2$ .

As can be seen from the  $c_{k, U}$  plots, the GGERM predicts that steady state conditions are approached between 900 s and 1800 s into the experiment. This is consistent with the experimental procedure which involved steady-state gas sampling after approximately 1800 s [2].

The results for  $c_{CH_4, U}, c_{O_2, U},$  and  $c_{H_2, U}$  (the top and bottom plots of Figures 28 and the bottom plot of Figure 30, respectively) offer no surprises. The GGERM predicts that each of these mass fractions changes monotonically with time from its initial value to its steady state value. As required by the GGERM, note that the latter steady state values are consistent with the results of Figures 4, 5, and 9 or Figures 16, 17, and 21 for  $\phi = \phi^{(SS)} = 2.33$ .

The plots for  $c_{CO_2,U}$ ,  $c_{H_2O,U}$ , and  $c_{CO,U}$  (the top and bottom plots of Figures 29 and the top plot of Figure 30, respectively) predict the unusual result that each of these mass fractions will reach a local maximum during the transient portion of the experiment. (It is noteworthy that for each of these products of combustion the predicted maximum is actually larger than the maximum of the steady state values for  $\phi^{(SS)}$  in the range  $0 \leq \phi^{(SS)} < 2.33$ .) The local-maximum- $c_{k,U}$  result occurs because of the fact that during the transient portion of the experiment the upper layer environment participates in the combustion process by way of the feedback flow at times when the upper layer already contains relatively significant mass fractions of the combustion products. Thus, the products produced in the combustion process are added to the products that already exist in the layer. Instantaneously, the product concentrations of the reactor output at those times is analogous to the concentrations of the steady state upper-layer environment in a reference-[2]-type of experiment where the laboratory atmosphere, entrained into the fire plume from the lower layer and injected directly into the upper layer, is contaminated with a non-negligible amount of the products in question. In such experiments, the steady-state upper-layer mass fractions of these products, as a function of  $\phi^{(SS)}$ , would exceed the steady state mass fractions reported in [2].

While the overall results of the above GGERM simulation are qualitatively plausible, transient data is not now available to validate them quantitatively.

### The Combustion of Hexanes in Figure-31 Test Configurations - One of Two Hexane Experiments Reported in [3]

Consider the tests of [3]. The experimental configuration for these are depicted in Figure 31. This is similar to the configuration of Figure 3a except for the fact that the collector is a fully enclosed space which contains the fuel source. Air supplied to the lower layer is brought in, below the elevation of the fuel source, through a duct from the outside.

The time-dependent rate of air flow through the duct is measured during the course of an experiment. This air flow is not controlled. Rather, it occurs naturally as a result of cross-duct pressure differentials generated by buoyancy forces and buoyancy-driven flows within and through the collector enclosure.

The time-dependent pyrolysis rate of the fuel is measured by a fuel-bearing load cell.

A thermocouple tree measures temperatures in the enclosure as a function of time and elevation.

The GGERM was used to simulate the larger of the two hexane-burn experiments reported in [3]. For this experiment the thermocouple data indicate that the upper layer gases fill most of the enclosed space relatively early in the experiment. Therefore, throughout the simulation the upper-layer volume is assumed to be fixed at  $1.62 \text{ m}^3$ , approximately ninety percent of the volume of the enclosure above the elevation of the fuel surface. The temperature history of the upper layer is taken to be the temperature measured at the



elevation of thermocouple 4 of the thermocouple tree, which is approximately at the middle elevation of the assumed upper layer thickness. This temperature is assumed to be a representative value of the average layer temperature. The data from thermocouple 4 are presented in Figure 32. According to [10], these data are only valid up to approximately 700 C. Other measurements indicated final peak and relatively steady temperatures of 850 C. In the simulation, the upper layer temperature was calculated according to the two-line-segment approximation of the data, which is also plotted in the figure.

Measurements from the fuel load cell show the time-dependent hexane pyrolysis rate,  $\dot{m}_{\text{HEX}}$ , plotted at the top of Figure 33. In the simulation, the value of this, which is taken to be identical to  $\dot{P}_{\text{FUEL, FLOWIN}}$  in the analysis, was calculated according to a three-line-segment approximation to this data. This is also plotted in the figure.

Data from measurements of the duct air flow rate,  $\dot{m}_{\text{AIR}}$ , are plotted at the bottom of Figure 33. This air flow rate is used to approximate  $\dot{P}_{\text{AIR, FLOWIN}}$ , the instantaneous air flow rate introduced into the upper layer by entrainment from the lower layer to the plume. In the simulation, the value of  $\dot{P}_{\text{AIR, FLOWIN}}$  was calculated according to a two-line-segment approximation to the data. This is also plotted in the Figure 33.

Note that the  $\dot{m}_{\text{HEX}}$  and  $\dot{m}_{\text{AIR}}$  approximations follow the corresponding data which indicate a step change in these value at  $t = 0$ .

Using Eqs. (19), the time-dependent value of  $\phi^{(SS)}$  was calculated using the above-mentioned approximations for the time-dependent values of  $\dot{P}_{\text{FUEL, FLOWIN}}$  and  $\dot{P}_{\text{AIR, FLOWIN}}$ . This is plotted in Figure 34.

The GGERM simulation of this experiment was carried out twice, first using the real  $\text{C}_6\text{H}_{14}$  combustion model and then using the complete stoichiometric combustion model. Only the real-combustion-model simulation results will be presented here.

Since experimental data was acquired for the volume fraction concentration of  $\text{O}_2$ ,  $\text{CO}_2$ , and  $\text{CO}$ , all GGERM-computed results for the product mass fractions have been transformed into volume-fraction concentrations. The transformation was carried out with the assumption that the upper layer constituents include only: the six products of combustion, with mass fractions as computed from the GGERM; argon, with a specified mass fraction of 0.009; and nitrogen. The upper-layer volume or mole-fraction concentration of a product  $k$  will be designated here as  $c_{k,U}[\text{vol}]$ .

Results of the simulations for the real combustion model are presented in Figures 35-37 where the predicted volume fractions  $c_{k,U}(t)[\text{vol}]$  are plotted for  $k \rightarrow \text{C}_6\text{H}_{14}$ ,  $\text{O}_2$ ,  $\text{CO}_2$ ,  $\text{H}_2\text{O}$ ,  $\text{CO}$ , and  $\text{H}_2$ . Included in the plots for  $\text{O}_2$ ,  $\text{CO}_2$ , and  $\text{CO}$  are the data for the experimentally measured volume fractions of these products. Also included in Figures 35-37 are the time-dependent values of the  $c_{k,\text{REACTOUT}}^{(SS)}[\text{vol}]$ .

In Figure 34 it can be seen that the simulated step change in  $\dot{m}_{\text{HEX}}$  and  $\dot{m}_{\text{AIR}}$  leads to  $\phi^{(SS)} \approx 0.7$  at  $t = 0$ . This results in initial values of  $c_{k,\text{REACTOUT}}^{(SS)}$  which are different than the initial values of the  $c_{k,U}$ 's of the simulation, the latter being initialized at the concentrations of the ambient atmosphere.



To the extent that the  $c_{k,REACTOUT}^{(SS)}$  [vol] are good approximations to the  $c_{k,U}$  [vol] in the plots presented in Figures 35-37, the GGERM predicts that the upper layer environment is basically in a condition of quasi-steady state. As can be seen from the figures, in this particular experiment the GGERM simulation suggests that the quasi-steady state approximation is reasonable. Nonetheless, for those products of combustion where experimental data is available for comparison, i.e., for  $O_2$ ,  $CO_2$ , and  $CO$ , the transient GGERM predictions are seen to provide a superior estimate of the data than do the simple quasi-steady state predictions. To this extent, the favorable comparison between the data and the simulation results provides some validation of the GGERM.

The following additional observations and comments are offered:

1. The construction of the  $f_k$  functions for the combustion of hexane are based on the steady-state measurements of [6]. As can be seen in Figures 10-15, the maximum of the  $\phi$ 's in those experiments was approximately 1.8. Therefore, one's confidence in the present GGERM simulation beyond  $\phi$ 's of 1.6, i.e., beyond approximately  $t = 150$  s, should be coupled to one's confidence in the extrapolation of these  $f_k$ 's beyond 1.6. In other words, acquisition and use of new data in the high- $\phi$  range would lead to more confidence in high- $\phi$  GGERM simulations. This is of course true for  $CH_4$  and other fuels as well as for hexane.
2. From approximately 150 s to the end of the test, the measured value of  $c_{O_2,U}$  [vol] is reported to be 0.003 [10] whereas the predicted value is approximately 0.03 (see Figure 35). The measured value is not consistent with the Figure 34 and the  $c_{O_2}$  of Figure 23. For example, according to Figure 34, at 150 s the value of  $\phi^{(SS)} \approx 2$ . According to Figure 23, this corresponds to  $c_{k,REACTOUT}^{(SS)} \approx 0.04$ . Thus, for the same  $\phi$  the  $c_{O_2,U}$  results of the steady-state experiments of [6], on which Figure 23 and the present hexane combustion is based, is not consistent with the present quasi-steady experimental result of [3]. It has been determined that the discrepancy is the result of a non-negligible dependence of  $f_{O_2}$  on temperature. In particular, it is likely that for  $t > 150$  s the temperature of the upper layer in the presently simulated experiment is several hundreds degrees C higher than temperatures in the reference [6] experiments.

The effect of similar levels of temperature difference on the steady-state  $c_{O_2,U}$  in  $CH_4$ -burn experiments can be seen in Figure 5. In this figure, the data of Toner [5] were acquired at significantly higher upper-layer temperatures, as much as 200°C higher, than were those of all of the other data. For  $\phi \geq 1$ , the effect on  $c_{O_2,U}$  is significant and completely consistent with the effects on  $c_{O_2,U}$  presently observed during the burning of hexanes. Presumably, if the hexane burn data of [6] were acquired in a well-insulated collector with upper-layer temperatures in the 700-850 C range, the measured  $c_{O_2,U}$  at  $\phi \geq 1$  would be lowered from the order of a few percent to the order of a few tenths of a percent.

The expected qualitative effect of high temperature on  $c_{CO_2,U}$  and  $c_{CO,U}$  in the burning of hexanes can also be obtained from the corresponding

high temperature effects in the burning of  $\text{CH}_4$ . Thus, in Figure 6 for  $\phi \geq 1$ , the relatively high temperature of the upper layer in the experiments of Toner [5] is seen to have resulted in  $c_{\text{CO}_2, \text{U}}$  levels ten to twenty percent higher than the  $c_{\text{CO}_2, \text{U}}$  levels of the relatively low-temperature experiments of [2]. A similar result is noted for  $c_{\text{CO}, \text{U}}$  in Figure 8. Thus, for all three of the measured product concentrations, the high temperature effect in the hexane combustion model explains the late-time discrepancies between the present GGERM simulation and the experimental data.

It is noted that for an arbitrary fuel of interest, any significant dependence of the  $f_k$  on temperature, that may be determined in steady-state tests, could be easily incorporated into the GGERM.

### The Combustion of Hexanes in Figure-31 Test Configurations - A Hypothetical Reference-[3]-Type Hexane Experiment

It is important to validate the GGERM with data acquired in experiments which clearly display transient behavior in the development of the upper layer environment, especially at times of relatively large values of  $c_{\text{CO}}$ . In general, the experiments reported in [2] would be useful in this regard. The first experiment simulated above is an excellent case in point. The reference-[2] experimental program is continuing [11]. When transient data from these experiments are available it is recommended that they be compared with corresponding GGERM simulations.

It would appear that experimental conditions could be chosen so that reference-[3]-types of experiments would also clearly display the transient upper-layer environment of interest. As discussed earlier, the test run simulated above was somewhat limited in this regard in that it displayed nearly-quasi-steady behavior during the interesting times of relatively high  $c_{\text{CO}}$  [vol]. One reason for the nearly-quasi-steady behavior was that the magnitude of  $\dot{P}_{\text{FUEL, FLOWIN}}$  resulted in relatively large induced values of  $\dot{P}_{\text{AIR, FLOWIN}}$ . From the bottom of Figure 33, the latter flow rate is seen to have a characteristic value on the order of 0.07 kg/s. For a characteristic air density of 1 kg/m<sup>3</sup>, and for the assumed 1.62 m<sup>3</sup> upper layer volume, this corresponds to a relatively small characteristic residence time, on the order of 20 s, for flow exchange of the upper layer. (In contrast to this, the simulated reference-[2] experiment with a upper layer volume of 3.89 m<sup>3</sup> and  $\dot{P}_{\text{AIR, FLOWIN}}$  value of 0.010 kg/s has a characteristic residence time of 400 s.)

For the reference-[3] test configuration it is expected that a significantly reduced fuel flow rate, leading to a corresponding reduced air flow rate, would lead to a display of the transient behavior of current interest for upper layer development. This idea was investigated by using the GGERM to simulate a hypothetical hexane-burn experiment involving values of  $\dot{P}_{\text{FUEL, FLOWIN}}$  and  $\dot{P}_{\text{AIR, FLOWIN}}$  one tenth as large as the Figure 33 values used previously. The actual approximation for these functions are plotted in Figure 38. All other parameters defining the experiment were assumed to be unchanged from the previous simulation. The hypothetical experiment was assumed to last 500 s, where all input parameters were assumed to be constant for the last 250 s. The results of the new simulation are plotted in Figures 39-41 in a manner completely analogous to the Figure 35-37 results of the



previous calculation. Favorable comparisons between  $c_{k,U}$  data from an actual experiment (similar to this hypothetical experiment) and  $c_{k,U}$  results of its GGERM simulation would be an important validation of GGERM capabilities.

## SUMMARY AND CONCLUSIONS

The Generalized Global Equivalence Ratio Model (GGERM) was developed to predict the generation rates of oxygen, fuel, and other products of combustion in rooms containing fires [1]. The GGERM extends to general transient conditions the global equivalence ratio model established during times of steady-state in experimental studies involving two-layer compartment fires. The present work used the GGERM to predict upper layer mass fractions of products of combustion (fuel, oxygen, CO, and others) in these two-layer fire experiments, but during times of transient response.

Implementation of the GGERM requires knowledge of the  $f_k(\phi)$  function for each product  $k$  of combustion of a fuel of interest. A  $f_k$  function predicts the steady-state generation rate of product  $k$  when the fuel burns in Figure-3-type configurations. The  $f_k$  would be constructed from data acquired in experiments of the type described in references [2]-[9]. Generic rules were developed for constructing the  $f_k$  from the steady-state data. The rules were then applied to data of [2] and [6]. This resulted in prototype models (i.e., the  $f_k$ ) for the steady-state combustion of methane ( $\text{CH}_4$ ) and hexanes ( $\text{C}_6\text{H}_{14}$ ) in Figure-3-type fire scenarios. The products of combustion considered in these latter models include  $\text{O}_2$ ,  $\text{CO}_2$ ,  $\text{H}_2\text{O}$ ,  $\text{CO}$ ,  $\text{H}_2$ , and the fuel itself.

With the characterization of methane and hexane combustion in hand, the GGERM was used to simulate transient upper-layer environments in two-layer experiments reported in [2] (methane) and [3] (hexanes). One of these simulations produced the unusual result of local maxima in the mass fractions of  $\text{CO}_2$ ,  $\text{H}_2\text{O}$ , and  $\text{CO}$ . This was explained by the action of the GGERM feedback mechanism.

All predicted results of the GGERM simulations were found to be plausible and, where transient data were available (upper-layer volume fraction of  $\text{O}_2$ ,  $\text{CO}_2$ , and  $\text{CO}$  for the hexanes experiment of [3]), predicted and measured results for the upper layer concentrations of products of combustion compared favorably. The most significant discrepancies between experiment and prediction were attributed to differences between the (relatively high) layer temperatures of [3] and the (relatively low) layer temperatures in the steady-state  $f_k$  tests of [6]. For the most part it appears that these discrepancies could be removed with use of a reference-[6]-type data base having a more extensive layer temperature variation. Analysis of data presented in Chapter 5 of [2] supports this contention.

Since comparisons between simulation and experiment were limited, additional validation of the GGERM under more varied fire conditions is required before it can be used with confidence in two-layer zone-type compartment fire models.

A GGERM simulation of a hypothetical experiment in the reference-[3] facility was carried out in order to identify a set of experimental conditions in that facility that would be expected to highlight the transient character of the developing upper-layer environments. Calculations suggest that a GGERM simulation which accurately predicts the experimental data from such an experiment would be an important test of the GGERM capability.

## REFERENCES

- [1] Cooper, L.Y., A Model for Predicting the Generation Rate and Distribution of Products of Combustion in Two-Layer Fire Environments, NISTIR 4403, National Institute of Standards and Technology, Gaithersburg MD, September 1990.
- [2] Morehart, J.H., Zukoski, E.E., and Kubota, T., Species Produced in Fires Burning in Two-Layered and Homogeneous Vitiated Environments, GCR 90-585 of the National Institute of Standards and Technology (NIST), report of the California Institute of Technology to the NIST, Gaithersburg MD, August 1990.
- [3] Gottuck, D.T., and Roby, R.J., Carbon Monoxide Yields from Hexane-Fueled Compartment Fires, Chemical and Physical Processes in Combustion, Proceedings of the 1990 Fall Technical Meeting of the Eastern Section of the Combustion Institute, Orlando FL.
- [4] Zukoski, E.E., Toner, S.J., Morehart, J.H., and Kubota, T., Combustion Processes in Two-Layered Configurations, Fire Safety Science - Proceedings of the Second International Symposium, pp. 295-304, T. Wakumatsu et al., Eds., International Association of Fire Safety Science, Tokyo, June 13-17, 1988, Hemisphere Publishing Co., New York, 1989.
- [5] Toner, S.J., Zukoski, E.E., and Kubota, T., Entrainment, Chemistry and Structure of Fire Plumes, report under Grant No. 60NANB600638 by the California Institute of Technology to the U.S. National Bureau of Standards (presently National Institute of Standards and Technology), Gaithersburg MD, October, 1986.
- [6] Beyler, C.L., Development and Burning of a Layer of Products of Incomplete Combustion Generated By a Buoyant Diffusion Flame, Ph.D. Thesis, Harvard University, Cambridge MA, 1983.
- [7] Beyler, C.L., Major Species Production by Diffusion Flames in a Two-Layer Compartment Fire Environment, Fire Safety J1, 10, pp. 47-56, 1986.
- [8] Beyler, C.L., Major Species Production by Solid Fuels in a Two-Layer Compartment Fire Environment, Fire Safety Science - Proceedings of the First International Symposium, pp. 431-440, Grant C.E. and Pagni, P.J. Eds., International Association of Fire Safety Science, Gaithersburg, October 7-11, 1985, Hemisphere Publishing Co., New York, 1986.
- [9] Zukoski, E.E., Morehart, J.H., Kubota, T., and Toner, S.J., Species Production and Heat Release Rates in Two-Layered Natural Gas Fires, Combustion and Flame, 83, pp. 325-332, 1991.
- [10] Roby, R.J. and Gottuck, D.T., private communication.
- [11] Zukoski, E.E., Experimental Study of Heat Transfer and the Environment of a Room Fire, Summaries of Center for Fire Research In-House Projects and Grants - 1990, NISTIR 4440, Cherry, S.M., Editor, National Institute of Standards and Technology, Gaithersburg MD, October 1990.



## NOMENCLATURE

$c_{H_2O,N}^{(SS)}$ , $N = 1, 2$	constants, Eq. (61)
$c_{k,U}$	mass fraction of combustion product $k$ in the upper layer
$c_{k,U}[\text{vol}]$	volume fraction of combustion product $k$ in the upper layer
$c_{k,REACTOUT}$	mass fraction of combustion product $k$ in the reactor outflow
$c_{k,REACTOUT}[\text{vol}]$	volume fraction of combustion product $k$ in the reactor outflow
$c_{k,REACTOUT,STOICH}$	value of $c_{k,REACTOUT}$ for stoichiometric combustion
$c_{k,REACTOUT}^{(SS)}$	value of $c_{k,REACTOUT}$ under steady state conditions
$c_{k,REACTOUT}^{(SS)}[\text{vol}]$	value of $c_{k,REACTOUT}[\text{vol}]$ under steady state conditions
$c_{k,REACTOUT,STOICH}^{(SS)}$	value of $c_{k,REACTOUT,STOICH}$ under steady state conditions
$f_k(\phi)$	Eq. (3)
$f_k^{(STOICH)}$	value of $f_k(\phi)$ for stoichiometric combustion
$m_U$	total mass in the upper layer
$\dot{m}_{AIR}$	measured mass flow rate of air into reference-[3] facility
$\dot{m}_{HEX}$	measured mass pyrolysis rate of hexane in reference-[3] facility
$\dot{m}_{FEEDBK}$	mass flow rate to the reactor from the bulk of the upper layer
$\dot{m}_{FEEDBK,1}$	Eq. (27)
$\dot{m}_{FEEDBK,3}$	Eq. (28)
$\dot{m}_{FLOWIN} [\dot{m}_{FLOWOUT}]$	total mass flow rate into [out of] the upper layer
$(\dot{P}_{FUEL}/\dot{P}_{OXY})_{STOICH}$	stoichiometric fuel-to-oxygen ratio
$\dot{P}_{k,FLOWIN} [\dot{P}_{k,FLOWOUT}]$	sum of rates of flow of all components of product $k$ into [out of] the upper layer

$P_{k,U}$	mass of combustion product k in the lower [upper] layer
$\dot{P}_{k,U}$	net rates of combustion product k flowing to the upper layer
$\dot{P}_{k,REACTIN}$	net mass flow rate of combustion product k into the reactor
r	$(\dot{P}_{FUEL}/\dot{P}_{OXY})_{STOICH}$
$T_U$	temperature of the upper layer
$T_{U,INIT}$ [ $T_{U,FINAL}$ ]	initial [final] temperature of the upper layer
t	time
$\Gamma_k$	Eq. (51)
$\Gamma_{k,0}$	Eq. (32)
$\Gamma_{k,\infty}$	Eq. (42)
$\lambda_{CO,N}$ N = 1,2,3,4	constants, Eq. (69)
$\lambda_{CO2,1}$	a constant, Eq. (65)
$\lambda_{H2O,N}$ N = 1,2	constants, Eq. (67)
$\Lambda_k$	Eq. (17)
$\lambda_k$	Eq. (10)
$\sigma$	Eq. (56)
$\phi$	Eq. (2)
$\phi^{(SS)}$	value of $\phi$ under steady state conditions, Eq. (19)
$\phi_{FUEL}$	Eq. (29)
$\phi_{FUEL}^{(STOICH)}$	value of $\phi_{FUEL}$ under complete stoichiometric burning
$\phi_{k,STOICH1}$ , $\phi_{k,STOICH2}$	constants in representation of $f_k$ , see Eq. (73) and below Eq. (71)
$\phi_{O2}$	Eq. (30)
$\phi_{O2}^{(STOICH)}$	value of $\phi_{O2}$ under complete stoichiometric burning
$\dot{\omega}_k$	mass generation rate of combustion product k

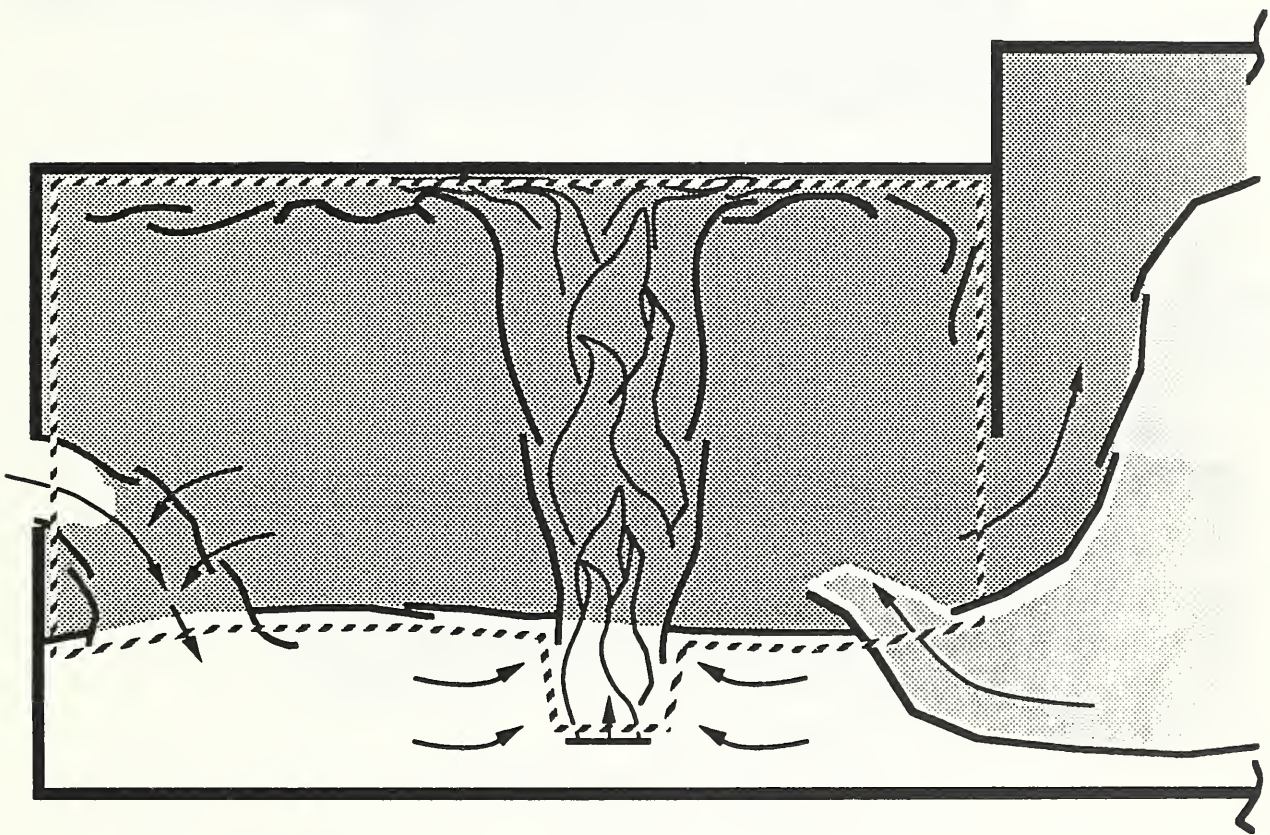


Figure 1. The extended upper layer in a room of fire origin which includes the assumed negligible-volume fire plume.

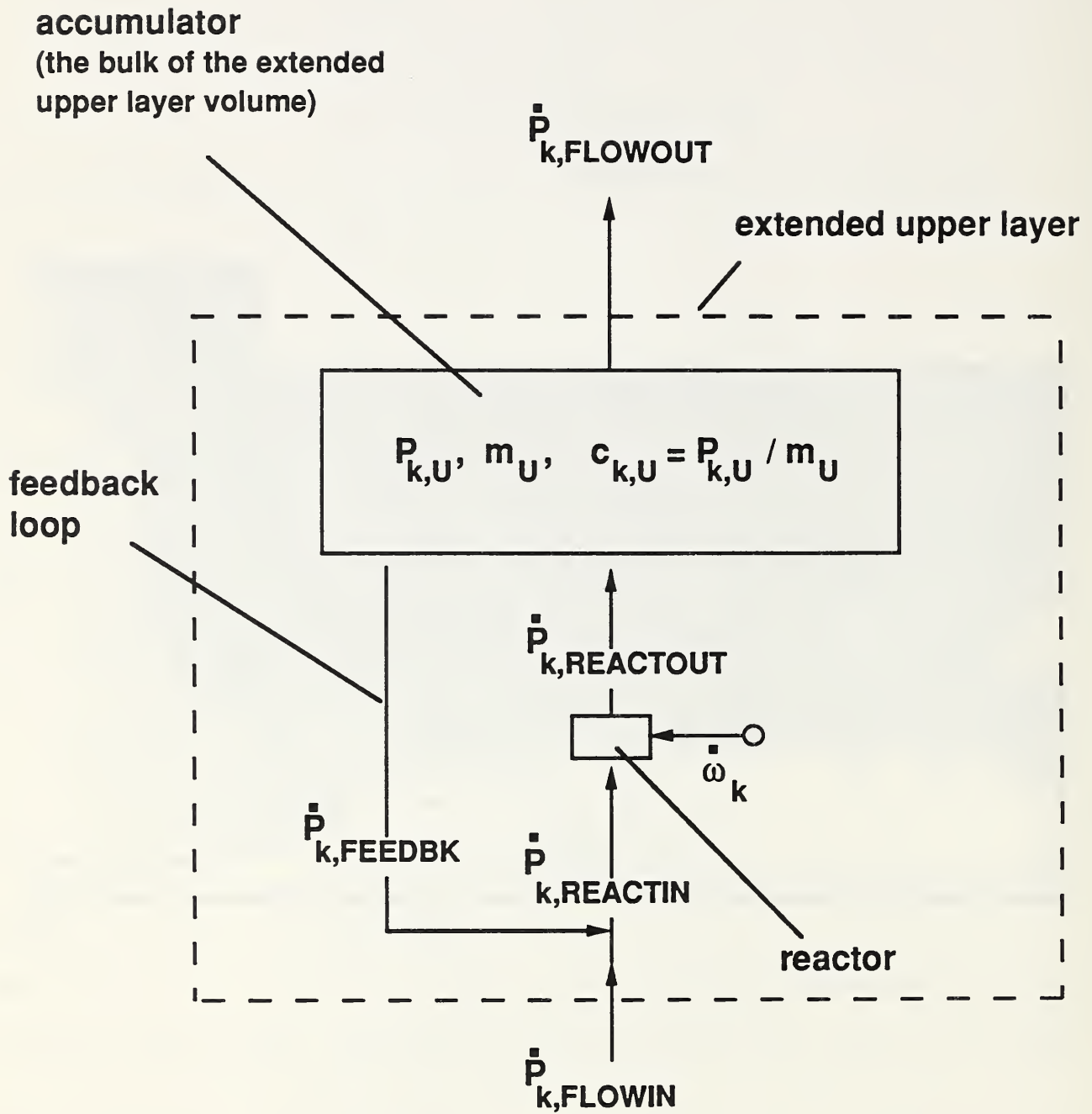
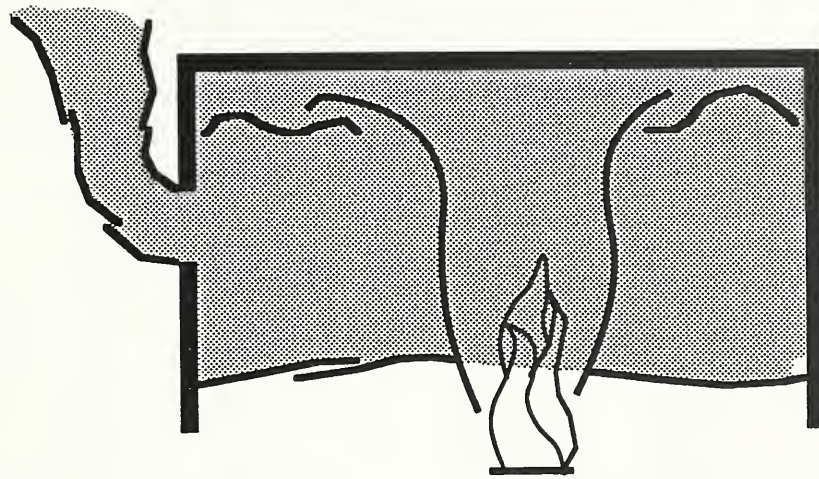
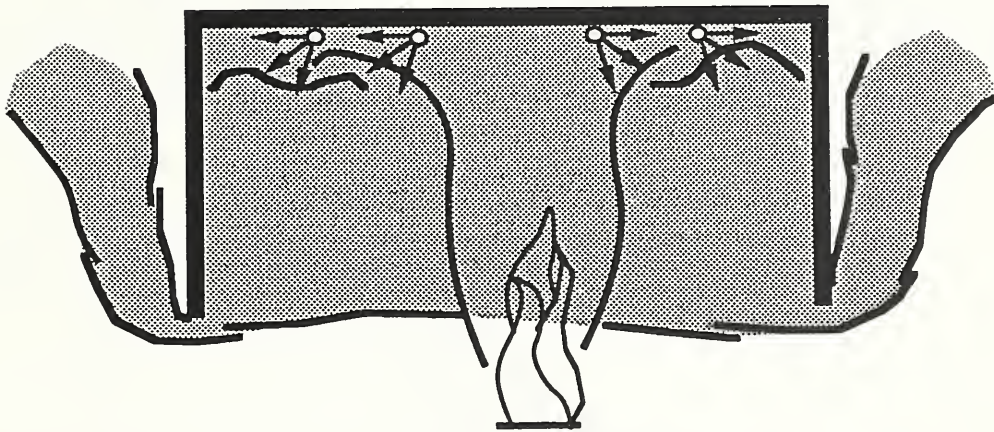


Figure 2. The GGERM representation of combustion and flow dynamics in the extended upper-layer of Figure 1.





(a)



(b)

Figure 3. The experimental configuration used in [6], [7], and [8] (a) and in [2], [4], [5], and [9] (b).

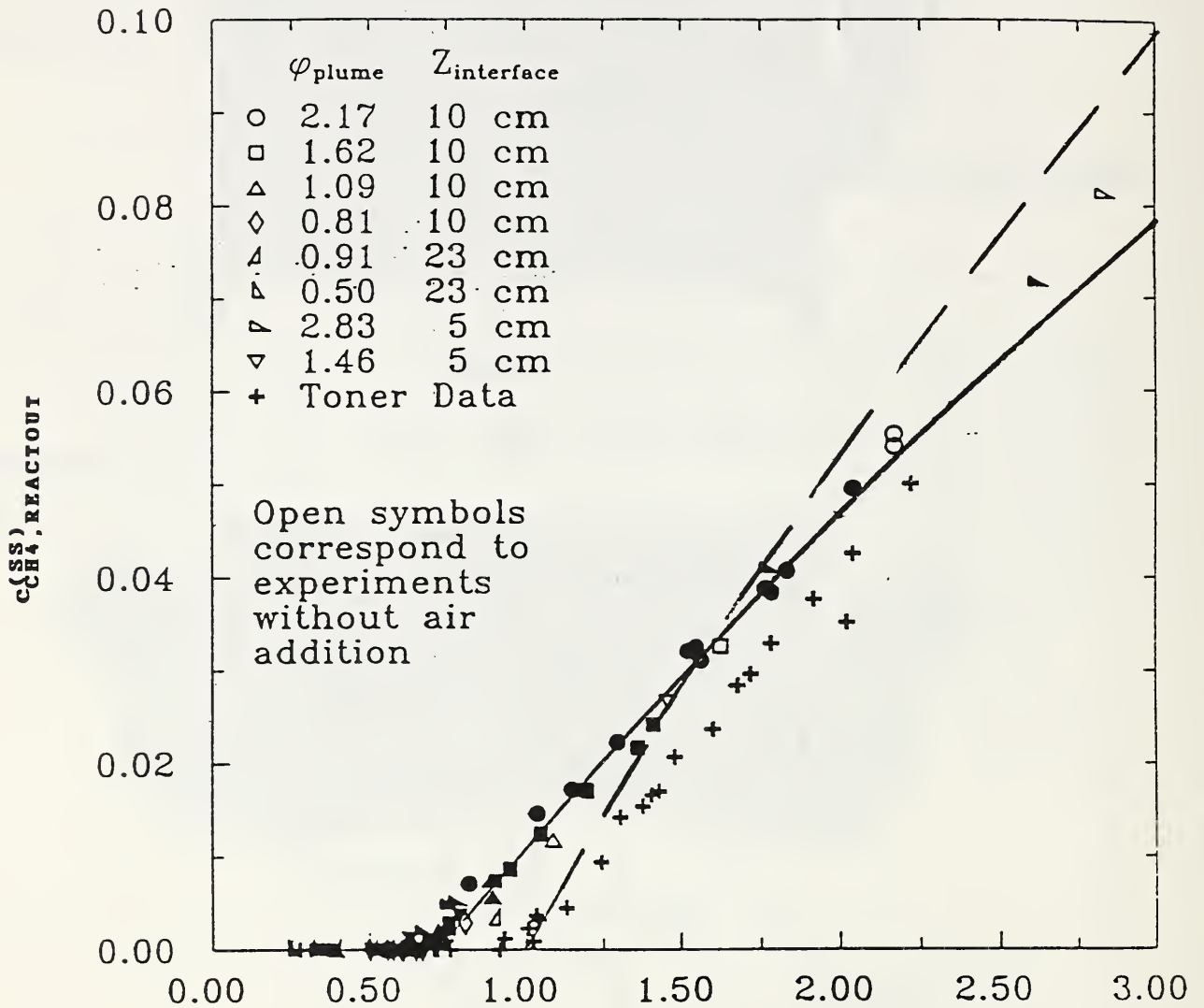


Figure 4. Combustion of methane ( $\text{CH}_4$ ). Data from [2]. Analytic representations of  $c_{\text{CH}_4, \text{REACTOUI}}^{(\text{SS})}$ : for complete stoichiometric combustion, Eqs. (51)-(53) or Eqs. (55) and (56) ( - - - ); and for the curve-fit of Eq. (58) ( — ).

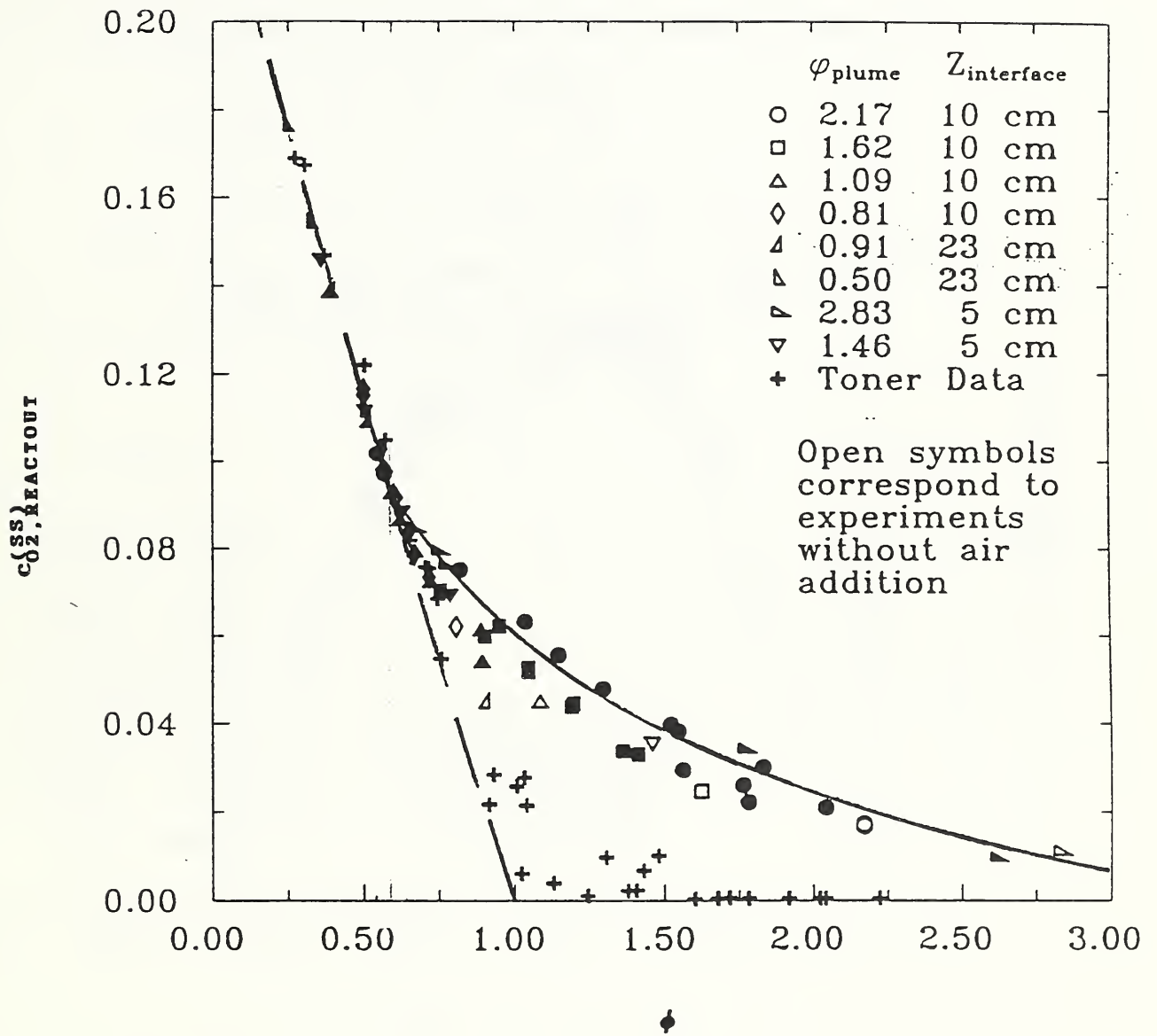


Figure 5. Combustion of methane ( $CH_4$ ). Data from [2]. Analytic representations of  $c_{O_2, REACTOUI}^{(SS)}$ : for complete stoichiometric combustion, Eq. (59) ( - - - ); and for the curve-fit of Eq. (61) ( — ).

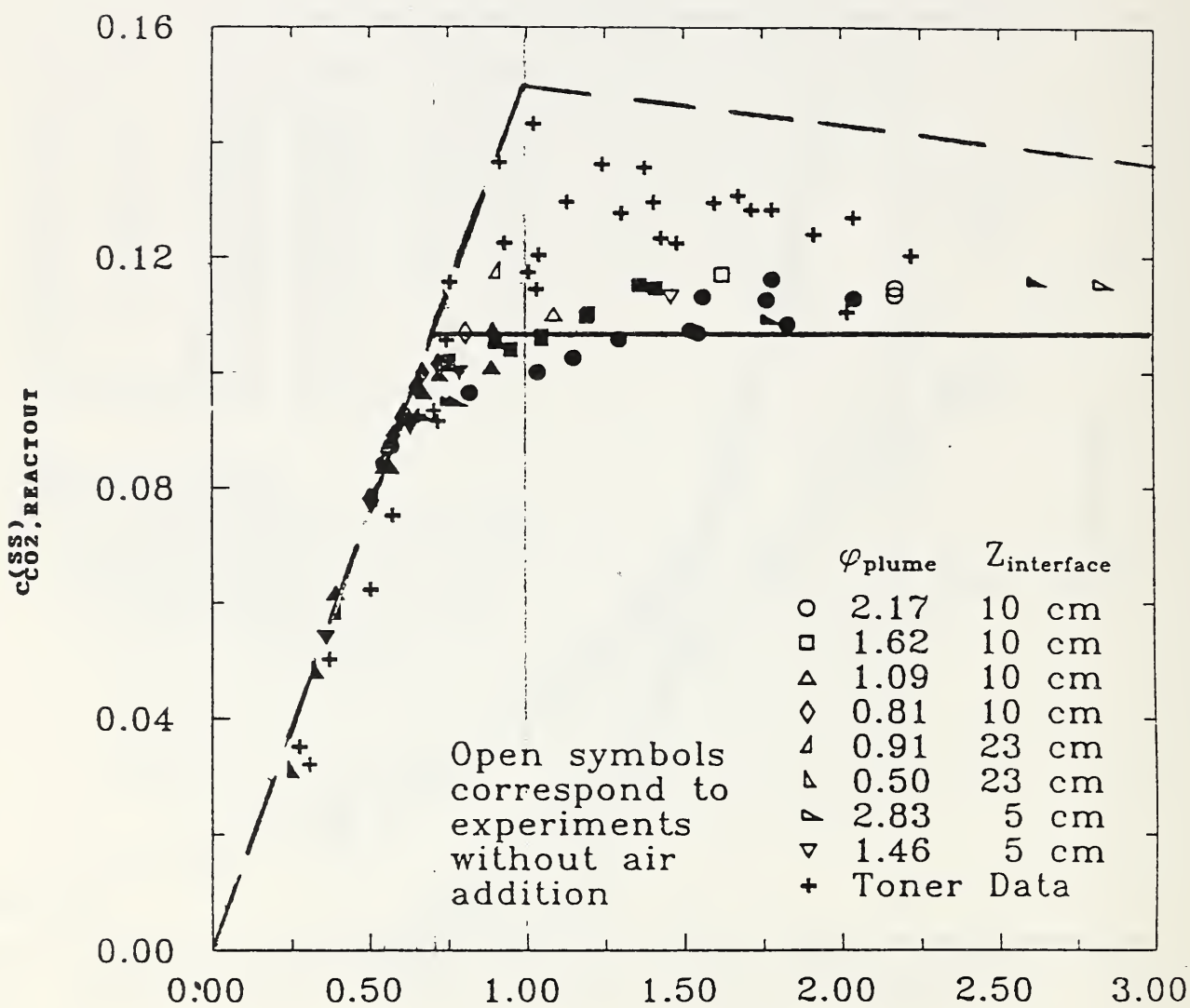


Figure 6. Combustion of methane ( $\text{CH}_4$ ). Data from [2]. Analytic representations of  $c_{\text{CO}_2, \text{REACTOUT}}^{(\text{SS})}$ : for complete stoichiometric combustion, Eq. (62) ( - - - ) and for the curve-fit of Eq. (64) and (65) ( — ).



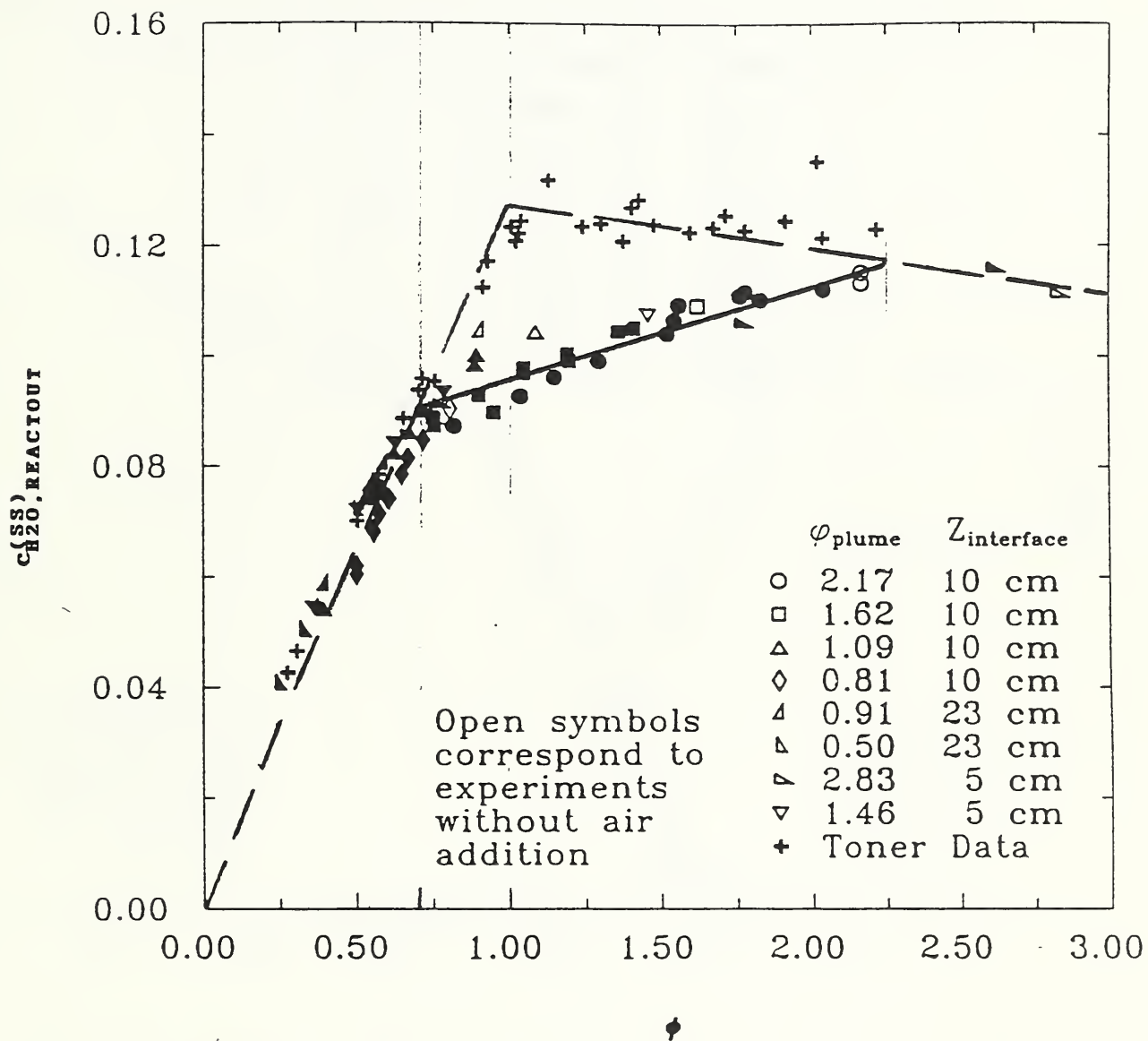


Figure 7. Combustion of methane ( $\text{CH}_4$ ). Data from [2]. Analytic representations of  $c_{\text{H}_2\text{O}, \text{REACTOUT}}^{(\text{SS})}$ : for complete stoichiometric combustion, Eq. (63) (---) and for the curve-fit of Eqs. (66) and (67) (—).

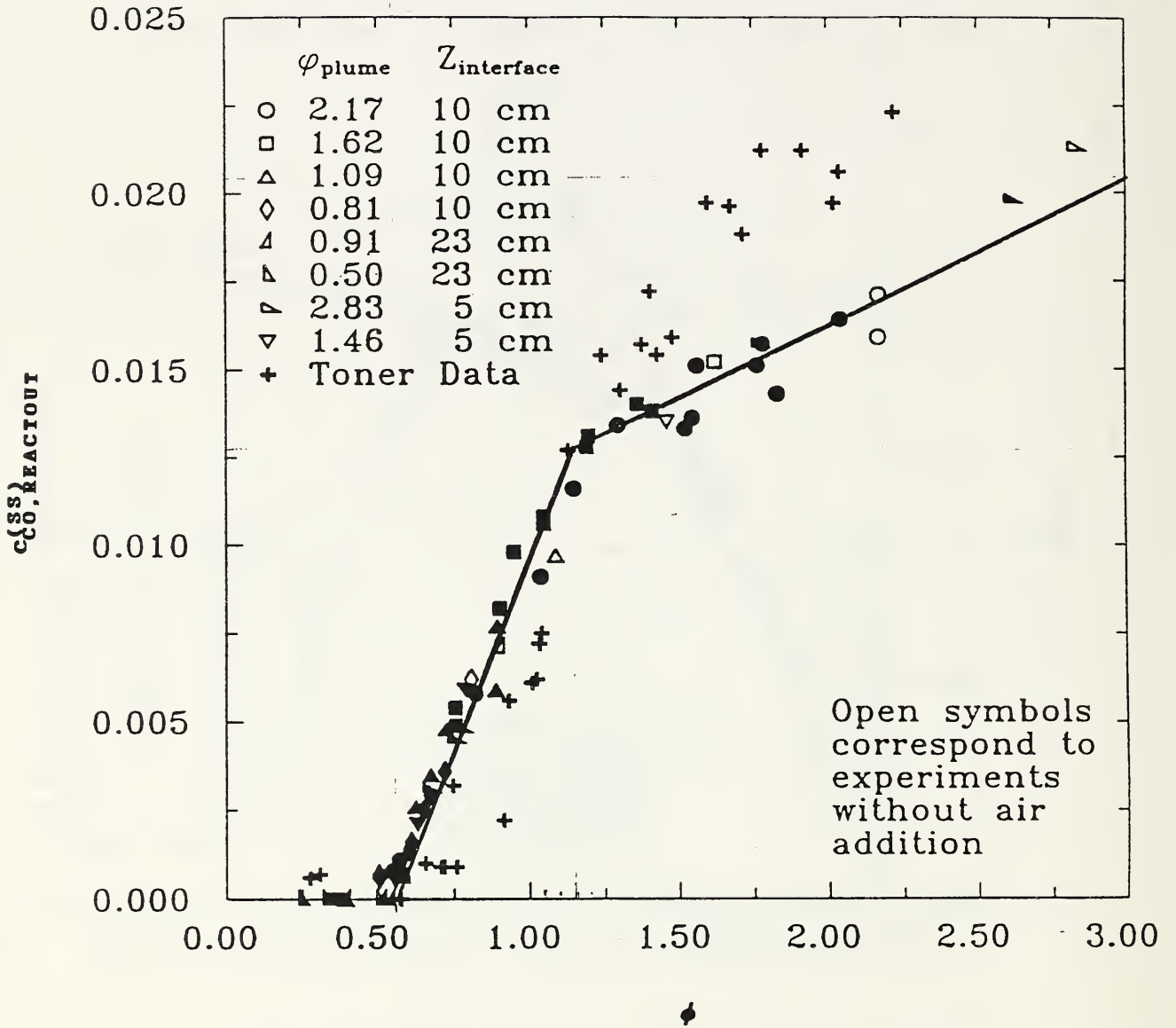


Figure 8. Combustion of methane ( $\text{CH}_4$ ). Data from [2]. Analytic representations of  $c_{\text{CO, REACTOUI}}^{\text{SS}}$  for the curve fit of Eqs. (68) and (69).

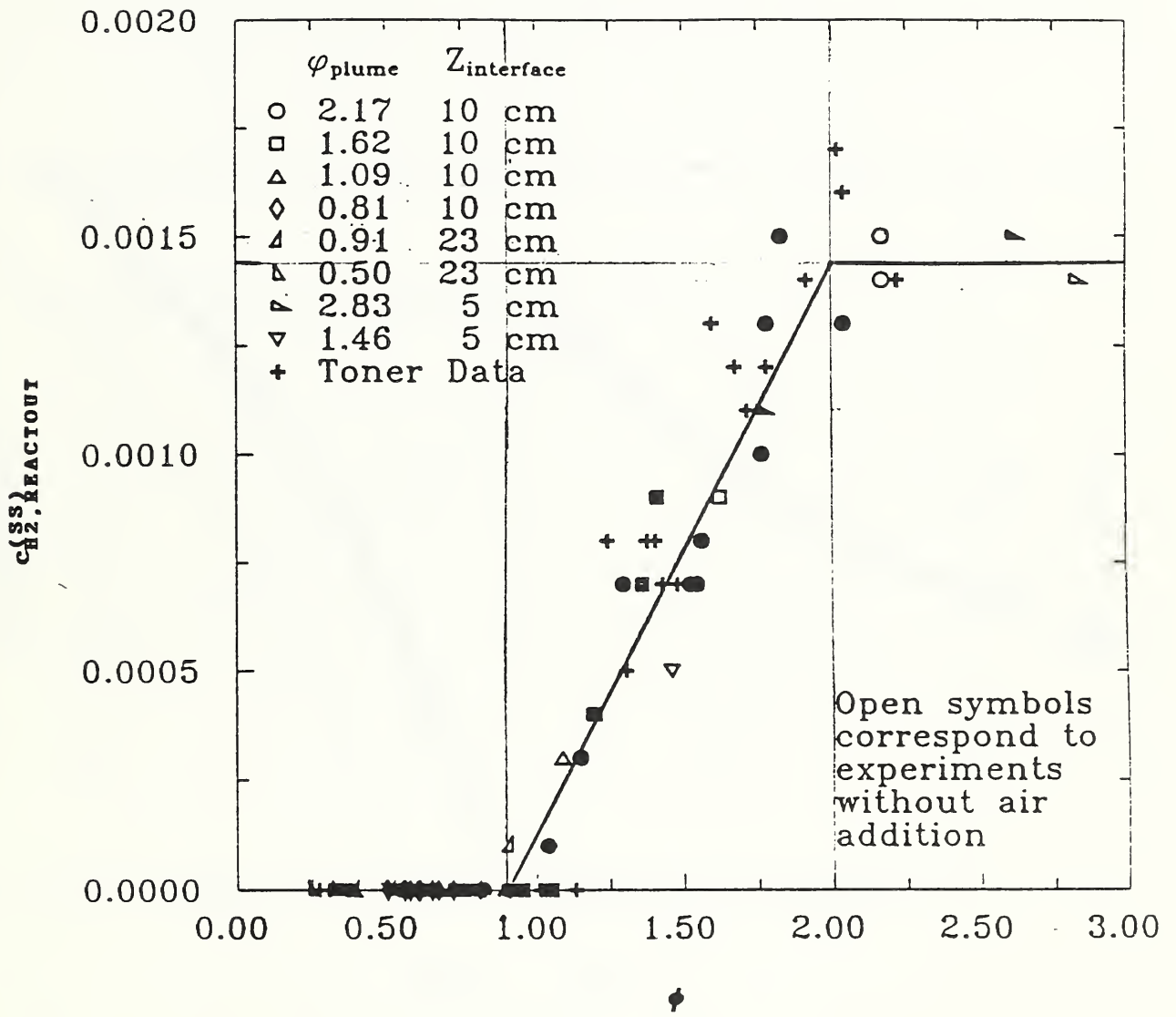


Figure 9. Combustion of methane ( $\text{CH}_4$ ). Data from [2]. Analytic representations of  $c_{\text{H}_2, \text{REACTOUI}}^{(\text{SS})}$  for the curve fit of Eq. (70).

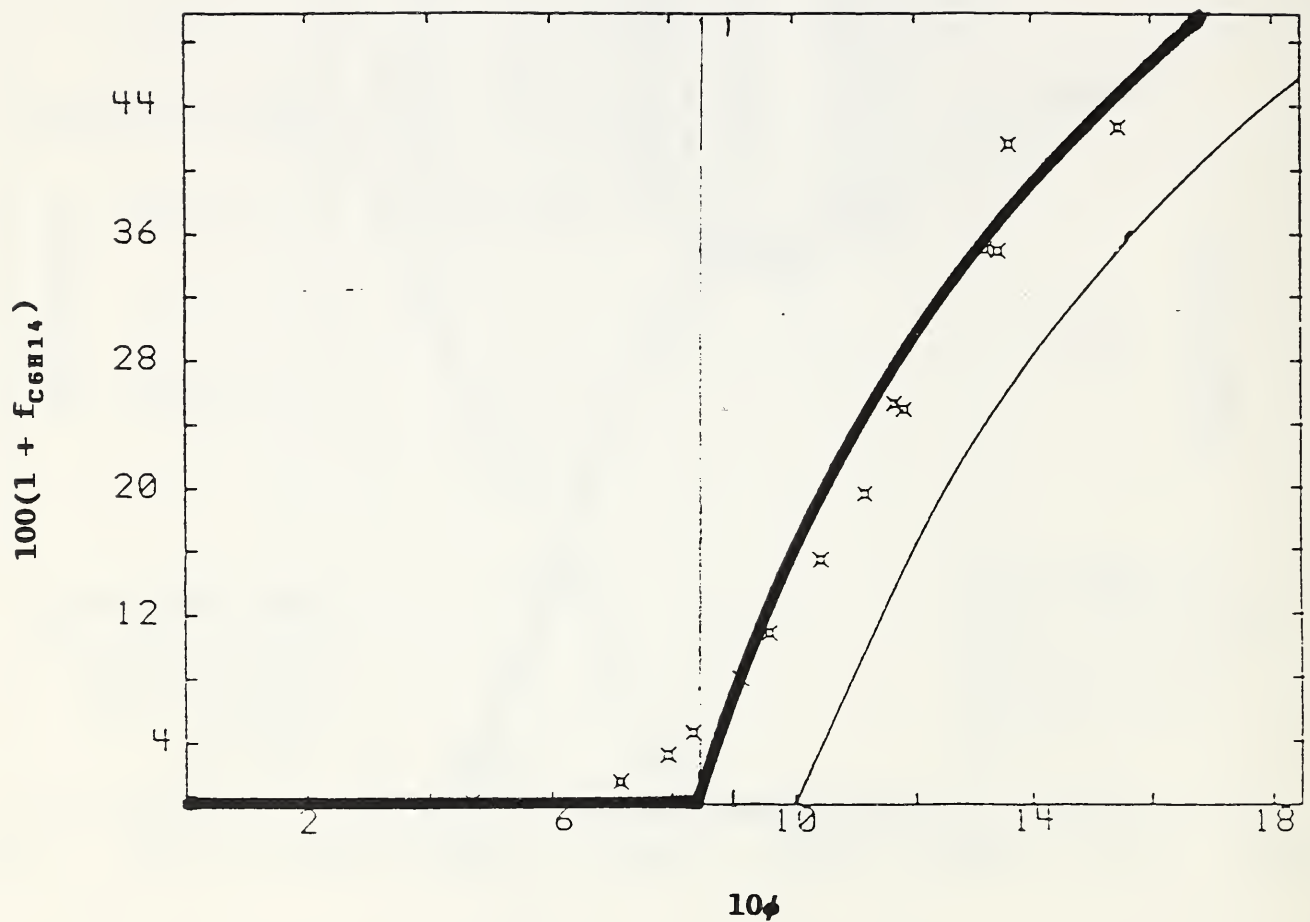


Figure 10. Combustion of hexanes ( $C_6H_{14}$ ). Data from [6]. Analytic representations of  $f_{C_6H_{14}}$ : for complete stoichiometric combustion, Eqs. (51)-(53) and (71) ( — ); and for the curve-fit of Eqs. (71)-(73) ( — ).



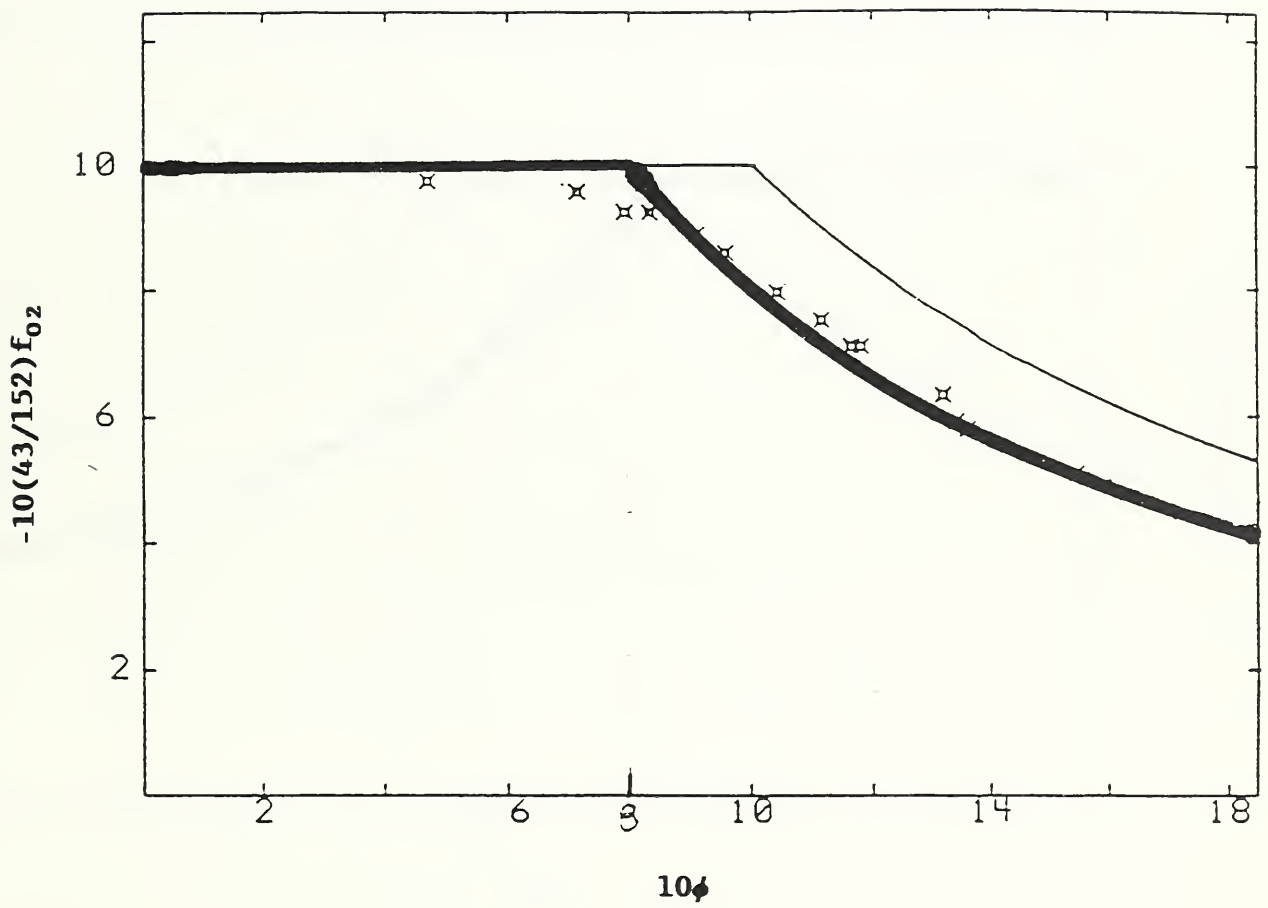


Figure 11. Combustion of hexanes ( $C_6H_{14}$ ). Data from [6]. Analytic representations of  $f_{O_2}$ : for complete stoichiometric combustion, Eqs. (51)-(53) and (71) ( — ); and for the curve-fit of Eqs. (71)-(73) ( — ).

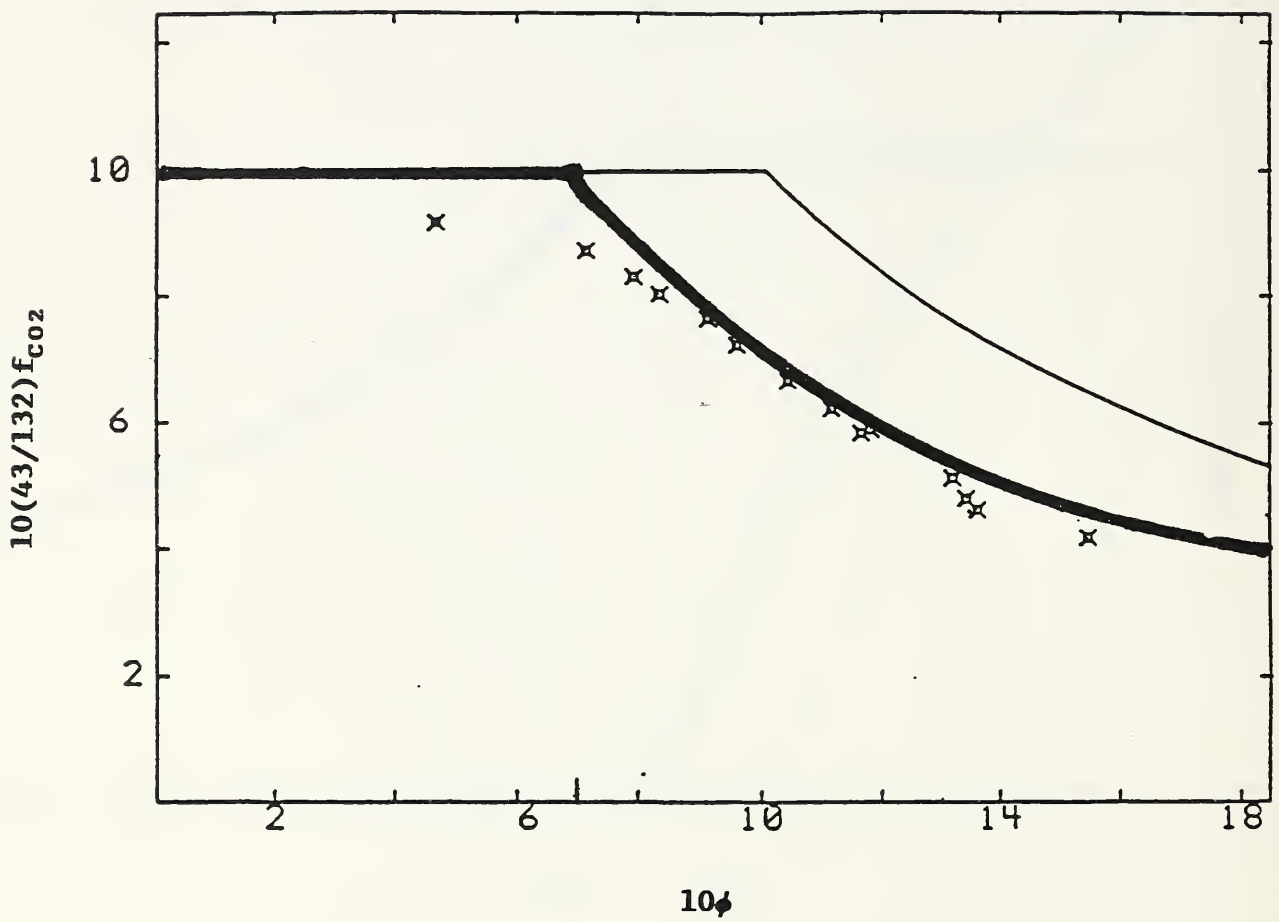


Figure 12. Combustion of hexanes ( $C_6H_{14}$ ). Data from [6]. Analytic representations of  $f_{CO_2}$ : for complete stoichiometric combustion, Eqs. (51)-(53) and (71) ( — ); and for the curve-fit of Eqs. (71)-(73) ( — ).

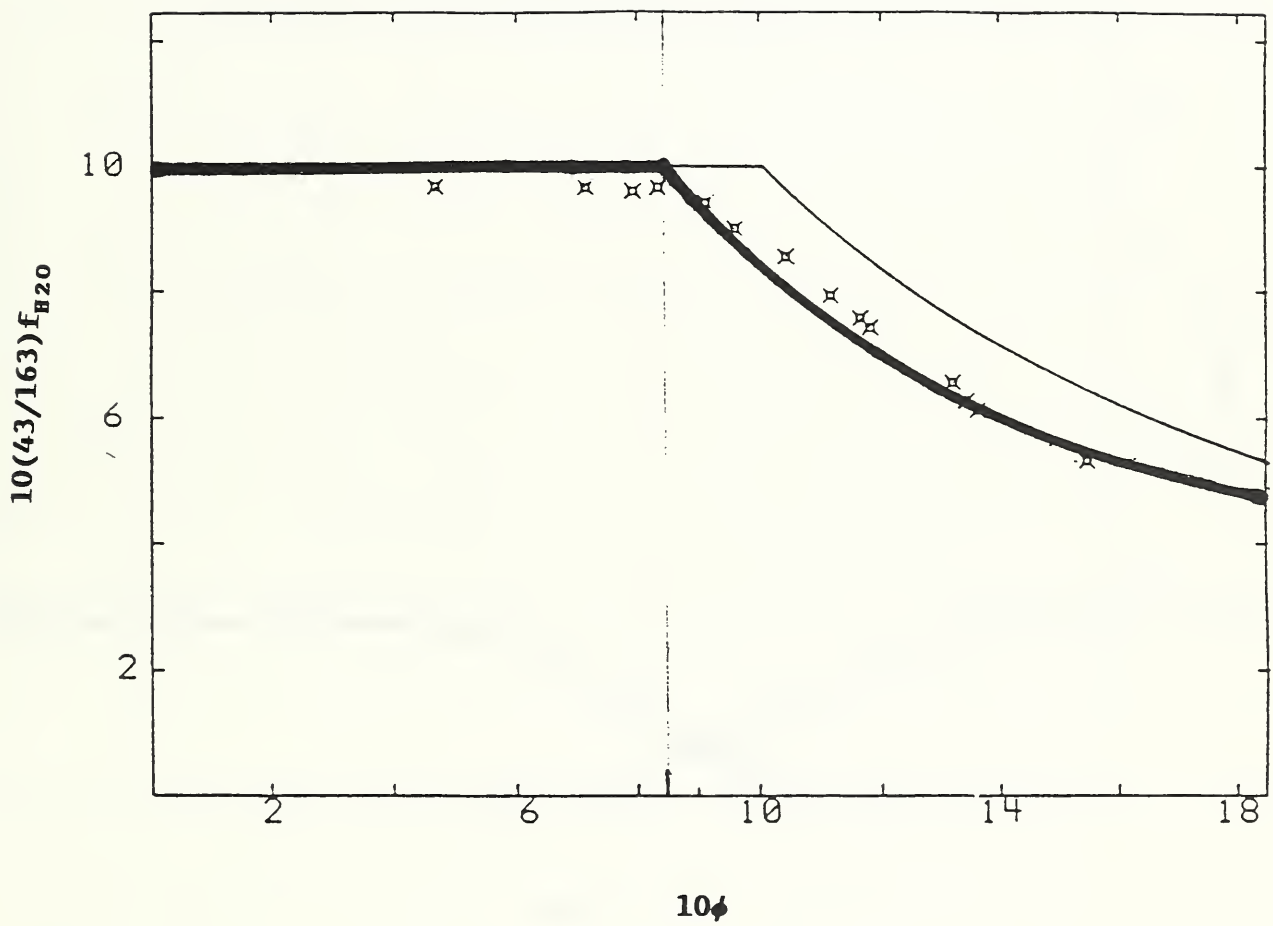


Figure 13. Combustion of hexanes ( $C_6H_{14}$ ). Data from [6]. Analytic representations of  $f_{H_2O}$ : for complete stoichiometric combustion, Eqs. (51)-(53) and (71) ( — ); and for the curve-fit of Eqs. (71)-(73) ( ——— ).

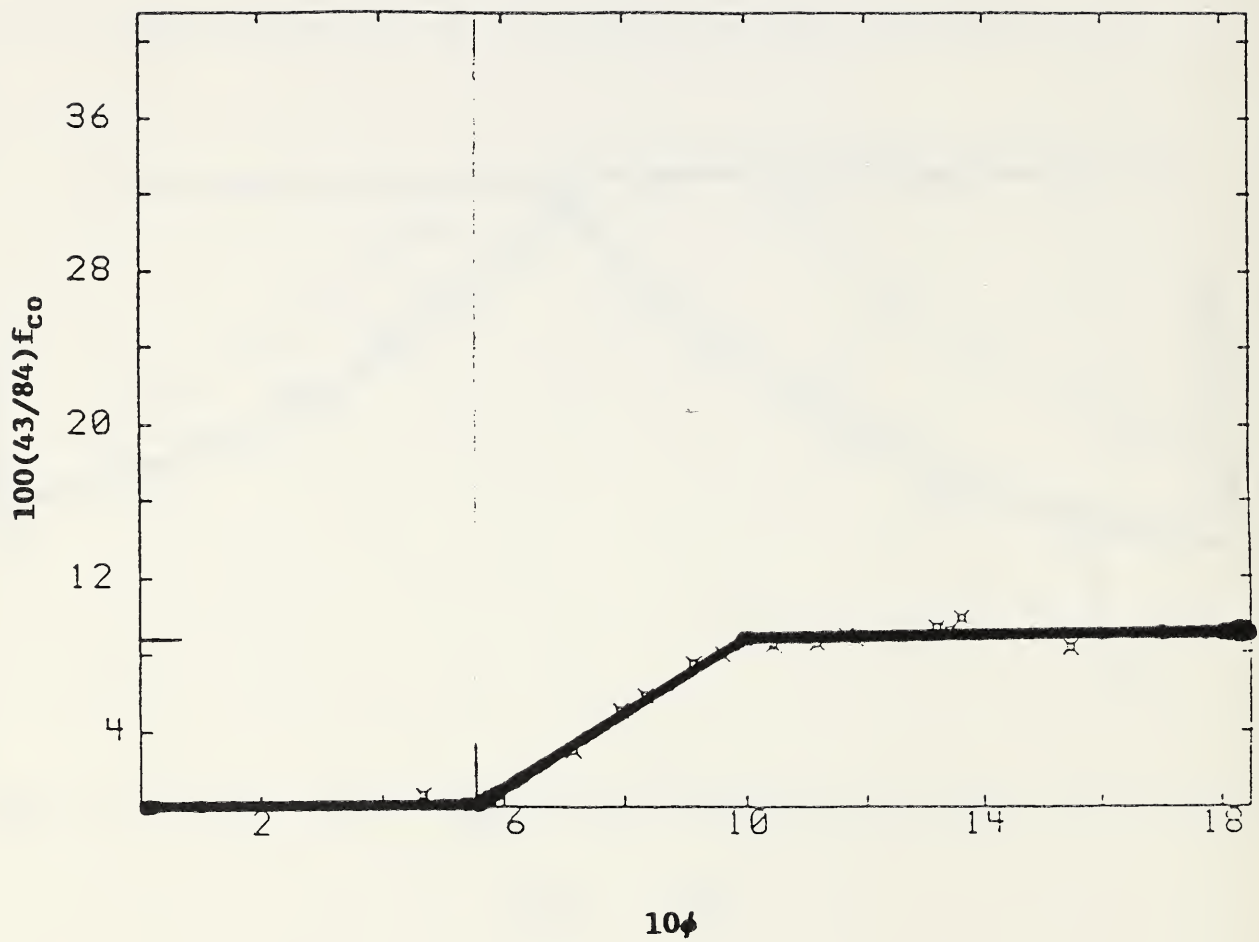


Figure 14. Combustion of hexanes ( $C_6H_{14}$ ). Data from [6]. Analytic representation of  $f_{CO}$  according to the curve fit of Eq. (74).



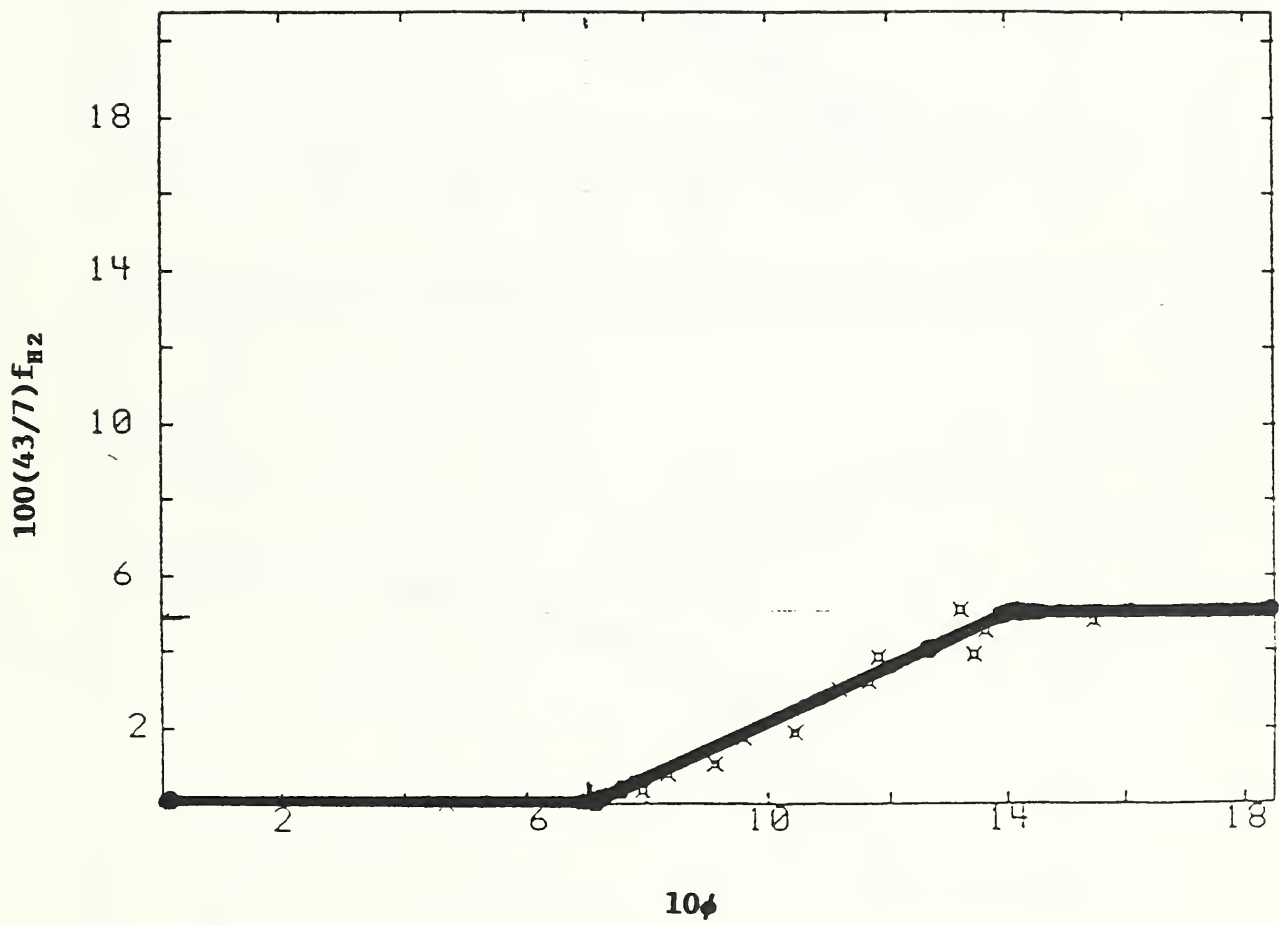


Figure 15. Combustion of hexanes ( $C_6H_{14}$ ). Data from [6]. Analytic representation of  $f_{H_2}$  according to the curve fit of Eq. (75).

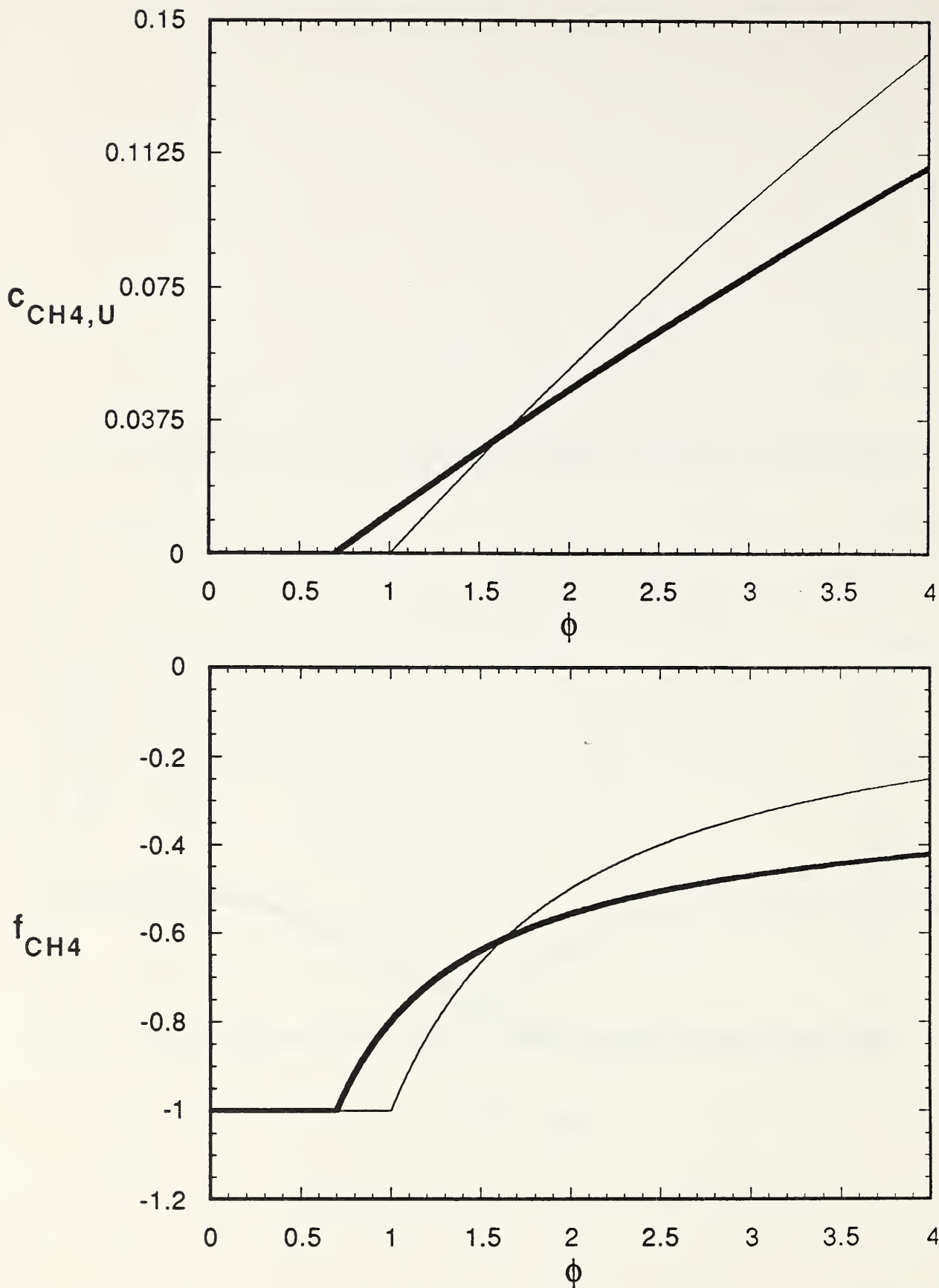


Figure 16. Combustion of methane ( $CH_4$ ). TOP - Analytic representations of  $c_{CH_4,U}^{(SS),REACTOUT}$ : for complete stoichiometric combustion, Eqs. (51)-(53) or Eqs. (55) and (56) ( — ); and for the curve-fit of Eq. (58) ( ——— ). BOTTOM - Corresponding analytic representations of  $f_{CH_4}$  according to Eq. (23).

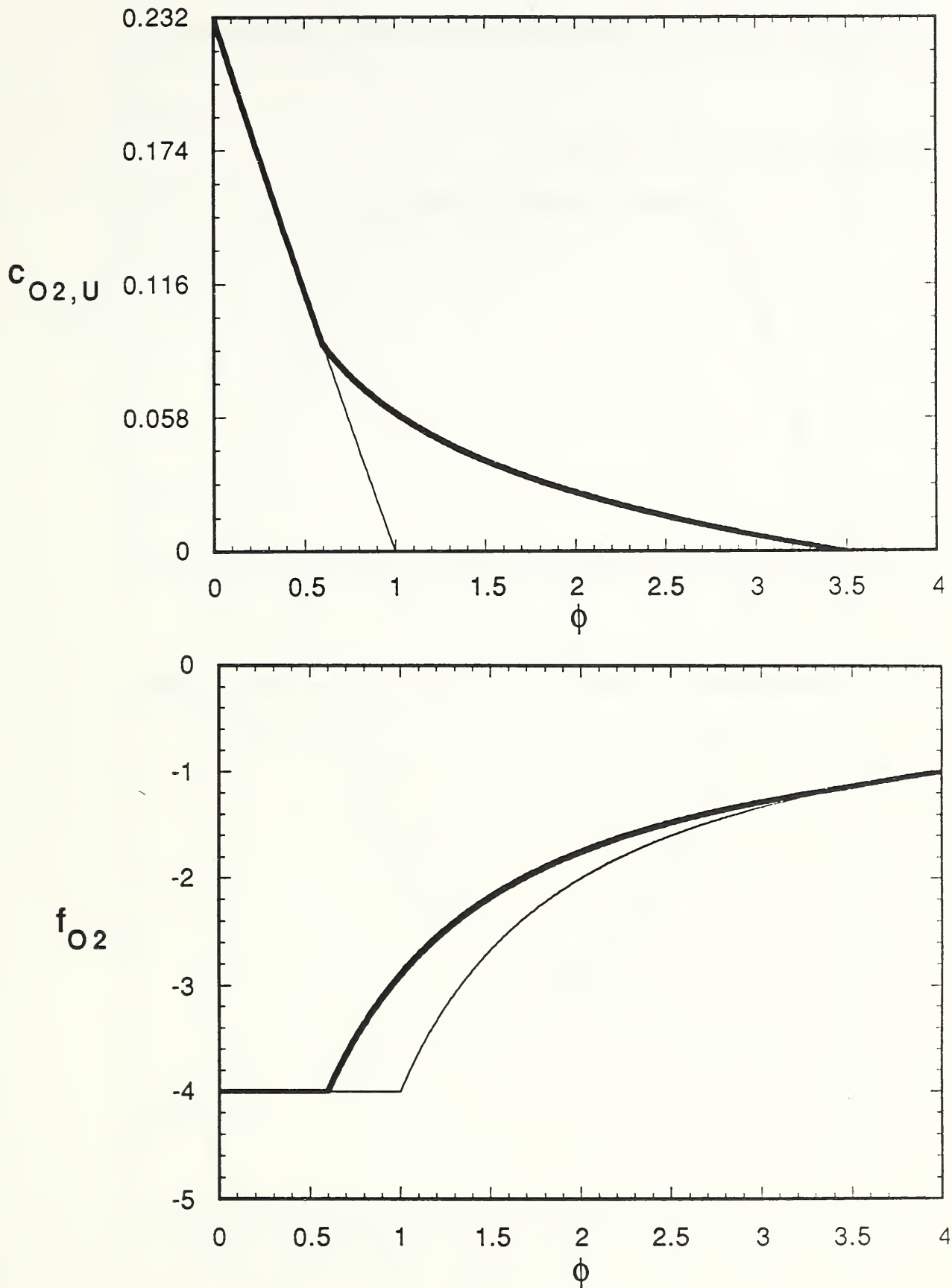


Figure 17. Combustion of methane ( $CH_4$ ): TOP - Analytic representations of  $C_{O_2,REACTOUT}^{(SS)}$ : for complete stoichiometric combustion, Eq. (59) (      ); and for the curve fit of Eq. (61) (      ). BOTTOM - Corresponding analytic representations of  $f_{O_2}$  according to Eq. (24).

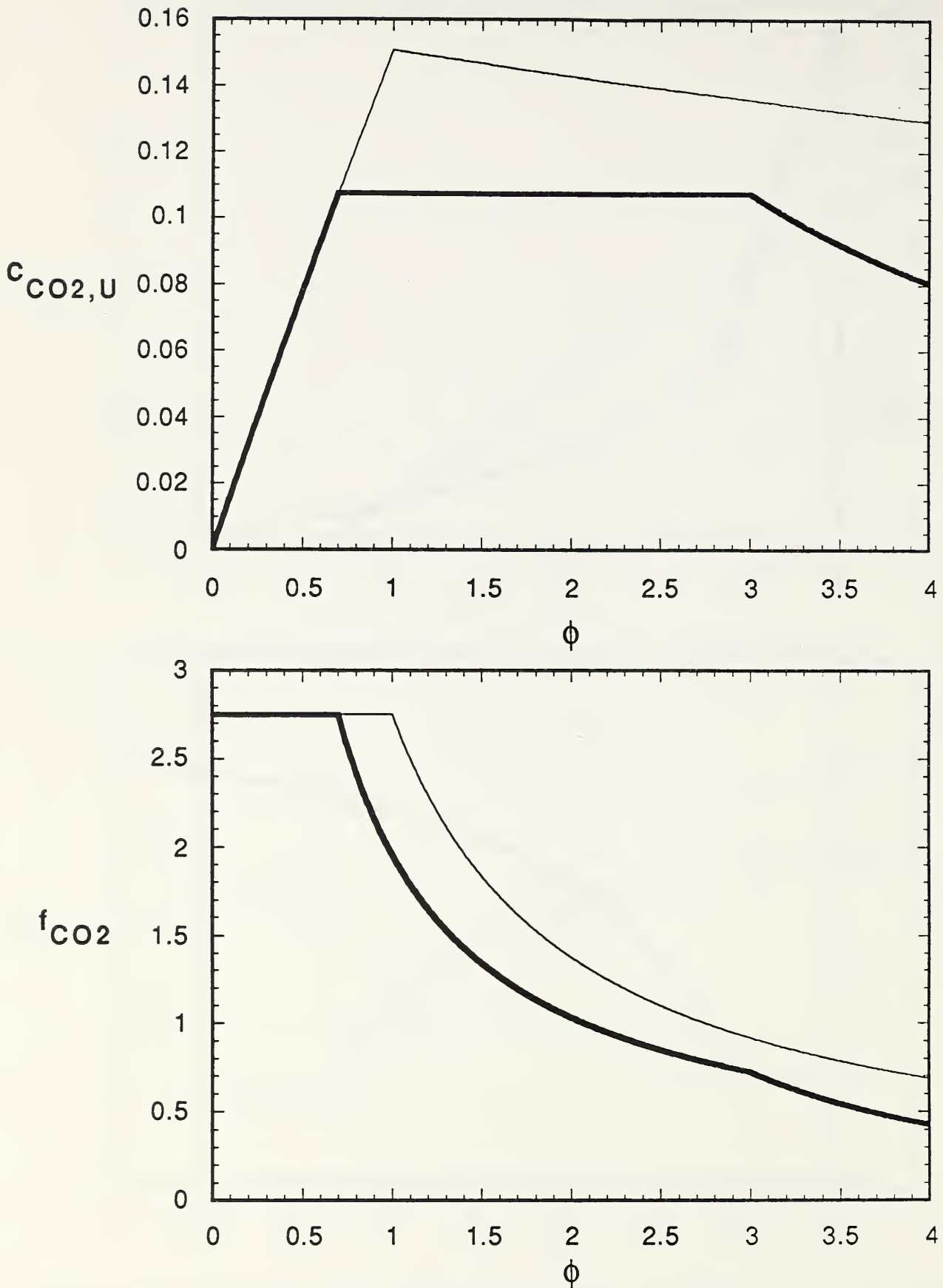


Figure 18. Combustion of methane ( $CH_4$ ): TOP - Analytic representations of  $c_{CO_2,REACTOUM}^{(SS)}$  for complete stoichiometric combustion, Eq. (62) (        ), and for the curve fit of Eq. (64) and (65) ( **—** ). BOTTOM - Corresponding analytic representations of  $f_{CO_2}$  according to Eq. (25).



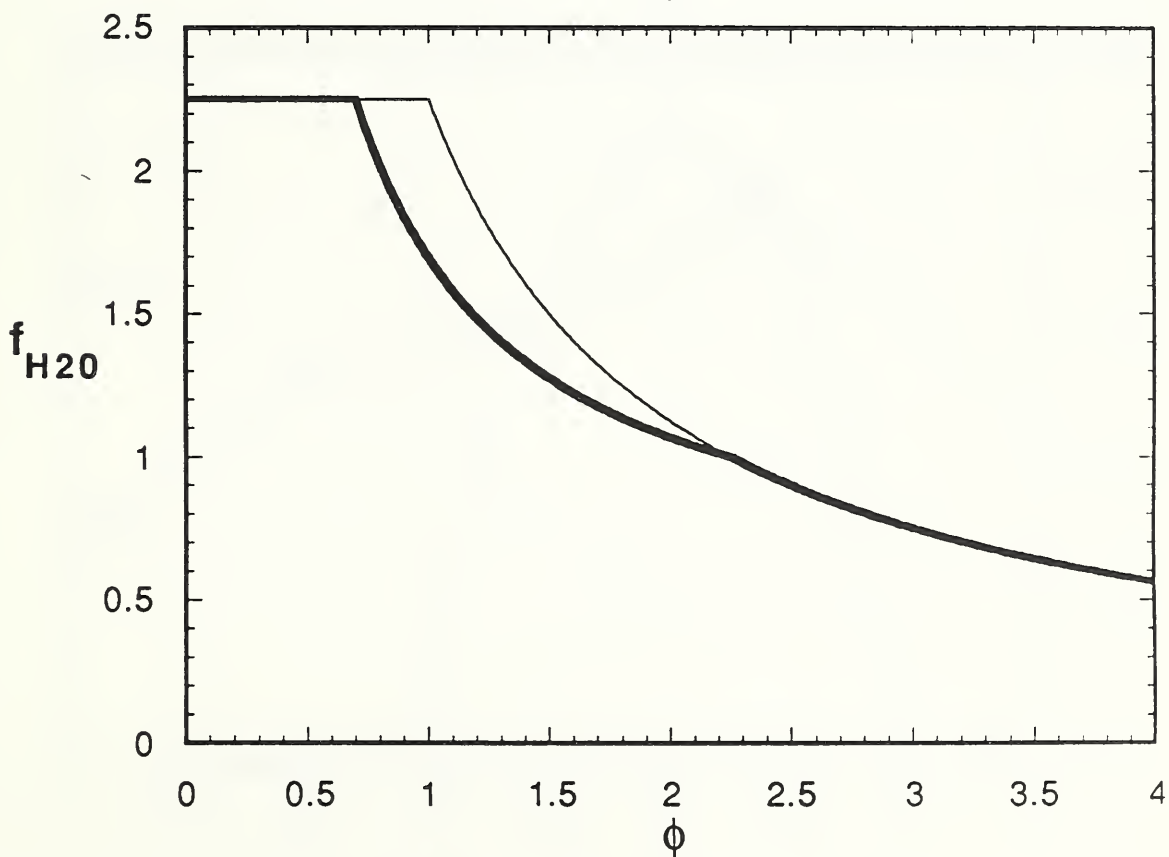
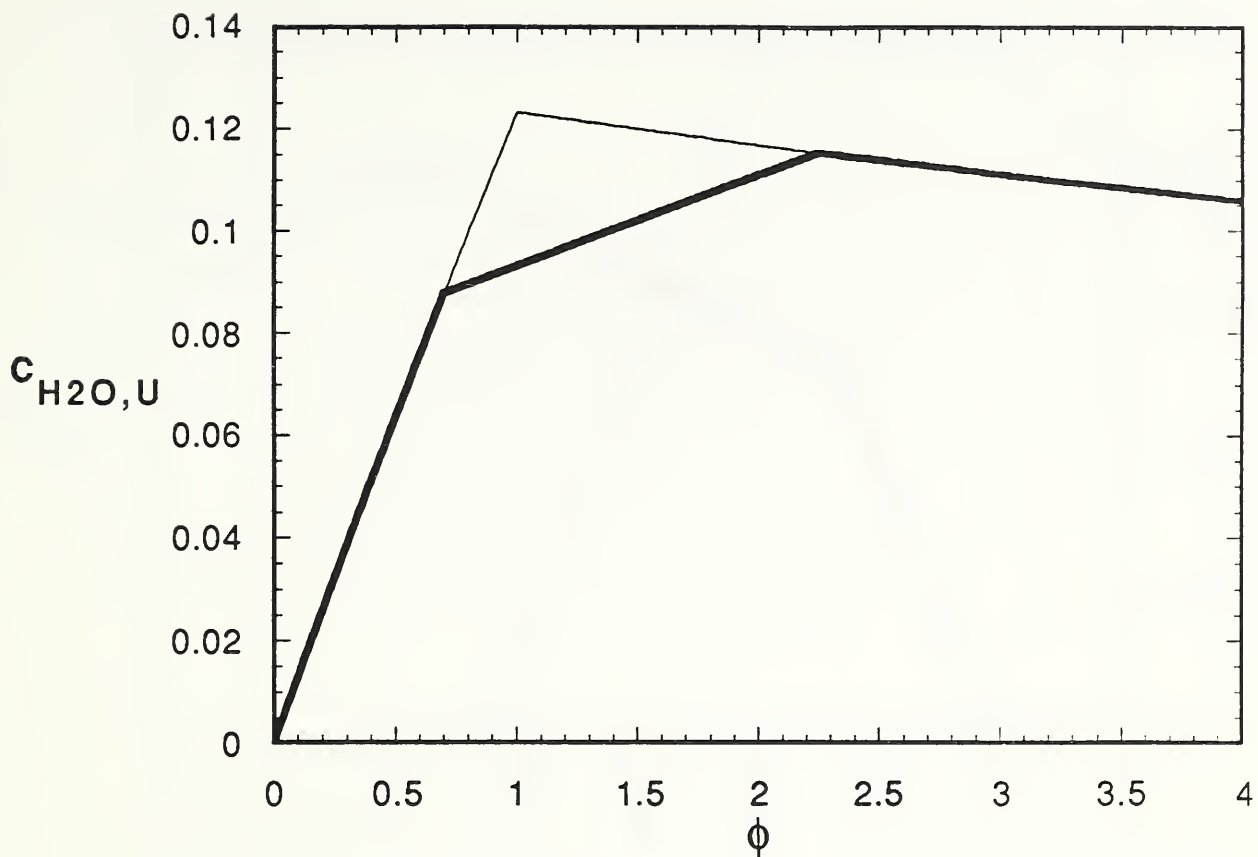


Figure 19. Combustion of methane ( $CH_4$ ): TOP - Analytic representations of  $C_{H_2O,REACTOUT}^{(SS)}$  for complete stoichiometric combustion, Eq. (63) (        ), and for the curve fit of Eqs. (66) and (67) (  ). BOTTOM - Corresponding analytic representations of  $f_{H_2O}$  according to Eq. (25).

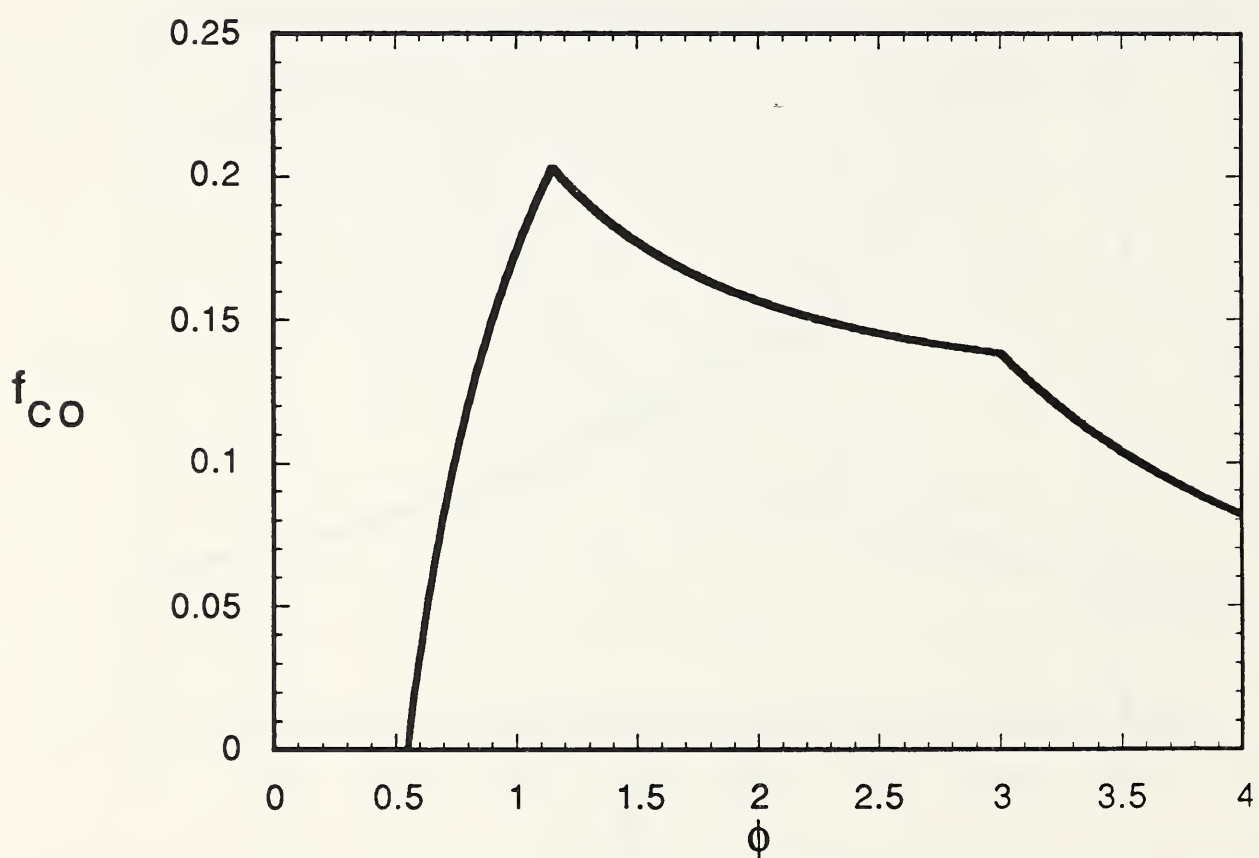
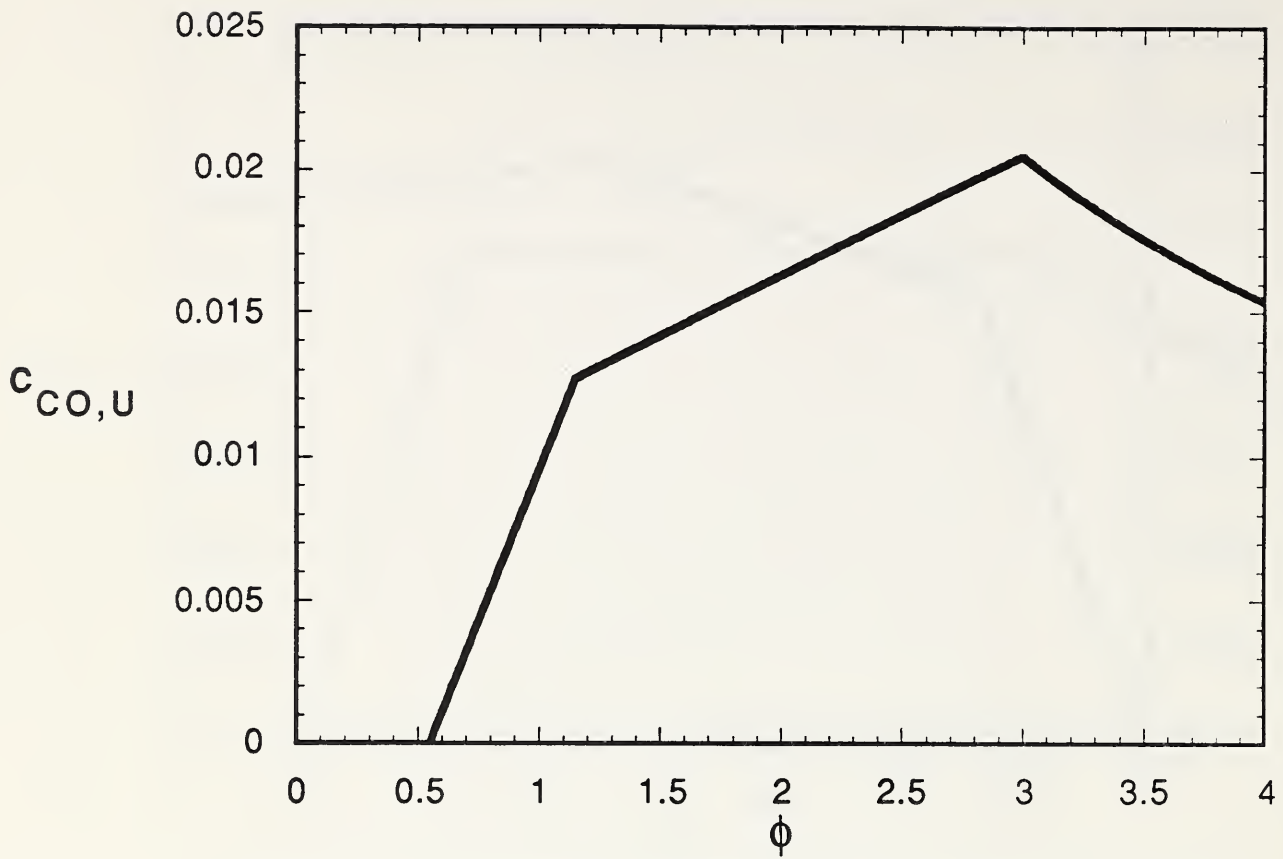


Figure 20. Combustion of methane ( $CH_4$ ): TOP - Analytic representation of  $c_{CO,REACTOUR}^{(SS)}$  according to Eqs. (68) and (69). BOTTOM - Corresponding analytic representations of  $f_{CO}$  according to Eq. (25).

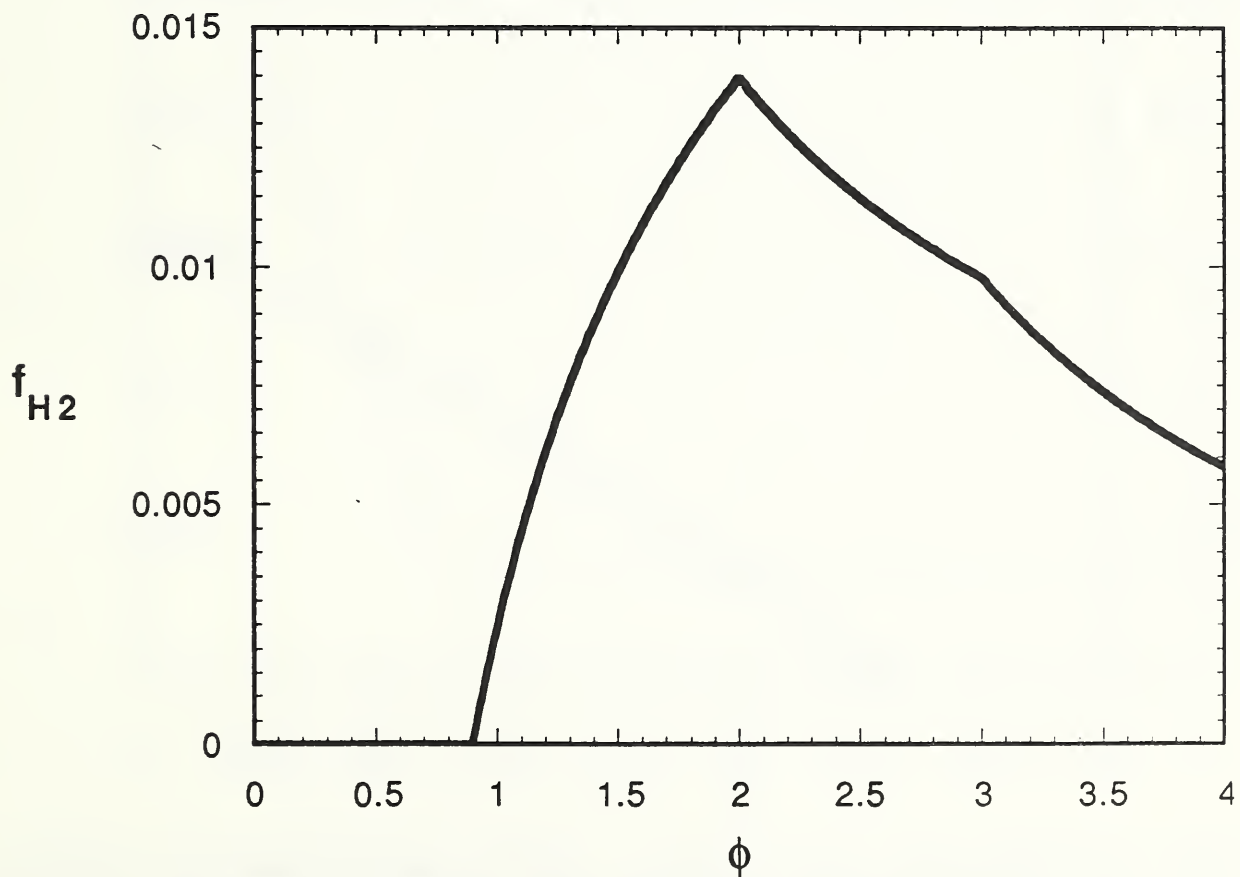
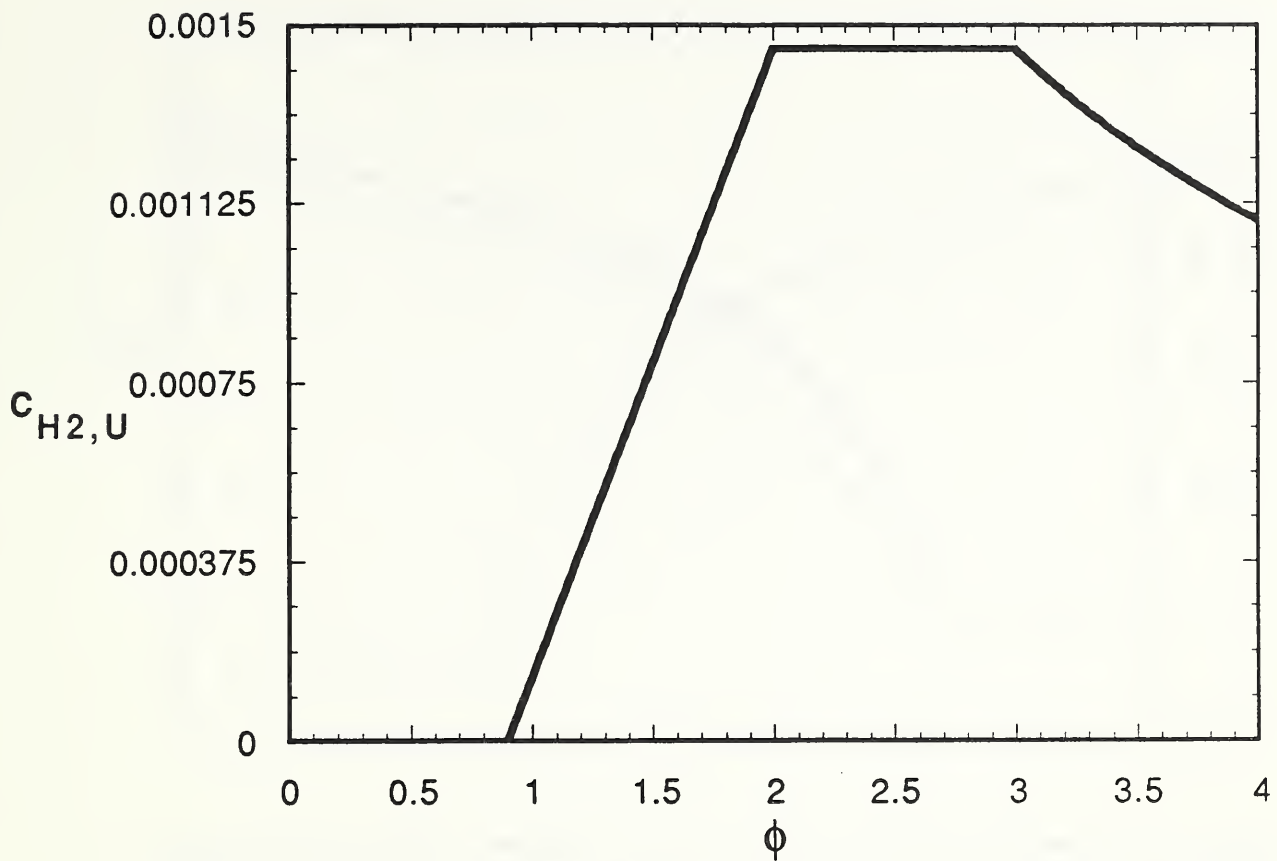


Figure 21. Combustion of methane ( $CH_4$ ): TOP - Analytic representation of  $c_{H_2,REACTOR}^{(SS)}$  according to Eq. (70). BOTTOM - Corresponding analytic representation of  $f_{H_2}$  according to Eq. (25).

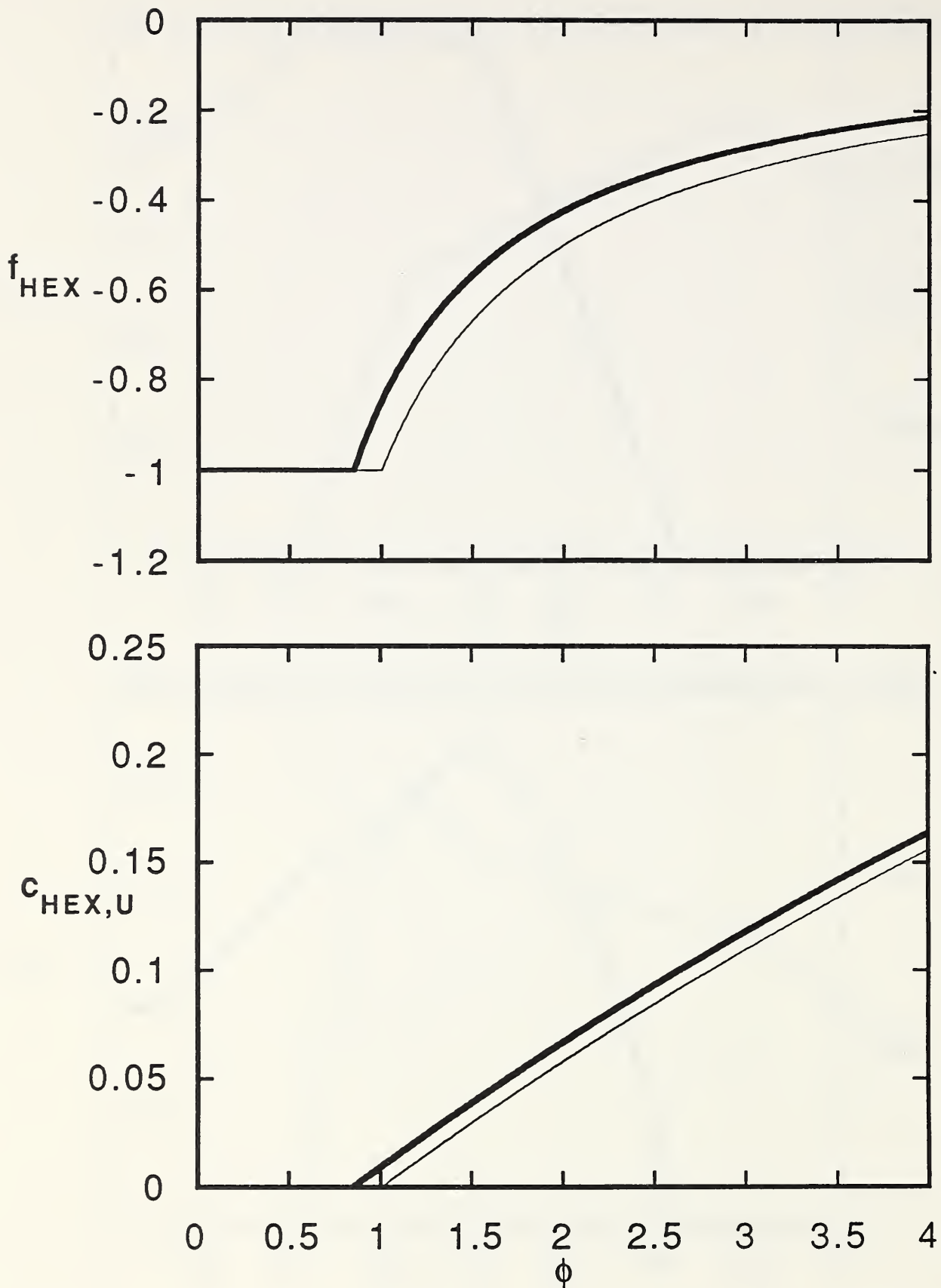


Figure 22. Combustion of hexanes ( $\text{C}_6\text{H}_{14}$ ): TOP - Analytic representations of  $f_{\text{C}_6\text{H}_{14}}$  for complete stoichiometric combustion, Eqs. (51)-(53) and (71) ( — ), and of the curve-fit of Eqs. (71)-(73) ( ——— ). BOTTOM - Corresponding analytic representations of  $c_{\text{C}_6\text{H}_{14},\text{REACTOUT}}^{\{\text{SS}\}}$  according to Eq. (20).



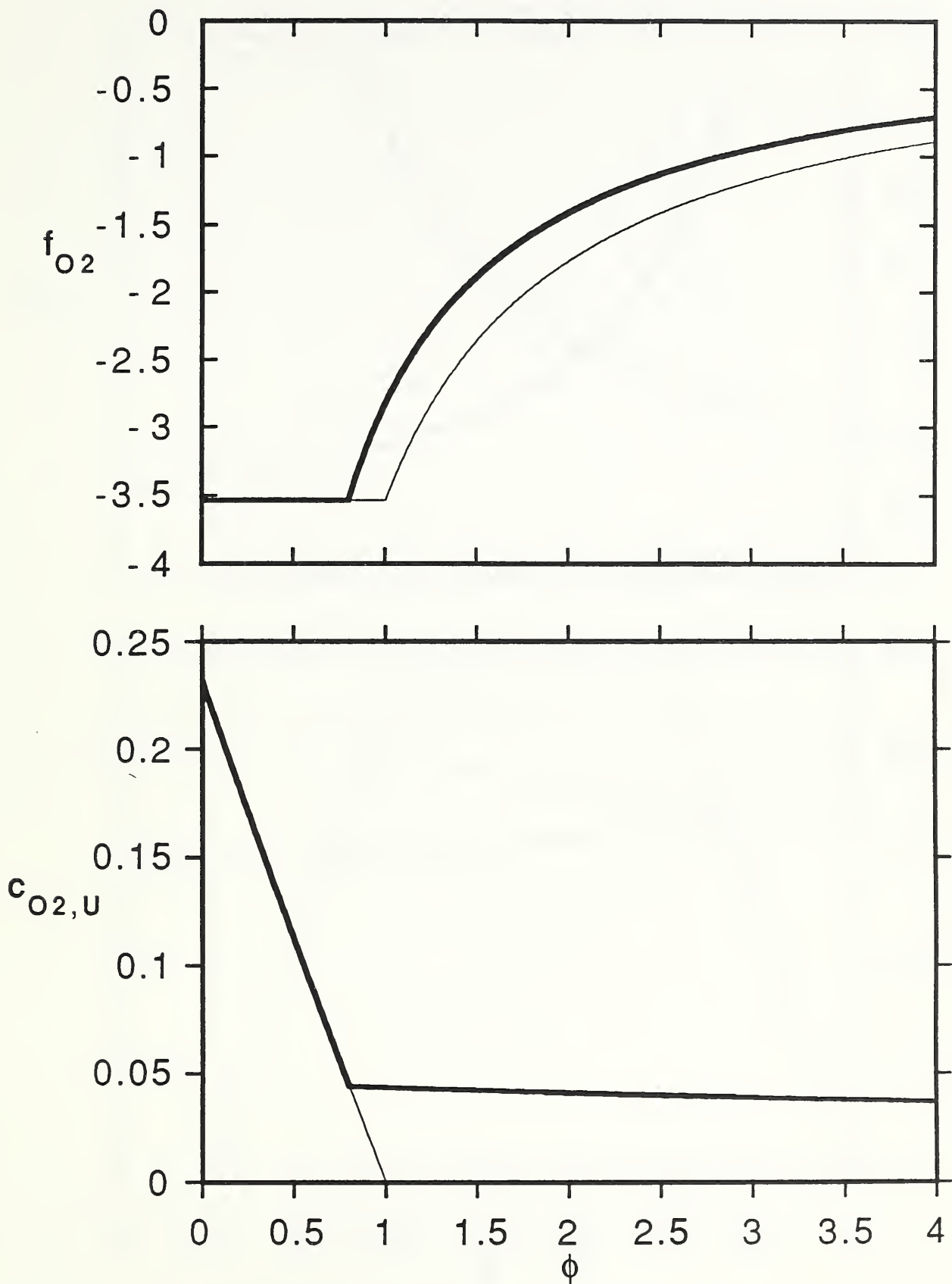


Figure 23. Combustion of hexanes ( $C_6H_{14}$ ): TOP - Analytic representations of  $f_{O_2}$  for complete stoichiometric combustion, Eqs. (51)-(53) and (71) ( ——— ), and of the curve-fit of Eqs. (71)-(73) ( ——— ). BOTTOM - Corresponding analytic representations of  $c_{O_2,U}^{(SS)} A_{TOUR}$  according to Eq. (21).

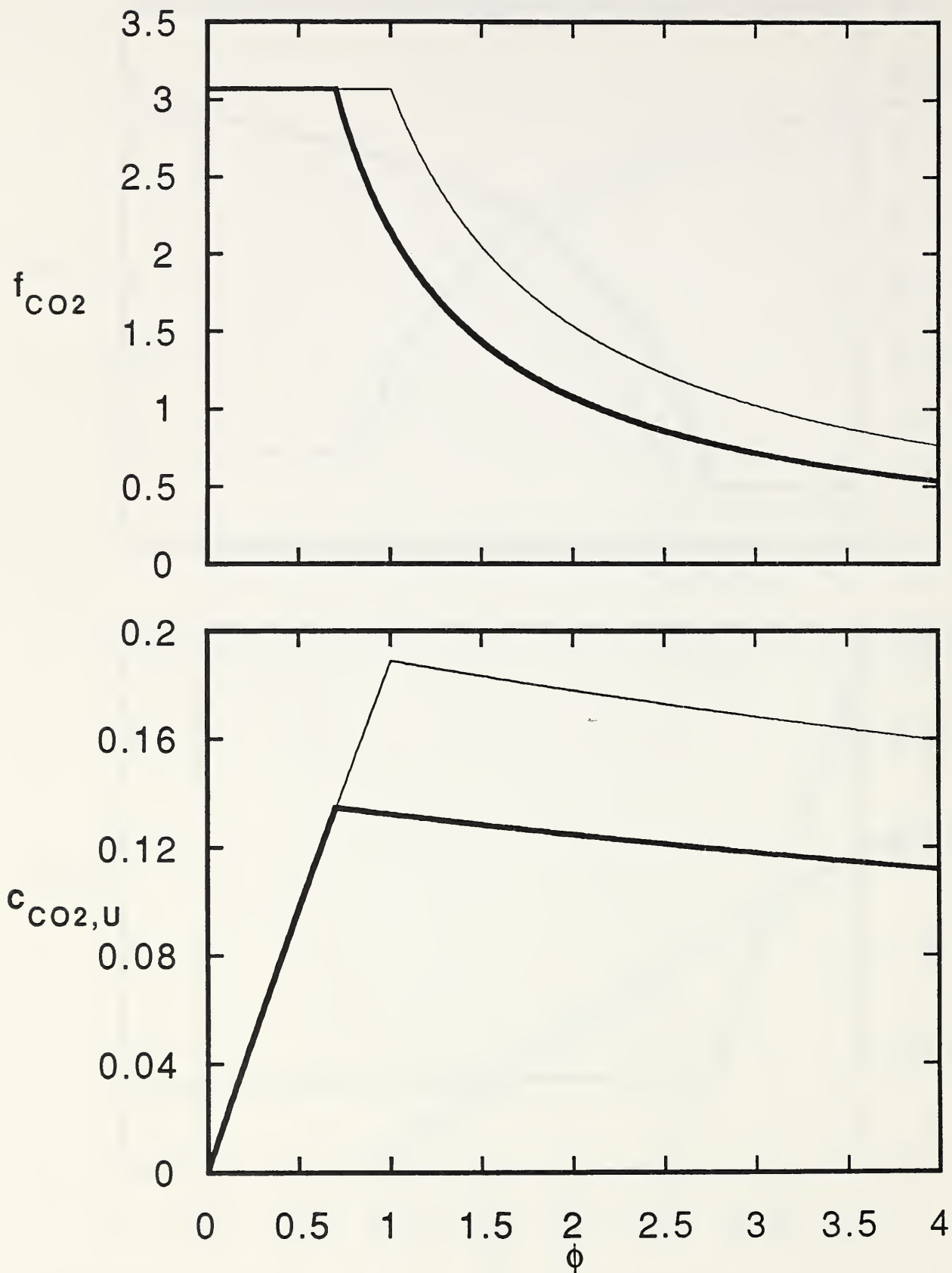


Figure 24. Combustion of hexanes ( $C_6H_{14}$ ): TOP - Analytic representations of  $f_{CO_2}$  for complete stoichiometric combustion, Eqs. (51)-(53) and (71) ( — ), and of the curve-fit of Eqs. (71)-(73) ( ——— ). BOTTOM - Corresponding analytic representations of  $c_{CO_2,REACTOUT}^{(SS)}$  according to Eq. (22).

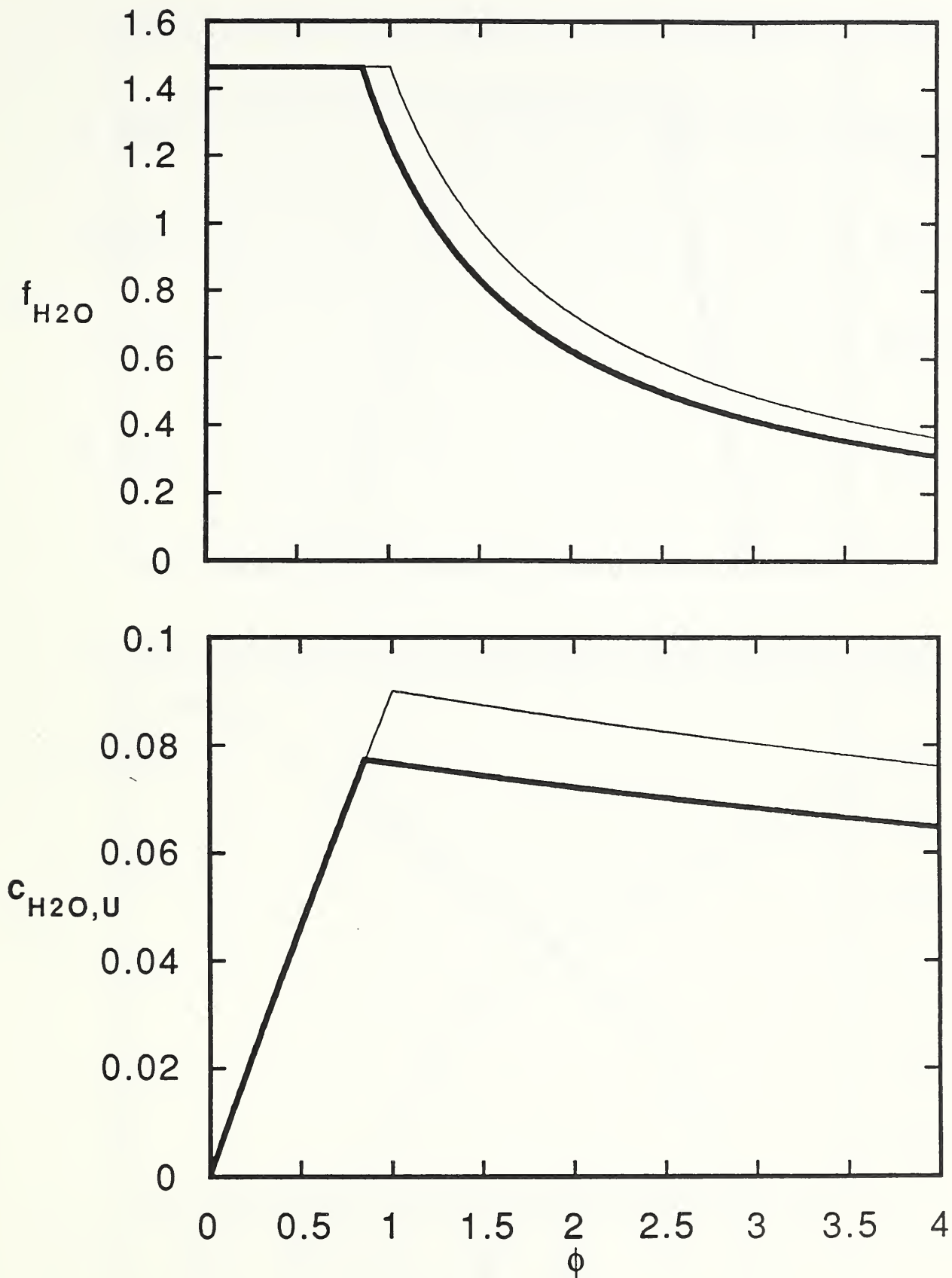


Figure 25. Combustion of hexanes ( $C_6H_{14}$ ): TOP - Analytic representations of  $f_{H_2O}$  for complete stoichiometric combustion, Eqs. (51)-(53) and (71) ( ——— ), and of the curve-fit of Eqs. (71)-(73) ( ——— ). BOTTOM - Corresponding analytic representations of  $c_{H_2O,REACTOUT}^{(SS)}$  according to Eq. (22).

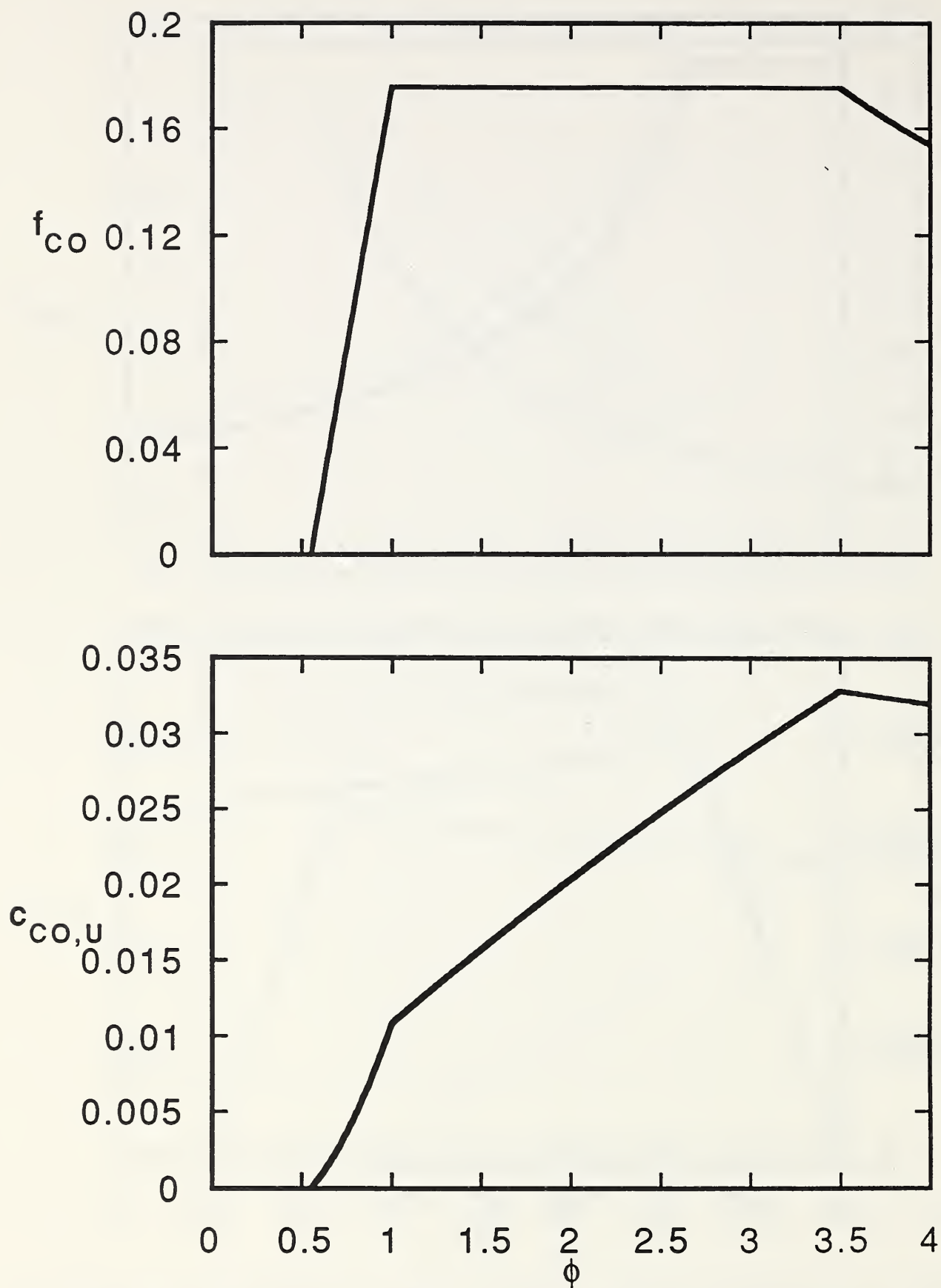


Figure 26. Combustion of hexanes ( $C_6H_{14}$ ): TOP - Analytic representations of  $f_{CO}$  for the curve-fit of Eq. (74). BOTTOM - Corresponding analytic representation of  $c_{CO,REACTOR}^{SS}$  according to Eq. (22).



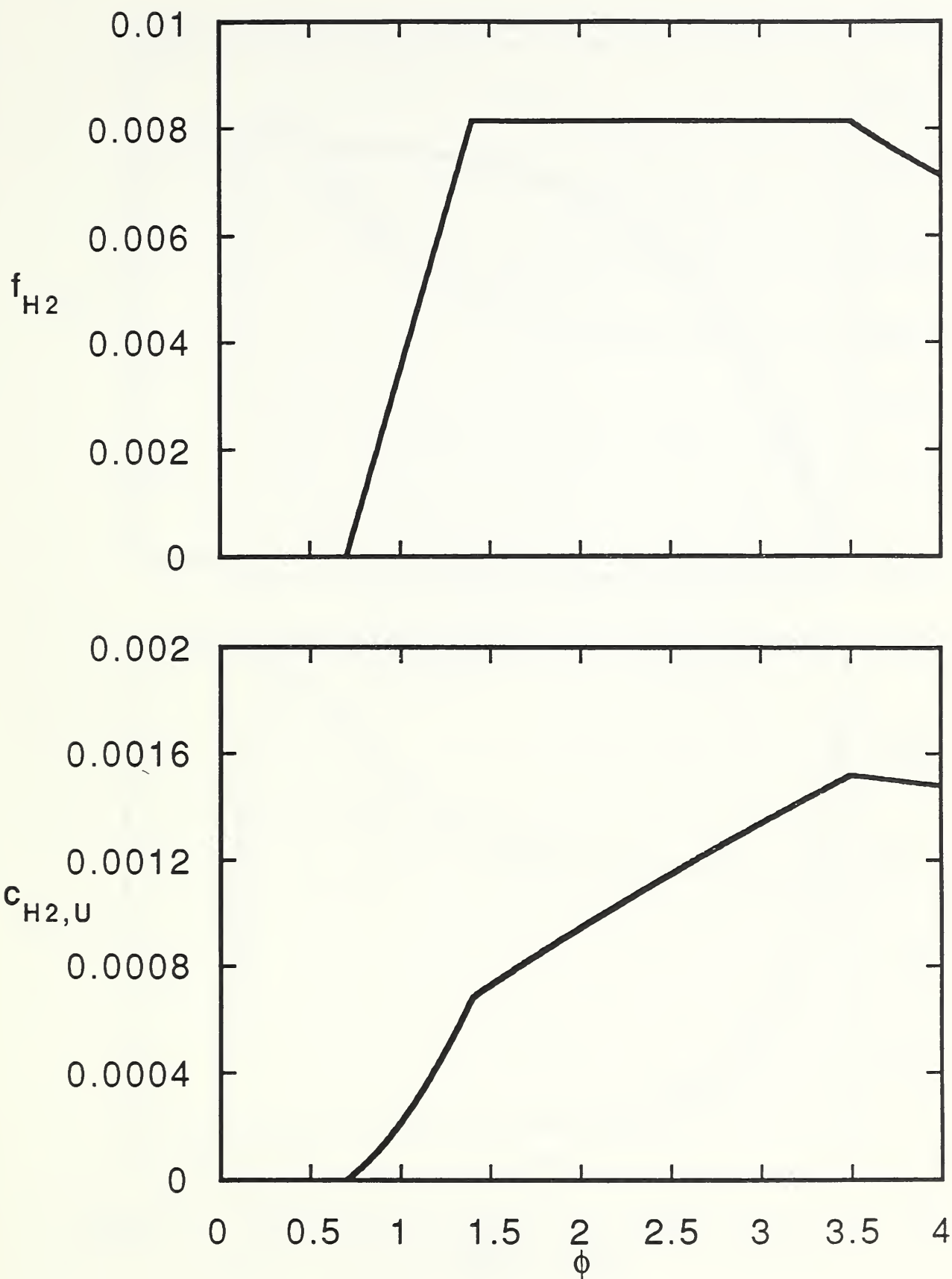


Figure 27. Combustion of hexanes ( $C_6H_{14}$ ): TOP - Analytic representations of  $f_{H_2}$  for the curve-fit of Eq. (75). BOTTOM - Corresponding analytic representation of  $C_{H_2,U}^{(SS)}$  according to Eq. (22).

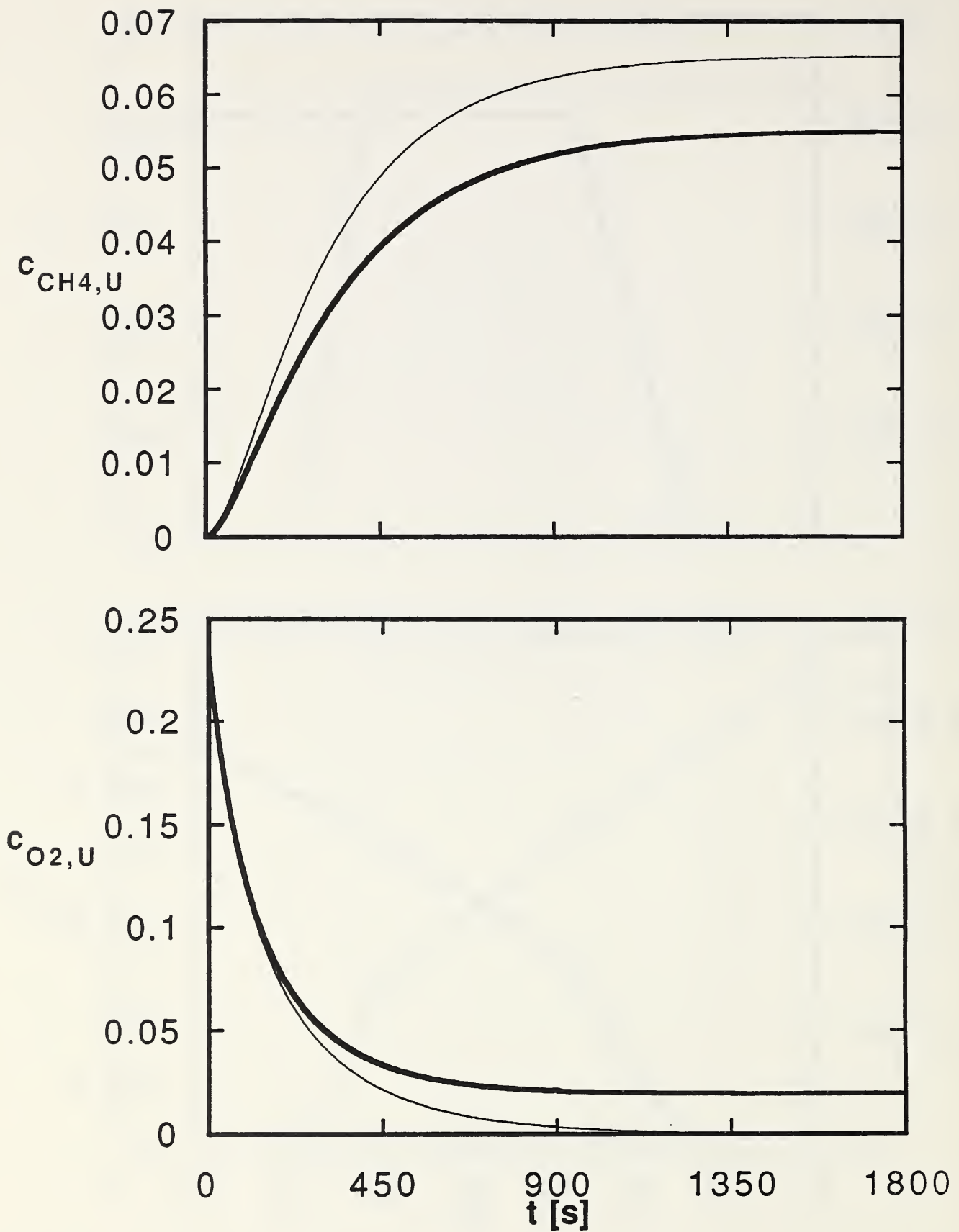


Figure 28. Results of GGERM simulation of test 1 of Appendix B of [2] using the real combustion model ( ——— ) and the complete stoichiometric combustion model ( ——— ). TOP: Plots of  $c_{CH_4,U}$ . BOTTOM: Plots of  $c_{O_2,U}$ .

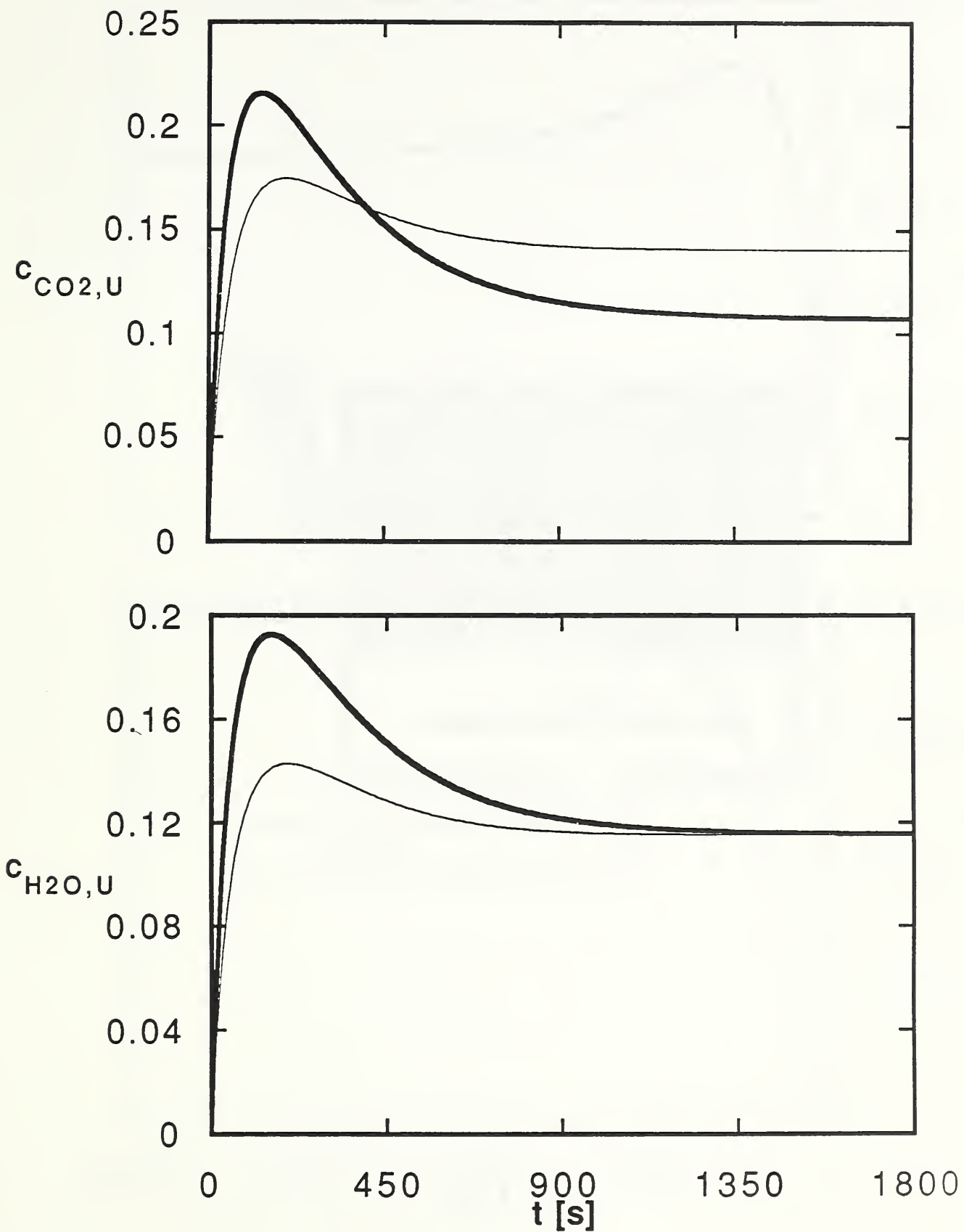


Figure 29. Results of GGERM simulation of test 1 of Appendix B of [2] using the real combustion model ( — ) and the complete stoichiometric combustion model ( — ). TOP: Plots of  $c_{CO_2,U}$ . BOTTOM: Plots of  $c_{H_2O,U}$ .

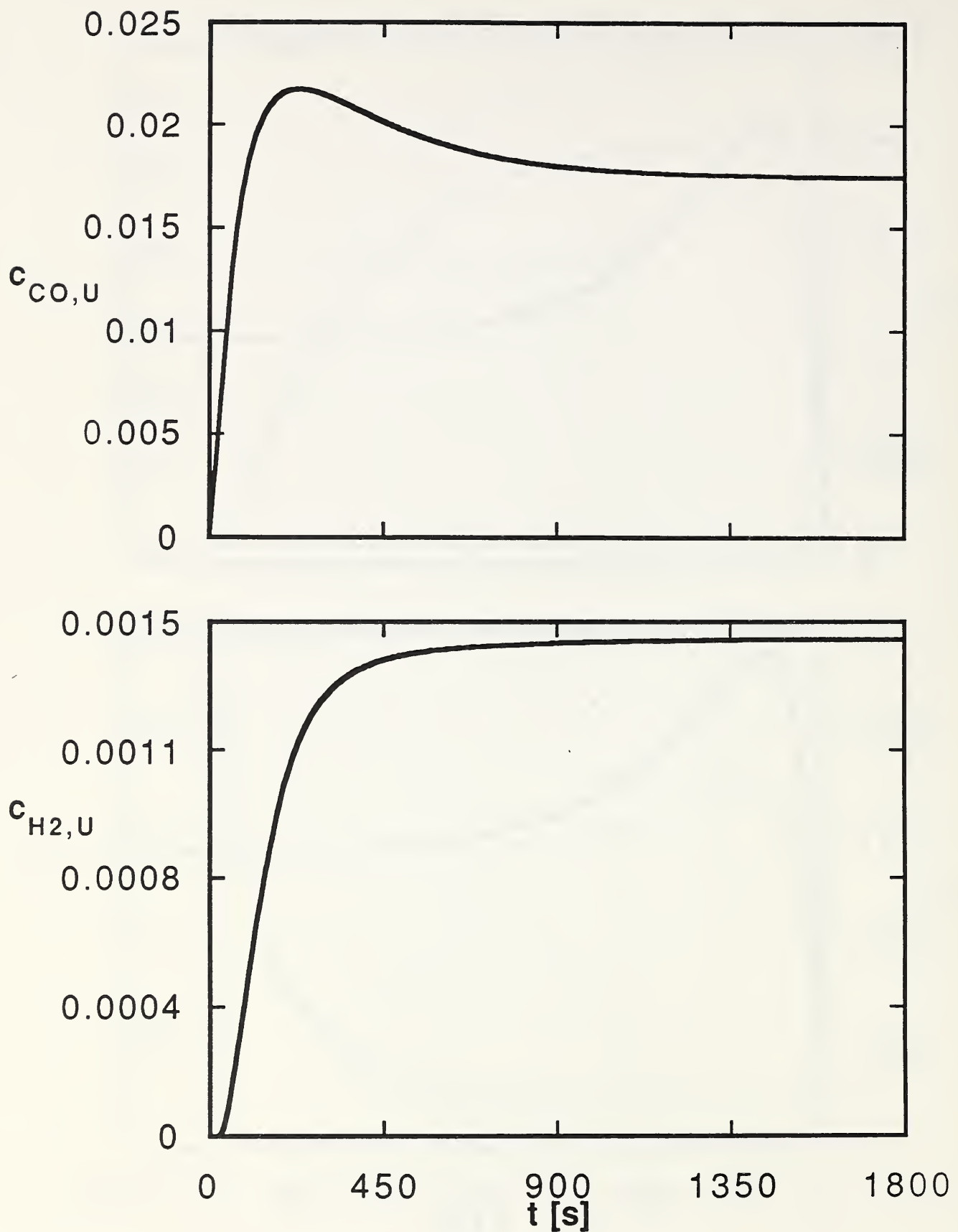


Figure 30. Results of GGERM simulation of test 1 of Appendix B of [2] using the real combustion model ( — ) and the complete stoichiometric combustion model ( - - ). TOP: Plots of  $c_{CO,U}$ . BOTTOM: Plots of  $c_{H2,U}$ .



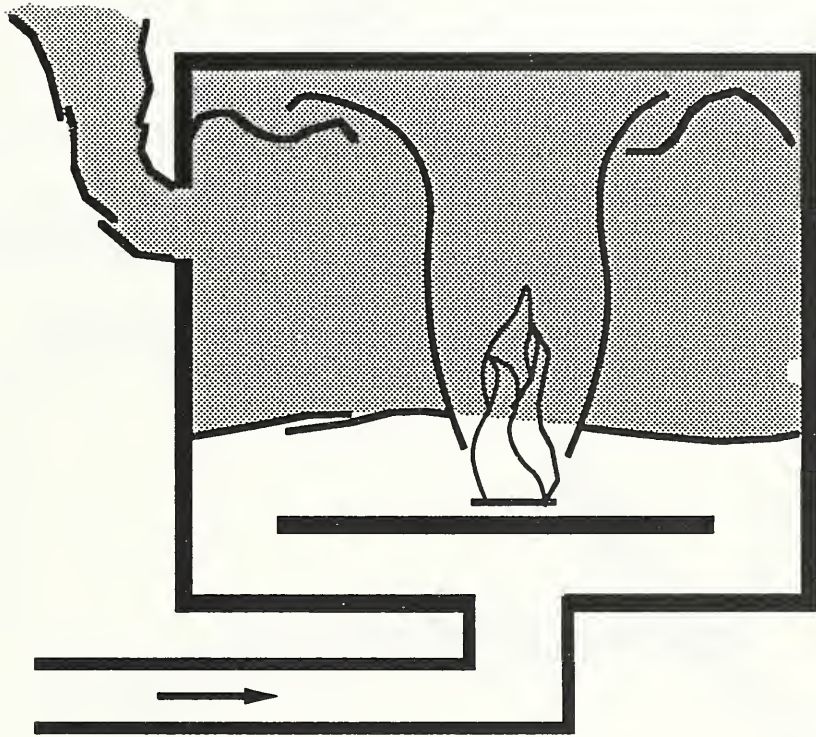


Figure 31. Test configuration for the experiments of [2].

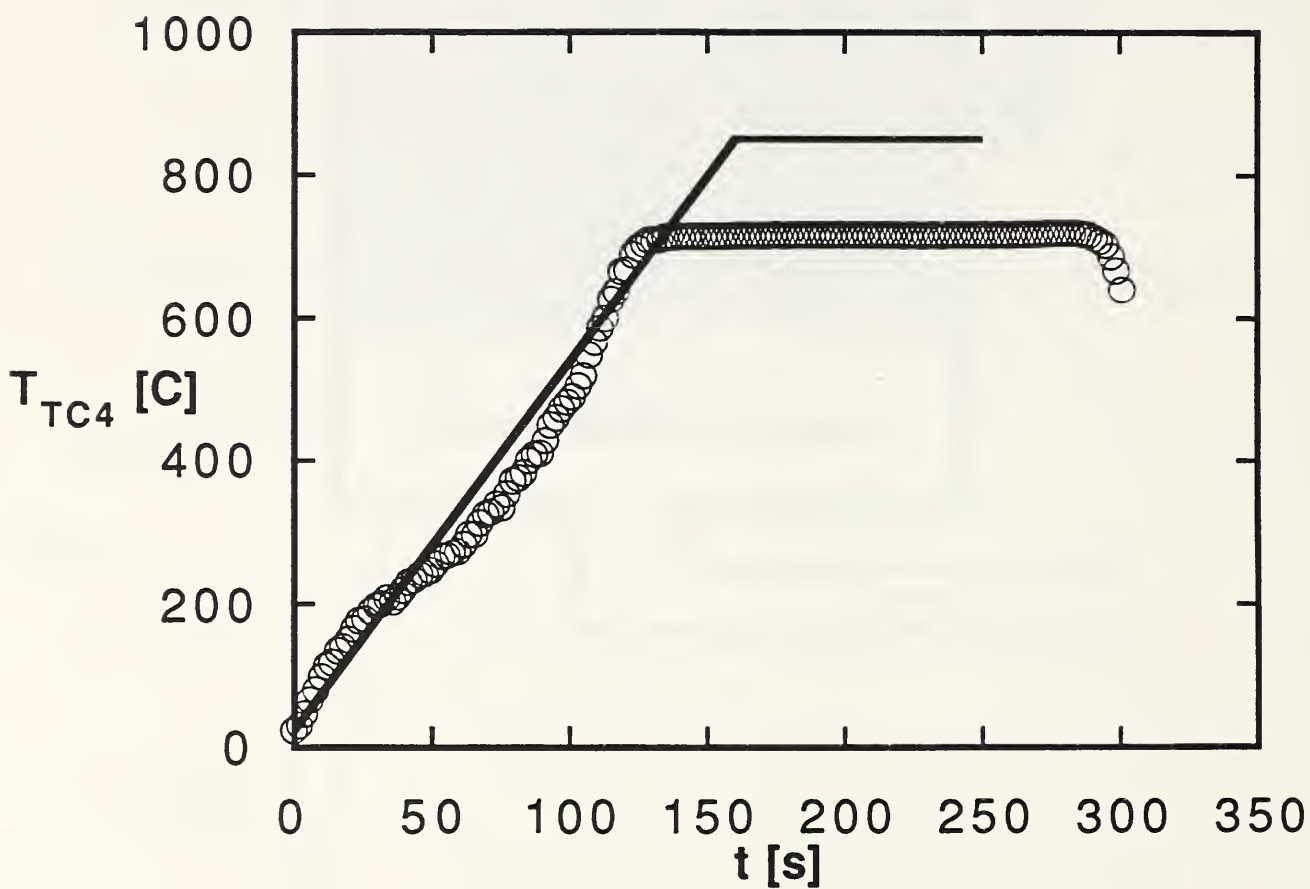


Figure 32. Large-burn hexane experiment of [3]. Temperature data from the thermocouple located approximately at the mid-elevation of the upper layer data. Curve fit of the data used in the analysis.

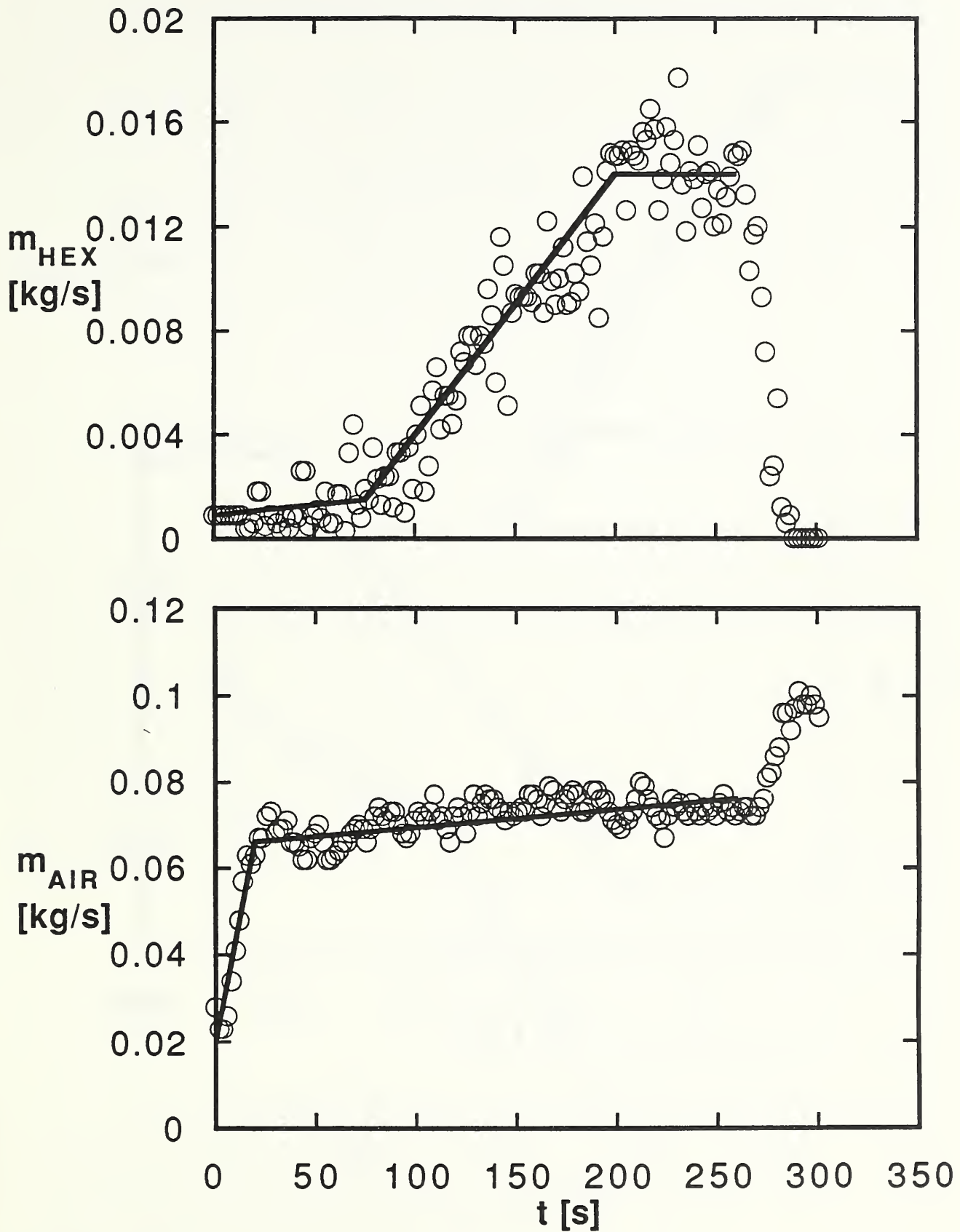


Figure 33. Large-burn hexane experiment of [3]. TOP - Hexane pyrolysis rate data and curve fit of the data used in the analysis; BOTTOM - airflow rate data and curve fit of the data used in the analysis to approximate  $\dot{P}_{\text{FUEL, FLOWIN}}$ .

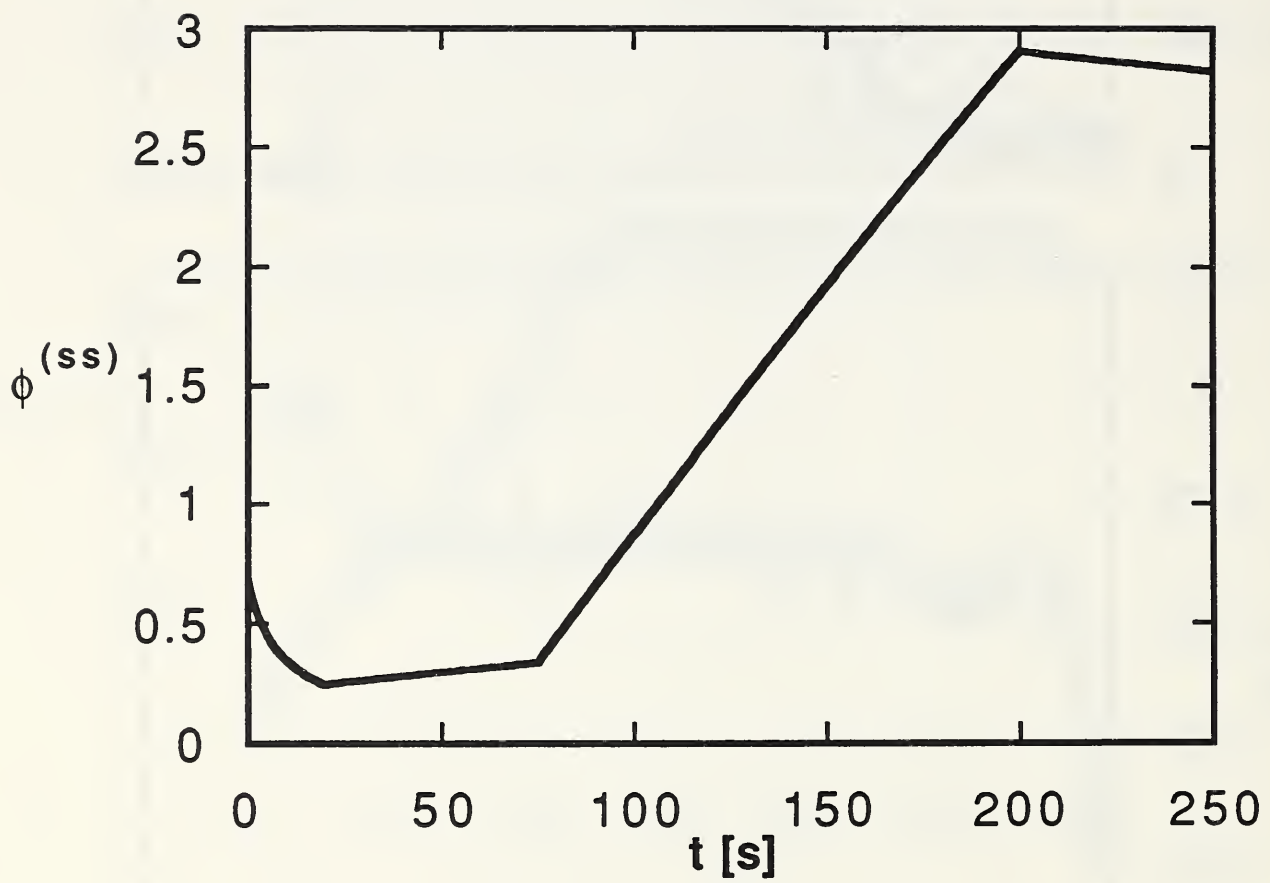


Figure 34. Plot of  $\phi^{(ss)}$  for the large-burn hexane experiment of [3]



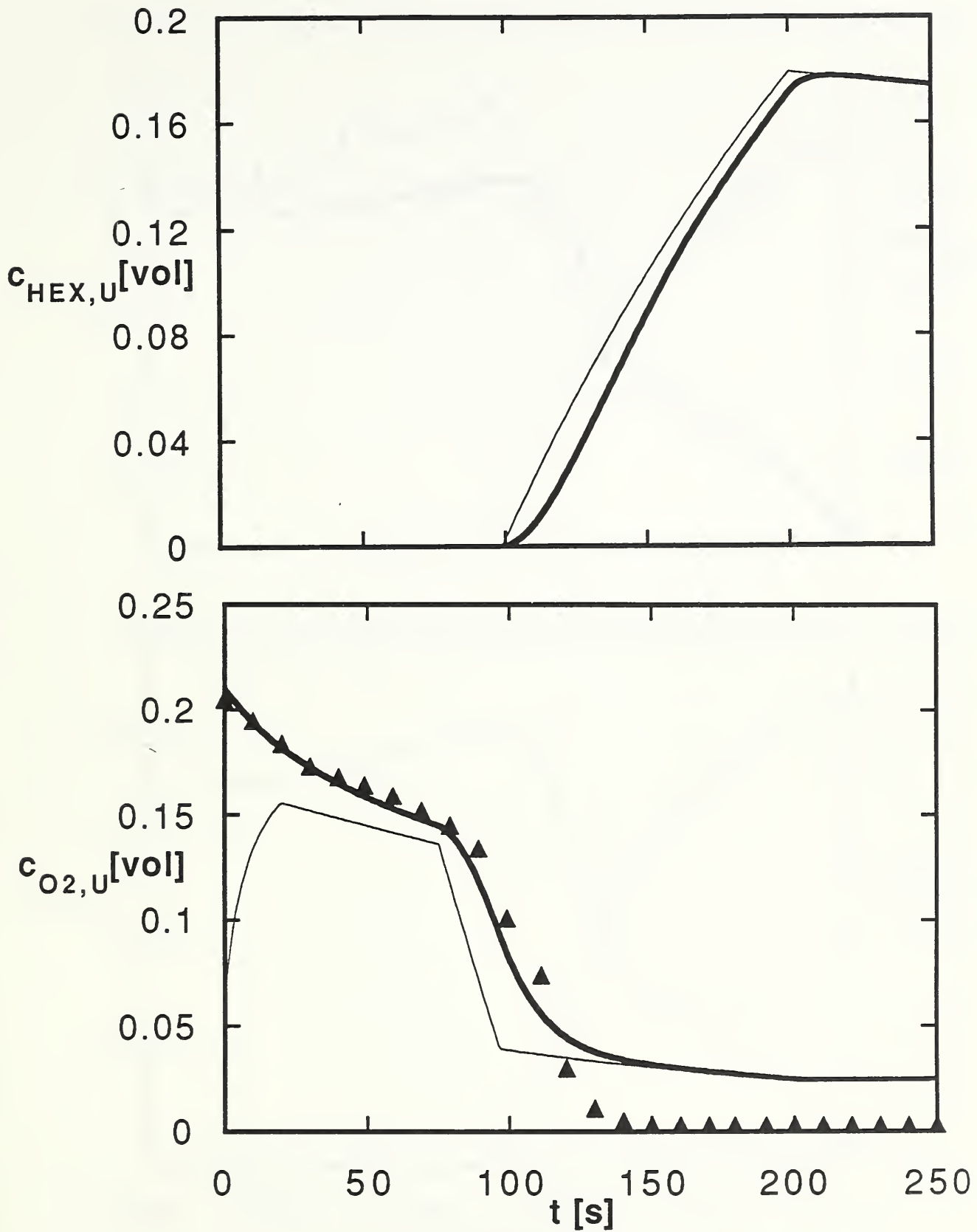


Figure 35. Results of simulating the large-burn hexane experiment of [3] using the real combustion model: The GGERM simulation (  $\text{—}$  ) and the quasi-steady approximation (  $\text{—}$  ). TOP: Plots of  $c_{\text{HEX},U}$  [vol]. BOTTOM: Plots of  $c_{\text{O}_2,U}$  [vol].

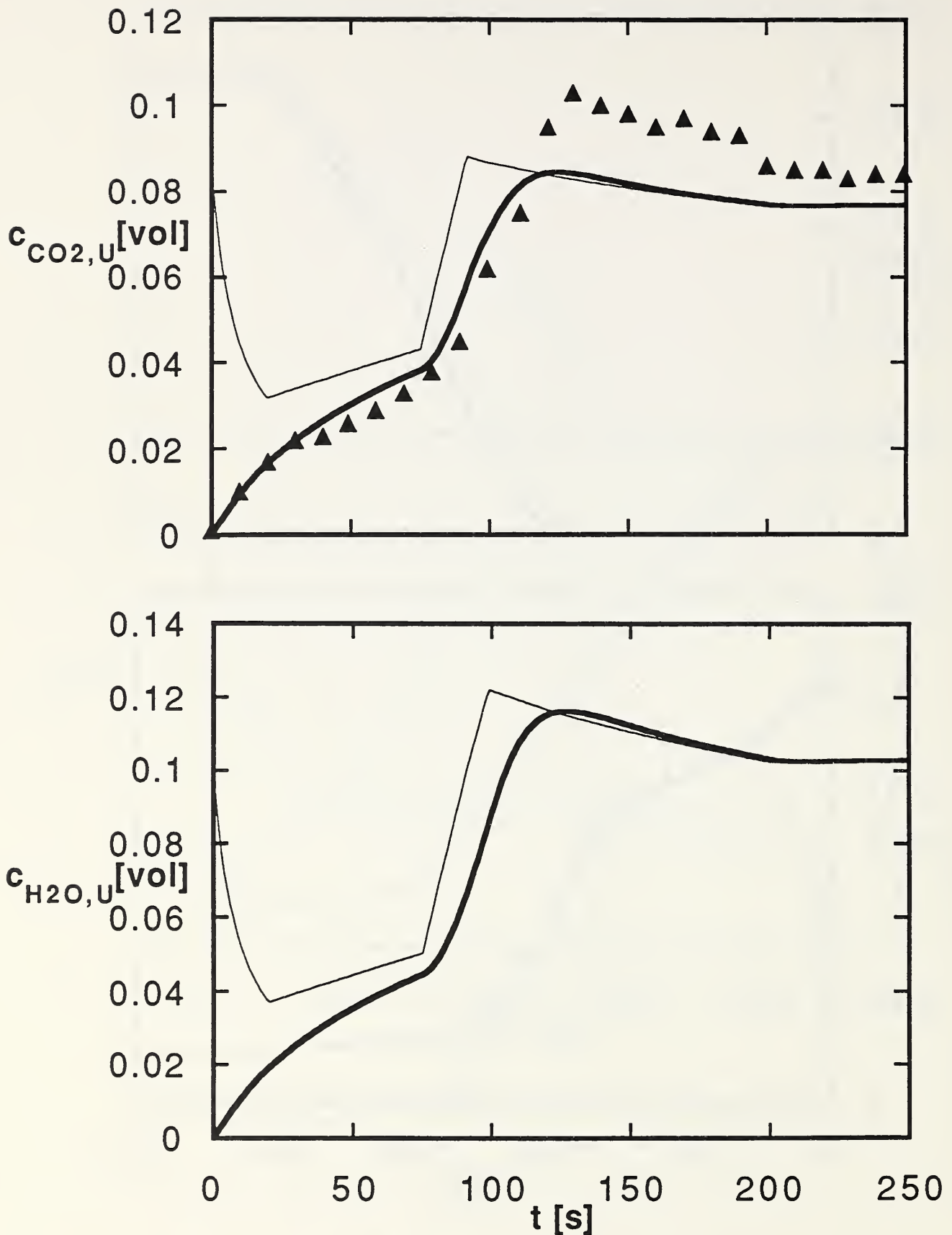


Figure 36. Results of simulating the large-burn hexane experiment of [3] using the real combustion model: The GGERM simulation ( **—** ) and the quasi-steady approximation ( **—** ). TOP: Plots of  $c_{\text{CO}_2, \text{U}}$  [vol]. BOTTOM: Plots of  $c_{\text{H}_2\text{O}, \text{U}}$  [vol].

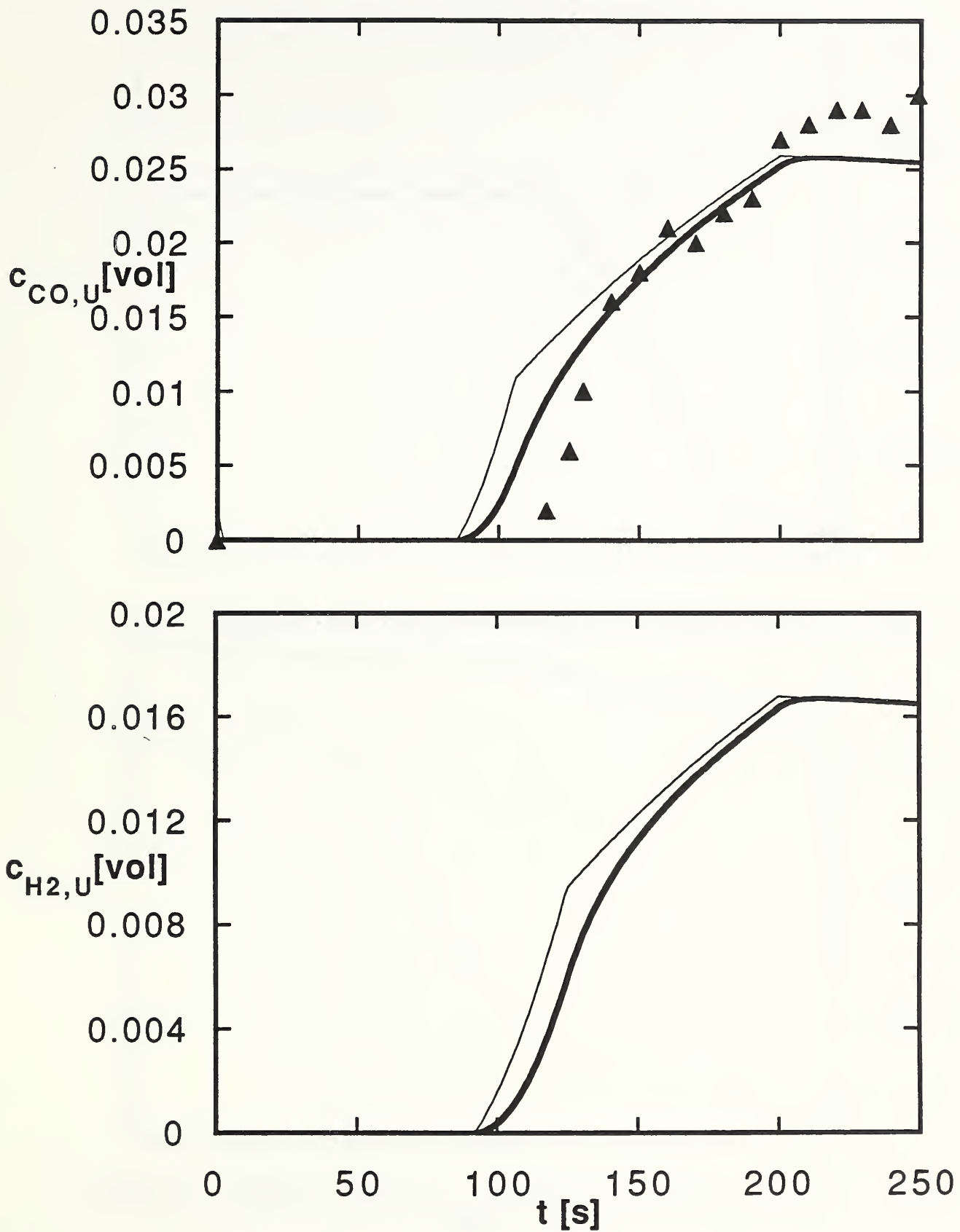


Figure 37. Results of simulating the large-burn hexane experiment of [3] using the real combustion model: The GGERM simulation ( **—** ) and the quasi-steady approximation ( **—** ). TOP: Plots of  $c_{CO,U}$  [vol]. BOTTOM: Plots of  $c_{H_2,U}$  [vol].

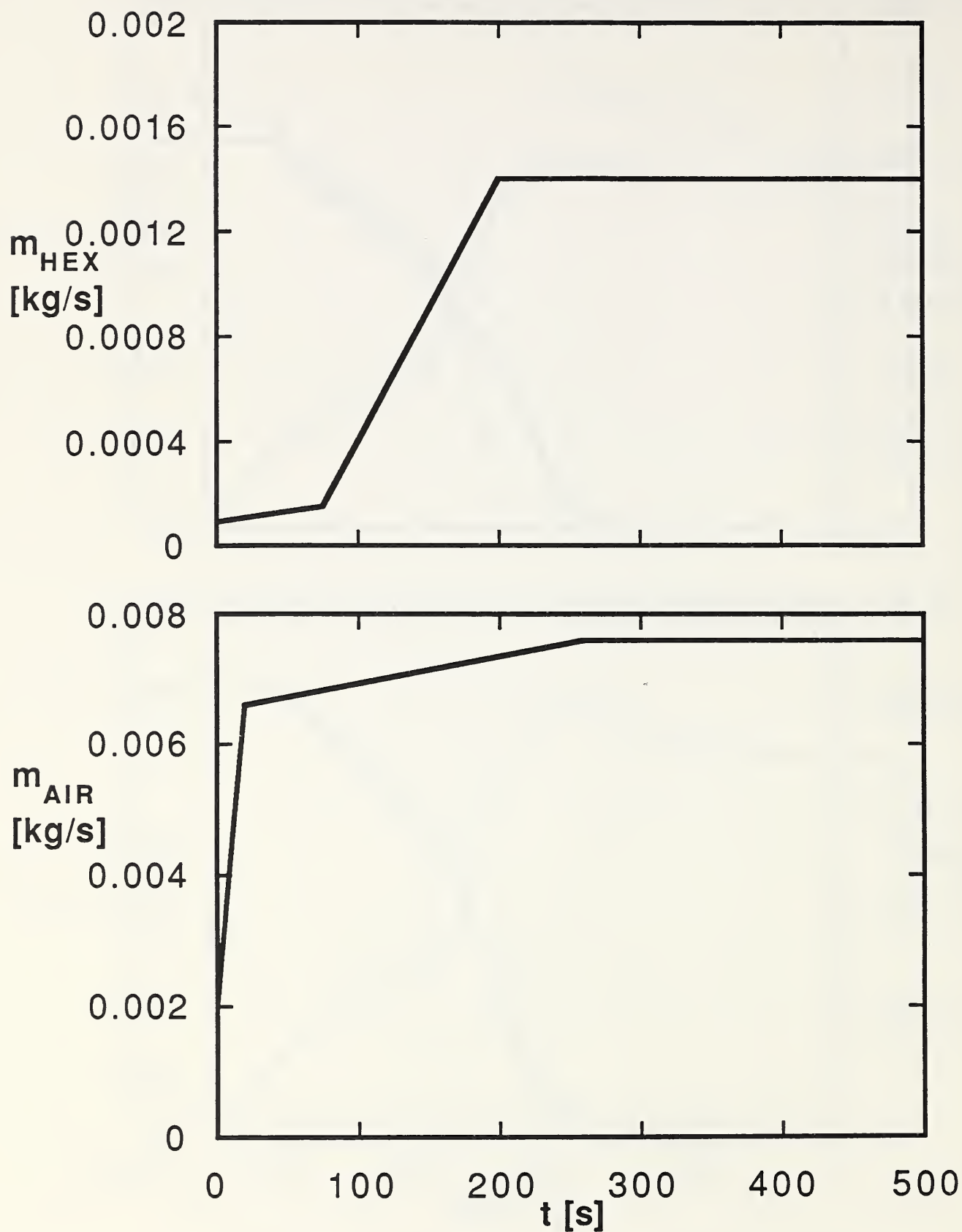


Figure 38. Hypothetical reference-[3]-type hexane experiment. TOP - Assumed hexane pyrolysis rate used in the analysis; BOTTOM - Assumed air flow rate used in the analysis.



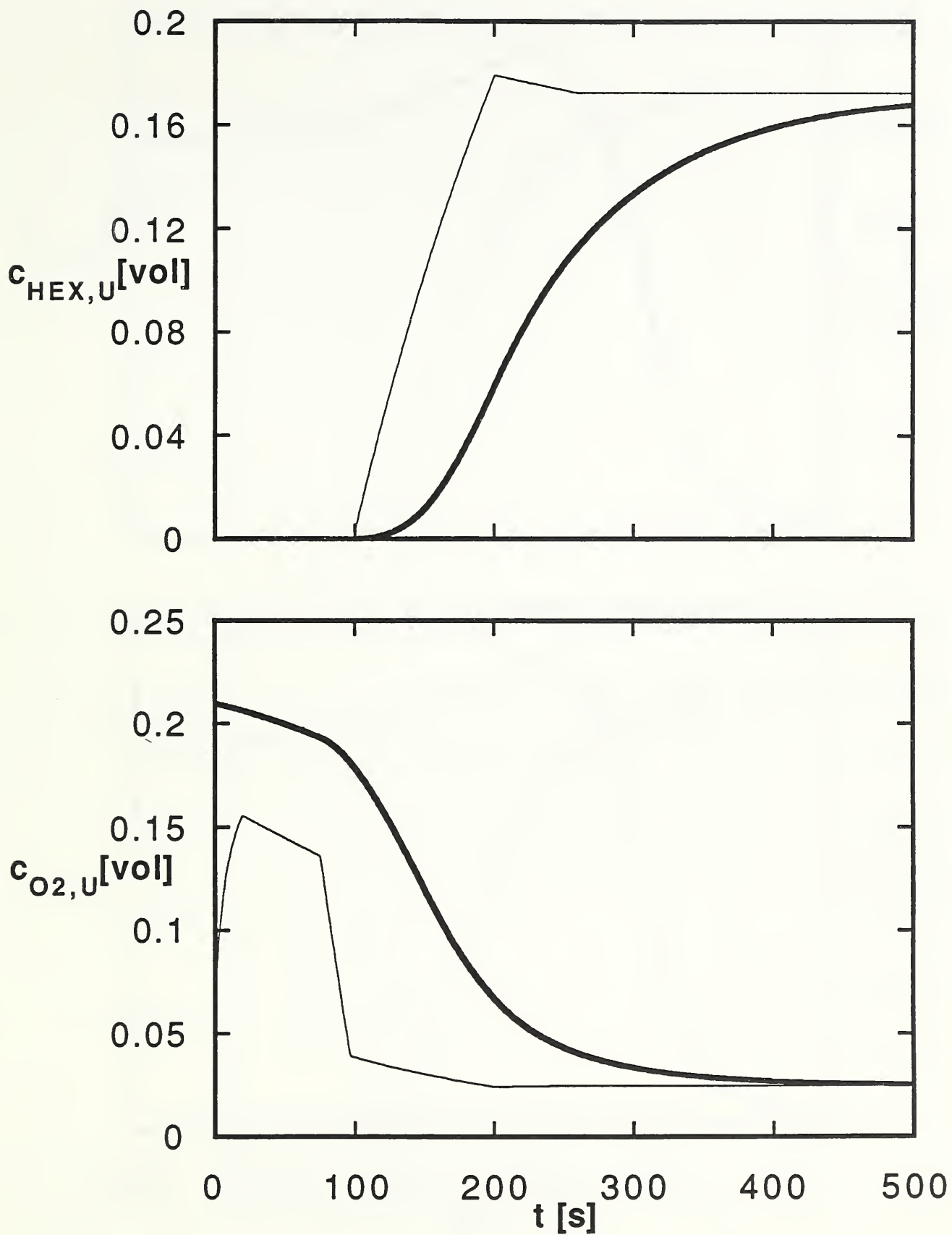


Figure 39. Results of simulating the hypothetical reference-[3]-type hexane experiment using the real combustion model: The GGERM simulation ( — ) and the quasi-steady approximation ( — ). TOP: Plots of  $c_{\text{HEX},U}$  [vol]. BOTTOM: Plots of  $c_{\text{O}_2,U}$  [vol].

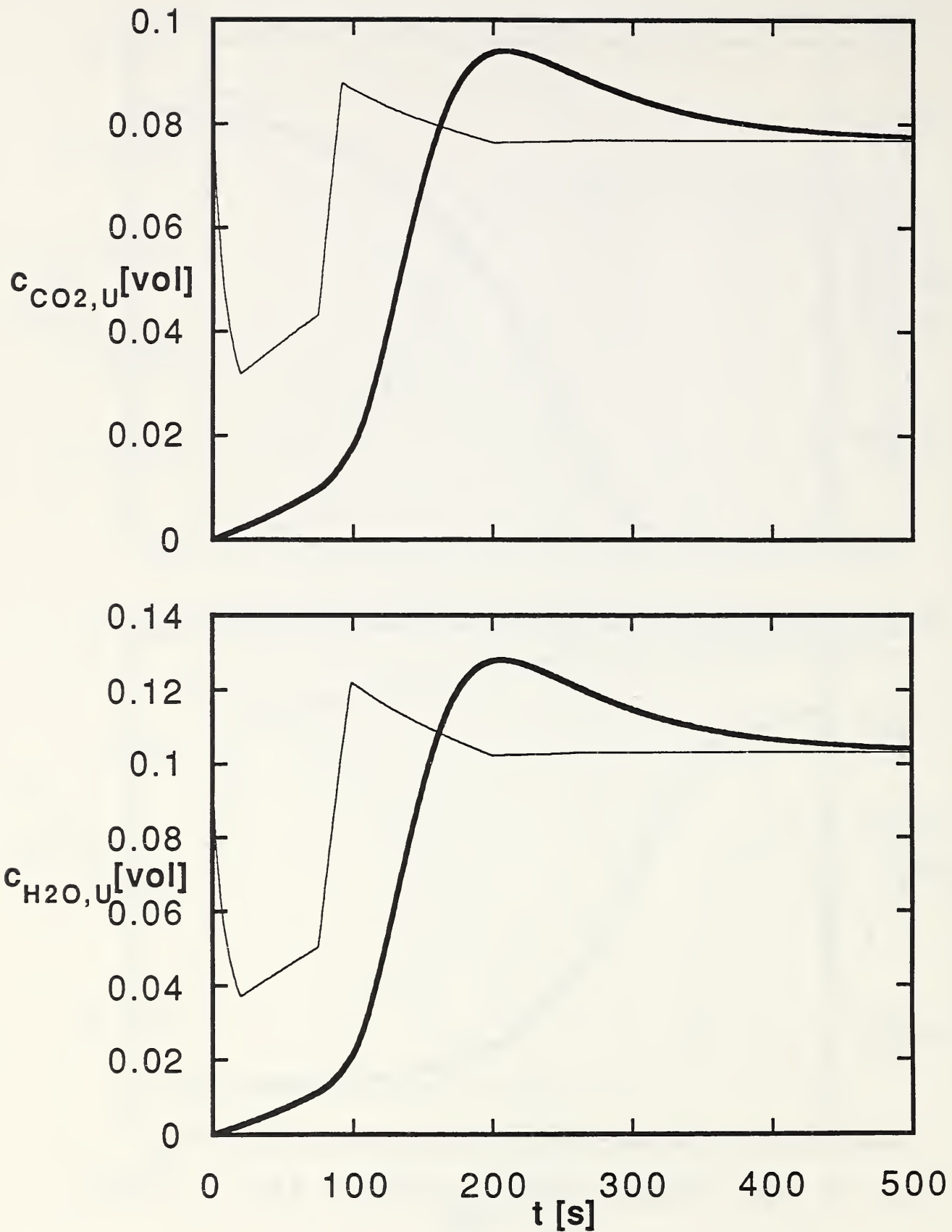


Figure 40. Results of simulating the hypothetical reference-[3]-type hexane experiment using the real combustion model: The GGERM simulation ( — ) and the quasi-steady approximation ( — ). TOP: Plots of  $c_{CO_2,U}$  [vol]. BOTTOM: Plots of  $c_{H_2O,U}$  [vol].

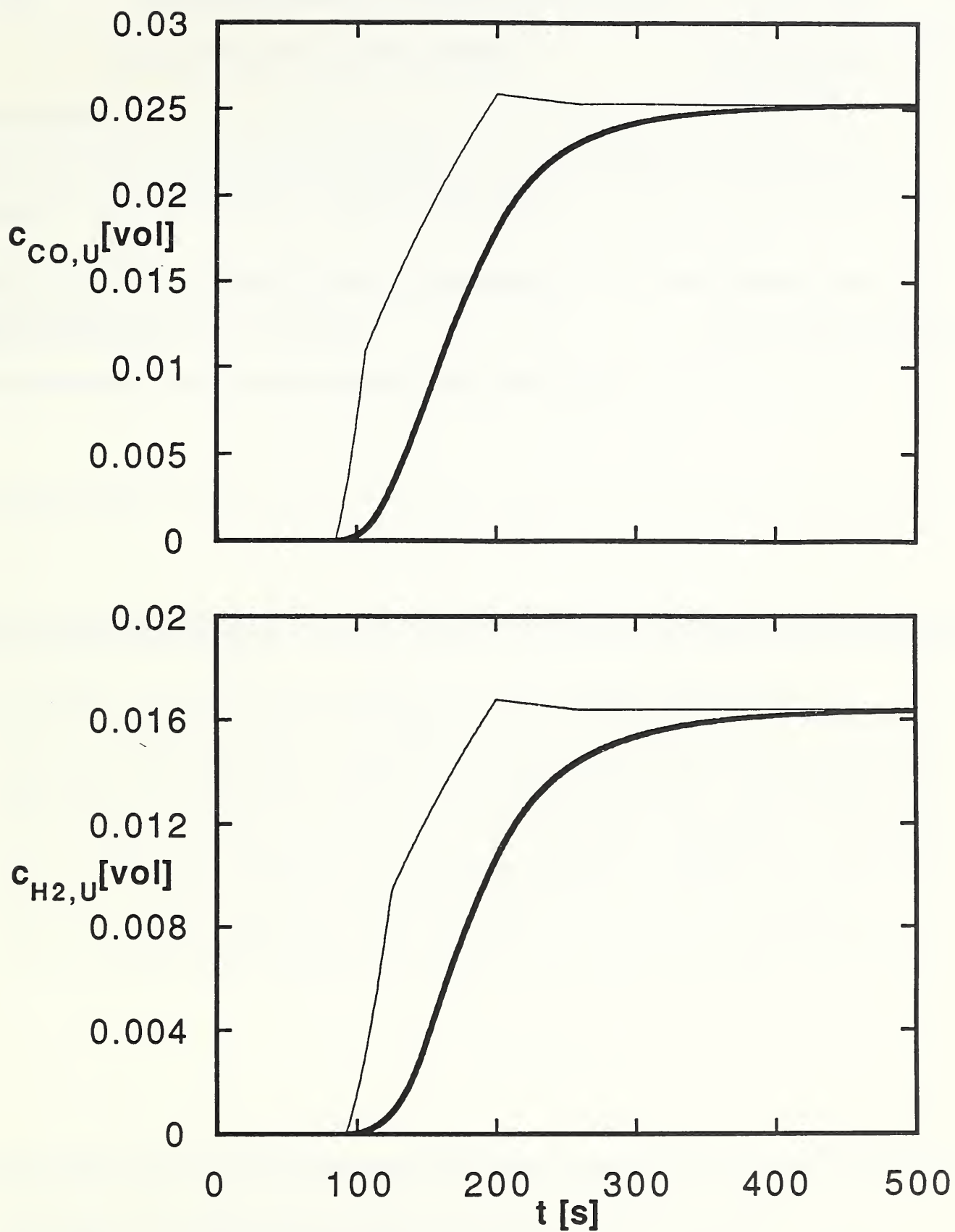


Figure 41. Results of simulating the hypothetical reference-[3]-type hexane experiment using the real combustion model: The GGERM simulation ( — ) and the quasi-steady approximation ( — ). TOP: Plots of  $c_{CO,U}$  [vol]. BOTTOM: Plots of  $c_{H2,U}$  [vol].



NIST-114A  
(REV. 3-90)

U.S. DEPARTMENT OF COMMERCE  
NATIONAL INSTITUTE OF STANDARDS AND TECHNOLOGY

1. PUBLICATION OR REPORT NUMBER

NISTIR 4590

2. PERFORMING ORGANIZATION REPORT NUMBER

3. PUBLICATION DATE

June 1991

## BIBLIOGRAPHIC DATA SHEET

4. TITLE AND SUBTITLE

Applications of the Generalized Global Equivalence Ratio Model (GGERM) for Predicting the Generation Rate and Distribution of Products of Combustion in Two-Layer Fire Environments--Methane and Hexanes

5. AUTHOR(S)

Leonard Y. Cooper

6. PERFORMING ORGANIZATION (IF JOINT OR OTHER THAN NIST, SEE INSTRUCTIONS)

U.S. DEPARTMENT OF COMMERCE  
NATIONAL INSTITUTE OF STANDARDS AND TECHNOLOGY  
GAITHERSBURG, MD 20899

7. CONTRACT/GRANT NUMBER

8. TYPE OF REPORT AND PERIOD COVERED

9. SPONSORING ORGANIZATION NAME AND COMPLETE ADDRESS (STREET, CITY, STATE, ZIP)

10. SUPPLEMENTARY NOTES

11. ABSTRACT (A 200-WORD OR LESS FACTUAL SUMMARY OF MOST SIGNIFICANT INFORMATION. IF DOCUMENT INCLUDES A SIGNIFICANT BIBLIOGRAPHY OR LITERATURE SURVEY, MENTION IT HERE.)

The Generalized Global Equivalence Ratio Model (GGERM) was developed to predict the generation rates of oxygen, fuel, and other products of combustion in rooms containing fires. The GGERM extends to general transient conditions the global equivalence ratio model established during times of steady-state in experimental studies involving two-layer compartment fires. The present work uses the GGERM to predict upper layer mass fractions of products of combustion (fuel, oxygen, CO, and others) in these two-layer fire experiments, but during times of transient response. All predicted results are found to be plausible and, where transient data are available, predicted and measured results compare favorably. However, available data are limited and additional validation of the GGERM under more varied fire conditions is required before it can be used with confidence in two-layer zone-type compartment fire models.

12. KEY WORDS (6 TO 12 ENTRIES; ALPHABETICAL ORDER; CAPITALIZE ONLY PROPER NAMES; AND SEPARATE KEY WORDS BY SEMICOLONS)

building fires; combustion; compartment fires; computer models;  
fire models; mathematical models; zone models.

13. AVAILABILITY

UNLIMITED

FOR OFFICIAL DISTRIBUTION. DO NOT RELEASE TO NATIONAL TECHNICAL INFORMATION SERVICE (NTIS).

ORDER FROM SUPERINTENDENT OF DOCUMENTS, U.S. GOVERNMENT PRINTING OFFICE,  
WASHINGTON, DC 20402.

ORDER FROM NATIONAL TECHNICAL INFORMATION SERVICE (NTIS), SPRINGFIELD, VA 22161.

14. NUMBER OF PRINTED PAGES

77

15. PRICE

A05







